AD-A086 115 UNIVERSITY OF SOUTHERN CALIFORNIA LOS ANGELES F/G 20/6
WAVEGUIDE STUDIES FOR FIBER OPTICS AND OPTICAL SIGNAL PROCESSIN--ETC(U)
APR 80 E GARMIRE F19628-77-C-0221
UNCLASSIFIED RADC-TR-80-82 NL

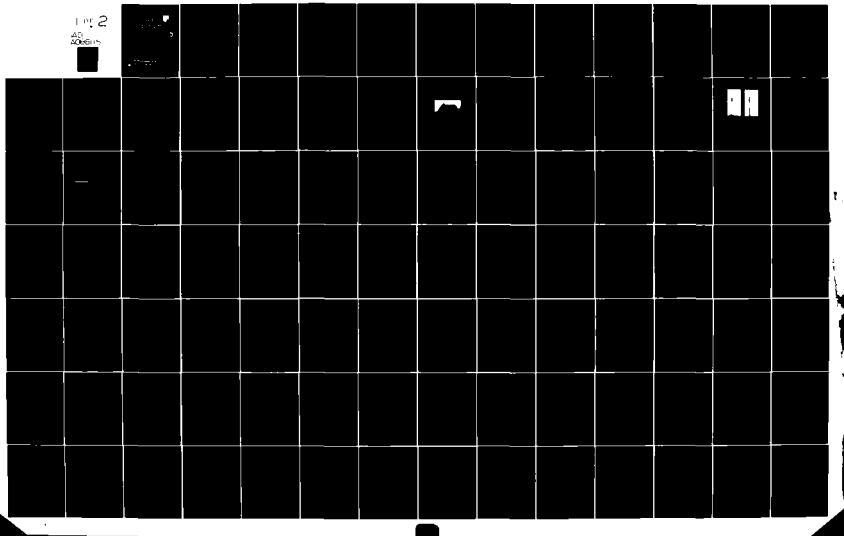

RADC-TR-80-82
Final Technical Report
April 1980

LEVEL II

12

WAVEGUIDE STUDIES FOR FIBER OPTICS AND OPTICAL SIGNAL PROCESSING APPLICATIONS

University of Southern California

Elsa Garmire

ROME AIR DEVELOPMENT CENTER
Air Force Systems Command
Griffiss Air Force Base, New York 13441

The Laboratory Contract Manager has a written policy governing the release of the copyright appearing on pages 66-68, which gives full permission to reproduce same.

This report has been reviewed by the RADC Public Affairs Office (PA) and is releasable to the National Technical Information Service (NTIS). At NTIS it will be releasable to the general public, including foreign nations.

RADC-TR-80-82 has been reviewed and is approved for publication.

APPROVED: Richard H. Picard

RICHARD H. PICARD
Project Engineer

APPROVED: Clarence D. Turner

CLARENCE D. TURNER, Acting Director
Solid State Sciences Division

FOR THE COMMANDER: John P. Huss

JOHN P. HUSS
Acting Chief, Plans Office

If your address has changed or if you wish to be removed from the RADC mailing list, or if the addressee is no longer employed by your organization, please notify RADC (ESO), Hanscom AFB MA 01731. This will assist us in maintaining a current mailing list.

Do not return this copy. Retain or destroy.

UNCLASSIFIED

SECURITY CLASSIFICATION OF THIS PAGE (When Data Entered)

REPORT DOCUMENTATION PAGE	READ INSTRUCTIONS BEFORE COMPLETING FORM
1. REPORT NUMBER: RADC-TR-80-82	2. GOVT ACCESSION NO.: AD-A086 115
	3. RECIPIENT'S CATALOG NUMBER:
4. TITLE (and Subtitle): WAVEGUIDE STUDIES FOR FIBER OPTICS AND OPTICAL SIGNAL PROCESSING APPLICATIONS	5. TYPE OF REPORT & PERIOD COVERED: Final Technical Report 11 Sep 77 — 10 Sep 79
	6. PERFORMING ORG. REPORT NUMBER: N/A
7. AUTHOR(s): Elsa Garmire	8. CONTRACT OR GRANT NUMBER(s): F19628-77-C-0221
9. PERFORMING ORGANIZATION NAME AND ADDRESS: University of Southern California, University Park, Los Angeles CA 90007	10. PROGRAM ELEMENT, PROJECT, TASK AREA & WORK UNIT NUMBERS: 61102F, 2306J228, 17 J2
11. CONTROLLING OFFICE NAME AND ADDRESS: Deputy for Electronic Technology (RADC/ESO), Hanscom AFB MA 01731	12. REPORT DATE: April 1980
	13. NUMBER OF PAGES: 117
14. MONITORING AGENCY NAME & ADDRESS (if different from Controlling Office): Same	15. SECURITY CLASS. (of this report): UNCLASSIFIED
	15a. DECLASSIFICATION DOWNGRADING SCHEDULE: N/A

16. DISTRIBUTION STATEMENT (of this Report)

Approved for public release; distribution unlimited

17. DISTRIBUTION STATEMENT (of the abstract entered in Block 20, if different from Report)

Same

18. SUPPLEMENTARY NOTES

RADC Project Engineer: Richard H. Picard (ESO)

19. KEY WORDS (Continue on reverse side if necessary and identify by block number)

Distributed Bragg reflectron lasers
Bragg deflectors
Sithium niobate waveguides
waveguide losses
multimode optical modulators and switches
electrothermal diffusion

20. ABSTRACT (Continue on reverse side if necessary and identify by block number)

This report describes investigations of waveguide components for use in multimode fiber optics and in optical signal processing. Measurements of beam expansion and polarization properties of distributed Bragg deflectors are described. Measurements of the characteristics of DBR lasers are detailed, with emphasis on those properties which are relevant to their use as sources to couple to the waveguide beam expander. Studies of the mechanisms for loss in $LiNbO_3$ waveguides are described —>

next Page

DD FORM 1 JAN 73 1473 EDITION OF 1 NOV 65 IS OBSOLETE

UNCLASSIFIED

SECURITY CLASSIFICATION OF THIS PAGE (When Data Entered)

361550

and techniques to reduce the waveguide loss in $LiNbO_3$ modulators are outlined. Finally, preliminary experiments on electro-thermal diffusion in $LiNbO_3$ are described.

EVALUATION

This report is the final technical report on the contract and covers research done in the period September 1977 to September 1979. It details work on distributed Bragg reflector lasers, waveguide grating beam expanders, lithium niobate waveguide loss mechanisms, and multimode lithium niobate waveguide fabrication. The work described should lead to increased understanding of waveguide components such as switches and sources for multimode fiber optic communications and optical signal processing. Hence, it supports both TPO R3B and TPO R5D of the RADC Technology Plan.

Richard H. Picard

RICHARD H. PICARD
Project Engineer

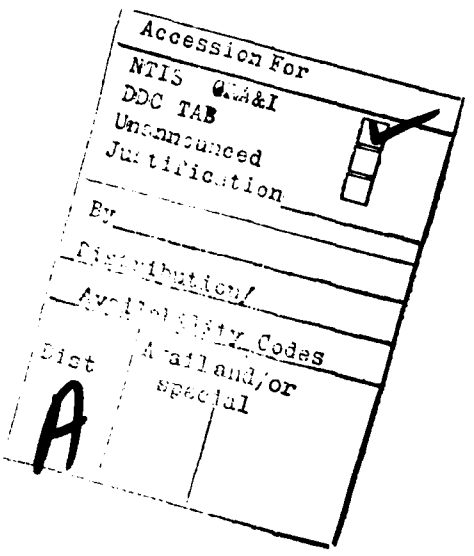

TABLE OF CONTENTS

INTRODUCTION

The purpose of this contract was to study beam expansion for multimode fiber optics and optical signal processing applications. It was proposed to integrate the beam expander monolithically with a DBR laser to provide an expanded beam about 75 μm wide. Simultaneous studies were begun to develop the beam expander to demonstrate the concept and also to fabricate DBR lasers. It was the intention of the program to integrate these two devices together during the second year of the contract. Within the first year, beam expansion was demonstrated using a distributed Bragg deflector (DBD) in passive material, and its unique polarization properties were characterized. However, unexpected difficulties were encountered in the fabrication of DBR lasers, and that part of the project was delayed by a year before a successful fabrication schedule was worked out. The details of the fabrication studies which went into the successful fabrication of DBR lasers is contained in Aerospace Report No. ATR-79(7739)-1, submitted by The Aerospace Corporation to University of Southern California on April 10, 1979.

During the second year DBR lasers were successfully fabricated and their properties were studied, in order to obtain information as to how successfully they would integrate with the beam expander. However, the contract ran out before the monolithic integration was achieved.

Because of the delay in DBR laser fabrication during the first year the program was broadened to include studies of bistable switches for fiber optics and optical signal processing applications. This program was very successful and led to five papers and four talks, listed in the tables at the end of the Introduction. This work was described in the RADC interim report (RADC-TR-79-112), and will only be summarized below. During the second year, the sponsorship of this work was picked up by AFOSR, and further research in this area is described in the interim scientific report submitted to AFOSR.

The realization of the polarization properties of the distributed Bragg deflector beam expander, which make it the integrated optics analog of the Glan-Thompson prism, suggested the possibility of using the DBD along with polarization modulation to made a multimode fiber optics switch. Work was therefore begun on developing $LiNbO_3$ waveguides with good optical properties to be used with the beam expander to make a multimode fiber optics switch.

Each of the efforts just described will be summarized in the following sections of the introduction and then will be described in separate chapters in the body of this report.

1. Waveguide Beam Expansion

In accordance with the proposal, studies of waveguide beam expansion were undertaken using a distributed Bragg deflector on VPE GaAs waveguides along with excitation by a 1.15 μm HeNe laser. The experiments resulted in a deflected beam with a width of 1300 μm, for an expansion factor of 26. This expansion was too large for the applications intended in the contract, however. The reason for the large expansion was the fact that the grating had a long coupling length. SEM photographs of the grating showed it to be of excellent quality but since the VPE waveguides had a large effective waveguide thickness, the coupling coefficient was weak. The result of this study was the prediction that the distributed Bragg deflector should provide adequate beam expansion when double heterostructure material is used.

The experiments demonstrated that the TE mode was not deflected when the grating spacing and angle were chosen to produce a 90° deflection. Only the TM mode was deflected, while the TE mode was transmitted through the DBD. Measurements indicated an extinction ratio of 343 between the transmitted components. This suggested the use of the DBD as a polarization analyzer, or as the integrated optics analog of the Glan-Thompson prism. However, it also indicated that the monolithically integrated beam expander would have to operate at 45°, rather than at 90°, since the DBR laser operates with the TE polarization.

At 45° beam expander was fabricated in VPE GaAs, although again the expanded beam was too large to be useful. The decision to use the 45° deflection angle led to a redesign of the beam expander, which could now use a first order grating. Measurements were made of the coupling coefficient of the gratings used in the DBR lasers and led to a prediction that expansion factors of 5, or deflected beams the order of 75 μm should be easily achieved. The result of this study is the assurance that, with the redesign to 45° beam deflection, expansion

factors as predicted in the proposal can be achieved in double heterostructure material which we have available at the present time.

2. DBR Lasers for Fiber Optics and Optical Signal Processing Sources

DBR lasers were successfully fabricated during the second year, and a number of studies were undertaken to evaluate their suitability as sources for multimode fiber optics and optical signal processing. We observed the single mode operation characteristic of the DBR lasers, but also observed that if the wavequide layer was too thick, two wavelengths appeared, separated by 40 Å. This is due to the fact that the waveguide supports two modes which have different propagation constants and therefore satisfy the Bragg condition at different wavelengths.

We made measurements of the front-to-rear power ratio emitted from the lasers in order to determine the coupling coefficient of the gratings causing retroreflection. The effective 1/e coupling lengths of the gratings were 192 μm and 106 μm, numbers which were in good agreement with estimations made from the tooth shape and heights and the waveguide effective thickness. These studies confirmed that the double heterostructure material could be used to make excellent beam expanders.

Finally, we measured the in-plane beam divergence of several DBR lasers and found one whose behavior was diffraction limited, right above threshold, and would be suitable for a beam expander. The other device, however, displayed multimode characteristics which would not be suitable for controlled beam expansion. This suggests that it will be necessary to control the spatial modes of the DBR laser in the same fashion as has been recently developed for Fabry-Perot lasers, using narrow stripes and tapered junctions, if optimum performance is desired.

3. Bistable Optical Switches for Multimode Fiber Optics and Optical Signal Processing Applications

When the output of any modulator or switch is detected and used to provide a voltage across that same modulator or switch, that device is bistable. This means that there is a regime of operation in which there are two stable final states, depending on the history of operation of the device (whether the steady state was reached with an incident signal below

or above its steady-state value). We demonstrated this concept in a bulk modulator and suggested that an integrated optics version with a multimode bistable optical switch could be used for multimode fiber optics and optical signal processing applications. For this reason we embarked on a study of these devices in the first year of this contract.

We demonstrated an integrated optics version of the bistable switch using a multimode out-diffused $LiNbO_3$ modulator which was only 2 mm long. Bistability was achieved, and the details are described in the pubications listed in Table I at the end of this introduction.

In addition, we made studies of the transient response of these bistable optical switches. In particular, we demonstrated the phenomenon of "critical slowing down". This is a delay in the switching of the device which occurs if the incident signal is near its critical value for switching. This phenomenon means that the switch signal must be bigger than its minimum value if long delays are to be avoided. It alsc means that estimates of the required switch energy based on steady-state values of incident signal and time constants will be wrong. Detailed understanding of this phenomenon and presentation of the experimental results are in the publications listed at the end of the Introduction.

In the past year, when support of the bistable switch as picked up by AFOSR, we have made progress in further understanding the transient behavior of these devices. In particular, we have studied the effects of overshoots which occur when the device has two time constants. In addition we have studied the distributed feedback non-linear optical device, which can also be bistable. These studies are described in the interim report to AFOSR.

4. Studies of $LiNbO_3$ Waveguide Loss

Motivated by the possibility of integrated optics multimode switches in $LiNbO_3$ which could be butt-coupled to multimode fiber optics, and by the interest in $LiNbO_3$ bistable devices for optical signal processing, studies were undertaken to improve the characteristics of $LiNbO_3$ waveguides. In Chapter 3, studies of the loss mechanisms in $LiNbO_3$ waveguides are described. The loss contributions are separated into

absorption, scattering from the surface of the waveguide and scattering from within the waveguide.

Absorption losses were measured calorimetrically and shown to be negligible. A theoretical study was undertaken which demonstrated that waveguides buried below the surface of the wafer should have considerably less scattering loss than those which are at the surface.

Experimental studies indicated that scattering from within the bulk of in-diffused waveguides was much smaller than the scattering from surface roughness. Finally, insertion loss studies were made to compare the relative importance of length-dependent and input coupling losses. The results show that the length-dependent losses in the waveguides we fabricated varied from 0.6 dB/cm in waveguides 20 μm wide to 1.1 dB/cm in waveguides 10 μm wide to 1.6 dB/cm in waveguides 3 μm wide. The input coupling loss was found to be between 0.6 and 2 dB.

Several experiments were undertaken in an attempt to reduce the insertion loss of $LiNbO_3$ butt-coupled multimode waveguides. These include polishing the surface and applying a high index cladding layer to the surface of the waveguide. The experiments did not reveal any sizeable improvement in waveguide performance as a result of these experiments.

5. Studies of Multimode Waveguide Fabrication in c-propagating $LiNbO_3$

The use of the DBD as an integrated optics Glan Prism suggested a multimode fiber optics switch based on electo-optic polarization modulation. This switch can work in $LiNbO_3$ for c-propagating light, when the electric field is parallel to the plane of the waveguide (as will occur for electrodes on either side of the channel waveguide). The geometry of this switch will be described in Chapter 4.

With the switch as motivation we began to study the fabrication of multimode waveguides in c-propagating $LiNbO_3$. We investigated the use of an electric field during the diffusion to assist in obtaining deep diffusions. The results were somewhat inconclusive, since the samples had a tendency to crack. Experiments were still underway at the end of the contract. The data in Chapter 4 represents a progress report to date, rather than a definitive estimation as to whether or not electro-thermal diffusion will be useful in the fabrication of multimode waveguides.

TABLE I PUBLICATIONS ARISING FROM THIS PROGRAM

Title	Authors	Reference
"Distributed Bragg Deflector: A Multifunctional Integrated Optical Device"	H. M. Stoll	Applied Optics 17 2562 (1978)
"High Brightness Lasers Using Integrated Optics"	H. M. Stoll	Proc. SPIE 139 113 (1978)
"Bragg-effect Polarizer-analyzers and Lens-less Waveguide Beam Expansion"	H. M. Stoll, W. E. Soady	To be published
"Optimally coupled, GaAs Distributed Bragg Reflection Lasers"	H. M. Stoll	To be published
"Multimode Integrated Optical Bistable switch"	E. Garmire, S. D. Allen J. Marburger, C. Verber	Optics Letters 3 69 (1978)
"Bistable Optical Devices for Integrated Optics and Fiber Optics Applications"	E. Garmire, S. D. Allen J. Marburger	Proc. SPIE 139 174 (1978)
"Bistable Optical Devices: An Overview"	J. Marburger, E. Garmire	Fiber Optics, Ed. B. Bendow, S. S. Mitra (Plenum Press, 1979) p. 395
"Bistable Optical Devices for Integrated Optics and Fiber Optics Applications"	E. Garmire, S. D. Allen J. Marburger	Optical Engineering 18, 194 (1979)
"Transient Response of Hybrid Bistable Optical Devices"	E. Garmire, J. H. Marburger, S.D. Allen, H. Winful	Appl. Phys. Lett., 34 374 (1979)
"Calorimetric measurement of $LiNbO_3$ Waveguide Absorption Losses"	S. D. Allen, E. Garmire M. Bass, B. Packer	Appl. Phys. Lett. 34 435 (1979)
"Comparison of Losses in Imperfect Surface-Diffused and buried Optical Waveguides"	T. Findakly, E. Garmire H. T. Moon	Optics Lett. 4 149 (1979)

TABLE II TALKS ARISING FROM THIS PROGRAM

Title	Authors	Meeting
"High Brightness Lasers Using Integrated Optics"	H. M. Stoll	SPIE, Washington, April, 1978
"Bistable Optical Devices for Integrated Optics and Fiber Optics Applications"	E. Garmire, S. D. Allen, J. H. Marburger	SPIE, Washington, April, 1978
"Optical Bistability Without Mirrors"	J. H. Marburger, S. D. Allen, E. Garmire M. Levenson, H. Winful	IQEC, Atlanta, June, 1978
"Bistable Optical Devices: An Overview"	J. H. Marburger, E. Garmire	Physics of Fiber Optics, Rhode Island, July, 1978.
"Transient Effects in Bistable Optical Devices"	S. D. Allen, E. Garmire, J. H. Marburger, H. Winful	OSA, San Francisco, October 1978
"Loss Mechanisms in $LiNbO_3$ Waveguides"	E. Garmire, T. Findakly, H. T. Moon	CLEA, Washington, June, 1979

CHAPTER 1. WAVEGUIDE BEAM EXPANSION

This program was begun to study waveguide beam expansion for use in fiber optics and signal processing applications. Beam expansion can be achieved by using a distributed Bragg deflector (DBD). This device consists of a corrugated waveguide, whose grating is slanted at an angle θ with respect to the incident beam. The geometry of the DBD is shown in Fig. 1. The incident beam enters from the left into a confined slab guide with a corrugated surface. Bragg reflection occurs from the grating, reflecting the beam at an angle equal to the incidence angle. However, the reflections from the corrugations add up coherently only if the Bragg condition is satisfied; that is,

$$\Lambda = \frac{\lambda m}{2n \sin \theta}. \tag{1-1}$$

In addition to beam expansion, applications of the DBD include beam splitters (power division), deflectors (as, for example, to create ring geometries), polarizers and analyzers (with 90° deflection) and multiplexers/demultiplexers (with chirped gratings).

The theoretical analysis of the device was completed during the initial phases of the contract and is presented in a paper, entitled, "Distributed Bragg Deflector: A Multifunctional Integrated Optical Device", H.M. Stoll, Applied Optics, 17 2562 (1978). For this reason, only the results of that theoretical analysis are presented here.

It was found that the incident light beam amplitude is reduced while traveling through the DBD region by an exponential factor with distance, $\exp(-\gamma z)$, due to deflection. The results of the calculation are:

$$\gamma_{TE} = \nu \cos^2\theta_B \tag{1-2}$$

and

$$\gamma_{TM} = \nu \left\{ \frac{2 n_2^2}{(n_2^2 - n_1^2)} \log\left(\frac{n_2}{n_1}\right) [\cos\theta_B - 1] - \cos\theta_B \right\}^2, \tag{1-3}$$

where

$$\nu = w \left\{ \frac{4\pi \left(n_2^2 - n_1^2\right) d^3}{3 \left(2\ell - 1\right) n_2 \lambda_o t_e^3} \right\}^2 . \qquad (1\text{-}4)$$

The quantities are as defined in Fig. 1-1, with λ_o the wavelength of incident light, ℓ the Bragg scattering order and t_e, the effective guide thickness. If the mode is near cutoff, $t_e = t + 1/\delta$, where δ is the exponential decay profile of the mode in the substrate.

Consider the deflection of a TM polarized beam at 90° which is the configuration of greatest interest for beam expander applications:

$$\gamma_\perp = \nu \left\{ \frac{2 n_2^2}{n_2^2 - 1} \log n_2 \right\}^2 . \qquad (1\text{-}5)$$

We have made use of the fact that n_1 = air = 1.

It will be convenient to relate these results to those of retroreflection in a corrugated waveguide. Coupled mode theory predicts that a corrugated waveguide will couple forward and backward waveguide modes with a coupling coefficient K. Light originally travelling forward transfers to the backward wave exponentially with length, with a coefficient given by K. Thus the effectiveness of a grating can be described by describing its coupling coefficient. For square corrugations such as those used to derive Eq. 1-3, the coupling coefficient is

$$K = \frac{2\pi^2 \Delta n^2}{3 \left(2\ell - 1\right) \lambda n_g} \left(\frac{d}{t_e}\right)^3 . \qquad (1\text{-}6)$$

A related parameter is the characteristic distance at which the power in the initial mode decreases by a factor of 1/e. This characteristic length is given by $L_g = (2K)^{-1}$.

We then write the DBD exponential coefficient as

$$\gamma_\perp = \left\{ \frac{4 n_g^2 \log n_g}{\pi \left(n_g^2 - 1\right)} \right\}^2 K^2 W . \qquad (1\text{-}7)$$

Since the deflected beam has an amplitude which decreases with distance along the DBD according to an exponential with a coefficient γ, the intensity width of the expanded beam will be approximately $1/2\gamma$.

Figure 1-1 Distribution Bragg deflector: (a) top view; (b) side cross-sectional view; and (c) end cross-sectional view. Small and large (solid) arrows in (a) represent incident and deflected beams respectively. Dashed sinusoid in (c) represents equivalent core field distribution in the y direction.

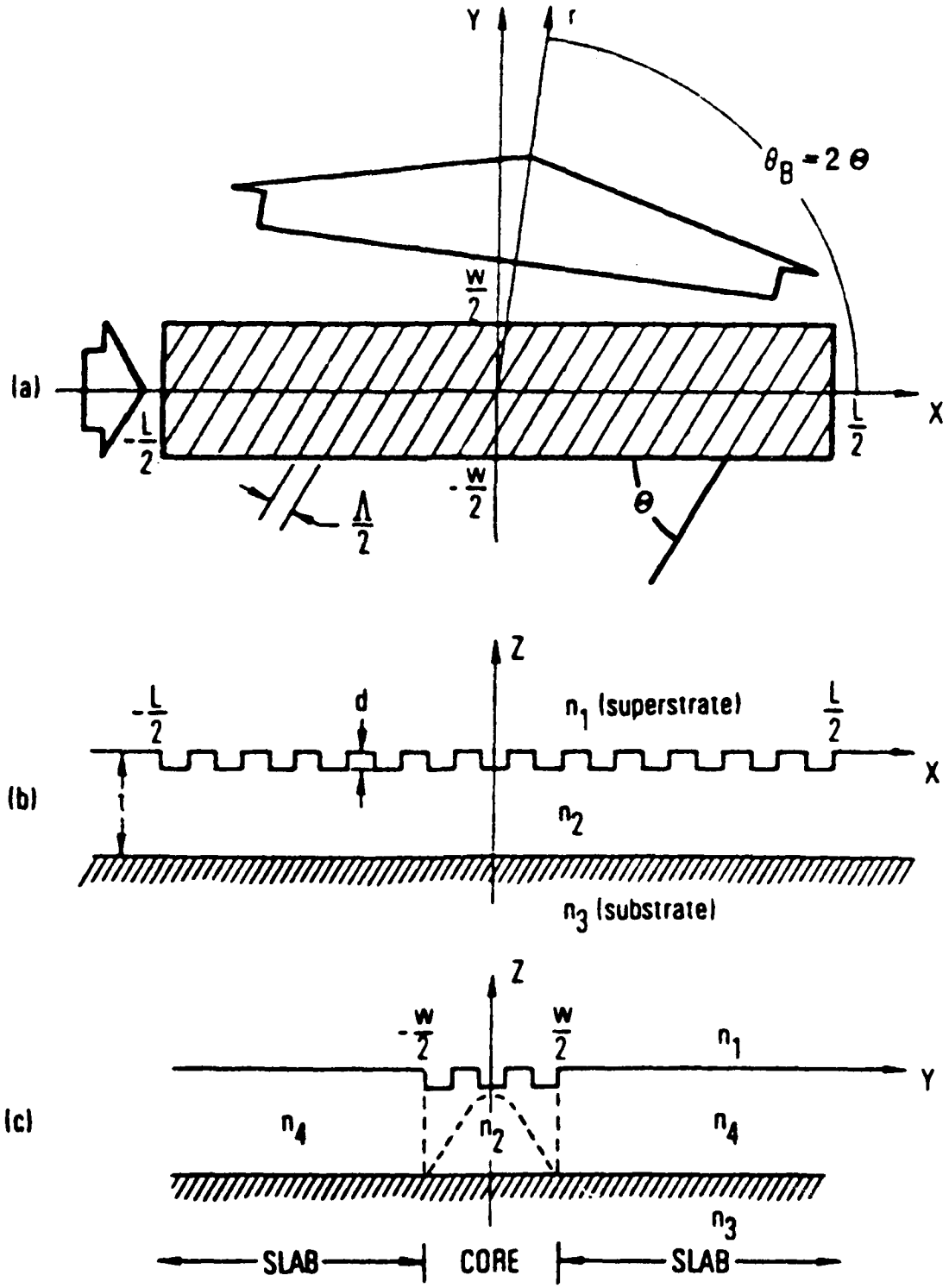

Defining the expansion factor as the width of the deflected beam divided by the incident beam width, we write the expansion factor as

$$F_{\perp} = \frac{1}{2\gamma_{\perp} W} = 2 \left\{ \frac{\pi (n_g^2 - 1)}{4 n_g^2 \log n_g} \right\}^2 \left(\frac{L_g}{W} \right)^2 \qquad (1\text{-}8)$$

$$\equiv 2f^2 \left(\frac{L_g}{W} \right)^2$$

where we have defined the grating by its characteristic length.

It can be seen that it is easy to obtain large expansion factors, since the characteristic length of gratings can be typically larger than W.

For the case of GaAs waveguides, $n_g = 3.6$, and $f = 0.56$. The intention of the program was to obtain expansion factors of roughly five; to expand the 20 μm emission from a GaAs stripe geometry laser to a 100 μm beam, which could be used for signal processing or which could be used with an output grating coupler to make a beam which could be butt-coupled to multimode fibers, discussed in Chapter 2. Expansion of a factor of 5 can be achieved if $L_g/W = 2.8$. For an incident beam of 20 μm, this requires $L_g = 56$ μm, or $K = .0089$. A grating with this coupling coefficient can be achieved if the waveguide is 1 μm thick and the tooth depth is 0.1 μm (Eq. 1-6).

Reflection with no expansion will occur when

$$W = \sqrt{2}\, \frac{\pi (n_g^2 - 1)}{4 n_g^2 \log n_g}\, L_g = \sqrt{2}\, f\, L_g. \qquad (1\text{-}9)$$

For GaAs, $W = 0.79\, L_g$ will ensure reflection with no expansion, at 90° deflection.

The research program was designed first to demonstrate beam expansion in high optical quality VPE GaAs waveguide material and then to apply the concept to LPE GaAs double heterostructures, so that the laser and beam expander could be combined into the same substrate.

Demonstration of beam expansion in VPE GaAs epilayers was successful. A perspective view of the Bragg-effect polarizer/analyzer which we fabricated is shown in Fig. 1-2. The asymmetric slab waveguide structure consisted of a 1 μm thick, n-type ($\lesssim 10^{16}$ cm^{-3}) GaAs layer epitaxially grown over a

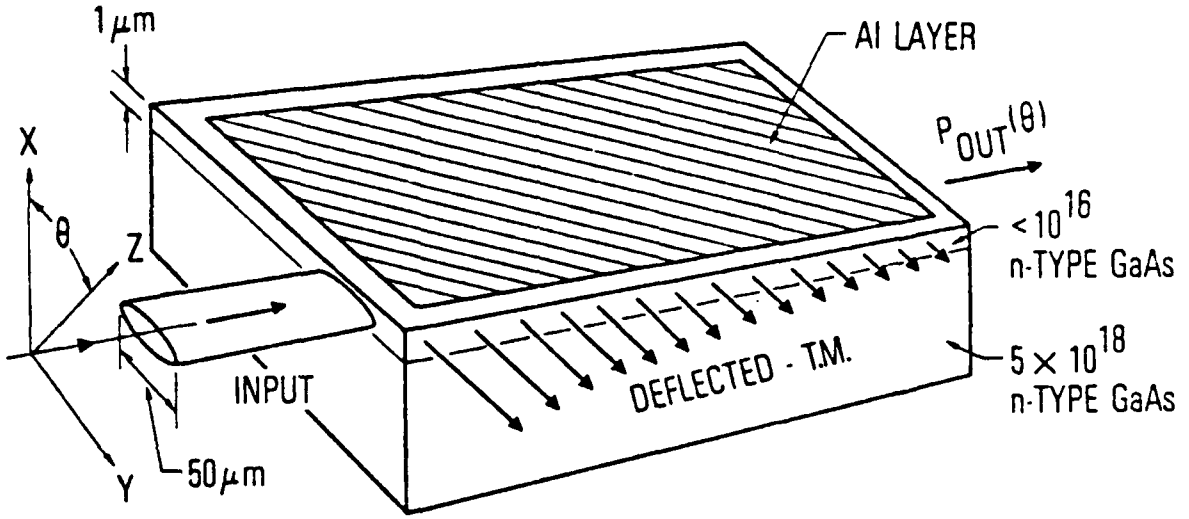

Figure 1-2 Perspective view of the Bragg-effect polarizer/analyzer which was tested. The electric field vector of the input beam is oriented at an angle θ to the waveguide surface normal.

heavily doped n-type ($\sim 5 \times 10^{18}$ cm^{-3}) GaAs substrate; it supported only the lowest order one-dimenional, T.E. - and T.M. - polarized modes. Ninety degree Bragg scattering of the incident 1.15 μm radiation was accomplished via a second order periodic surface corrugation (Λ = 0.478 μm) which was ion milled into the waveguide surface and overcoated with a 0.1 μm thick layer of aluminum ($n_1^2 \approx -69$) in order to increase its deflection efficiency. As revealed by SEM examination of a cross section through the device, the corrugations bore a nearly triangular tooth profile. A photograph of a typical grating is shown in Fig. 1-3. The total corrugation length, L, and input beam width, w, were 3.2 mm and 50 μm, respectively.

Figure 1-4 shows a semi-logarithmic plot of the near-field, deflected beam intensity profile of one of our 90° Bragg deflectors. The data shows that the deflected beam decreases of a factor of 1/e in 1.3 mm length. With in input beam of 50 μm, this corresponds to an expansion factor of 38, much larger than required for fiber optics applications. From this data it can be inferred that the effective coupling length of the grating was L_g = 385 μm, with a coupling coefficient of K = 0.0013. This coupling is too weak for fiber optics applications. The reason for the weak effect is use of VPE GaAs. The index change due to the reduction of the number of free carriers in the epilayer is very small. As a result, the guided mode extends into the substrate and the effective guide width is larger than the 1 μm physical thickness of the epilayer. For the physical parameters used in the experiment, the effective guide thickness was several microns, causing the coupling coefficient to be small.

Because of the weakness of guiding in the VPE material, the effective waveguide thickness was large and the grating coupling coefficient was small. As a result, the expanded beam was too large to be useful for more than demonstration of the principles. However, it was demonstrated that even a grating with a low coupling coefficient can be used successfully as a polarizer-analyzer. A study of this effect was undertaken and the results of this study have been submitted for publication (H.M. Stoll, W.E. Soady "Bragg-effect Polarizer/Analyzers and Lens-less Waveguide Beam Expansion") and are summarized in this report.

Operation of the DBD as a polarizer/analyzer can be seen by observing that $\gamma_{TE} = 0$ for a deflection angle of 90°. Polarizer/analyzer performance parameters of interest include the extinction ratio, ρ, which we define as

Ion Milled Grating

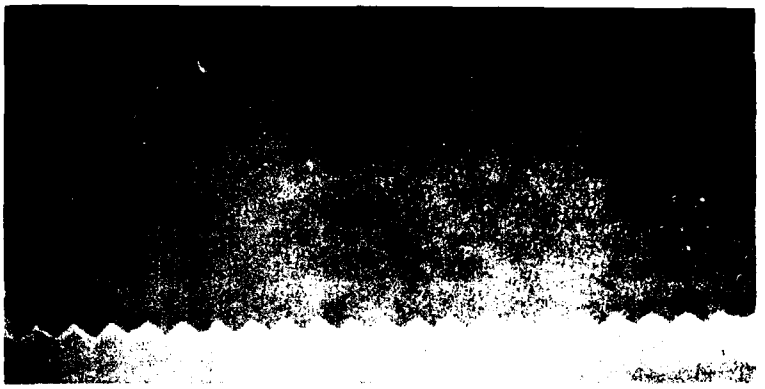

0.5 μm PERIOD

Figure 1-3 SEM photograph of cross-section of ion-milled grating in GaAs.

Figure 1-4 Semi-logarithmic plot of the near-field Bragg scattered beam intensity profile of a 90° deflector.

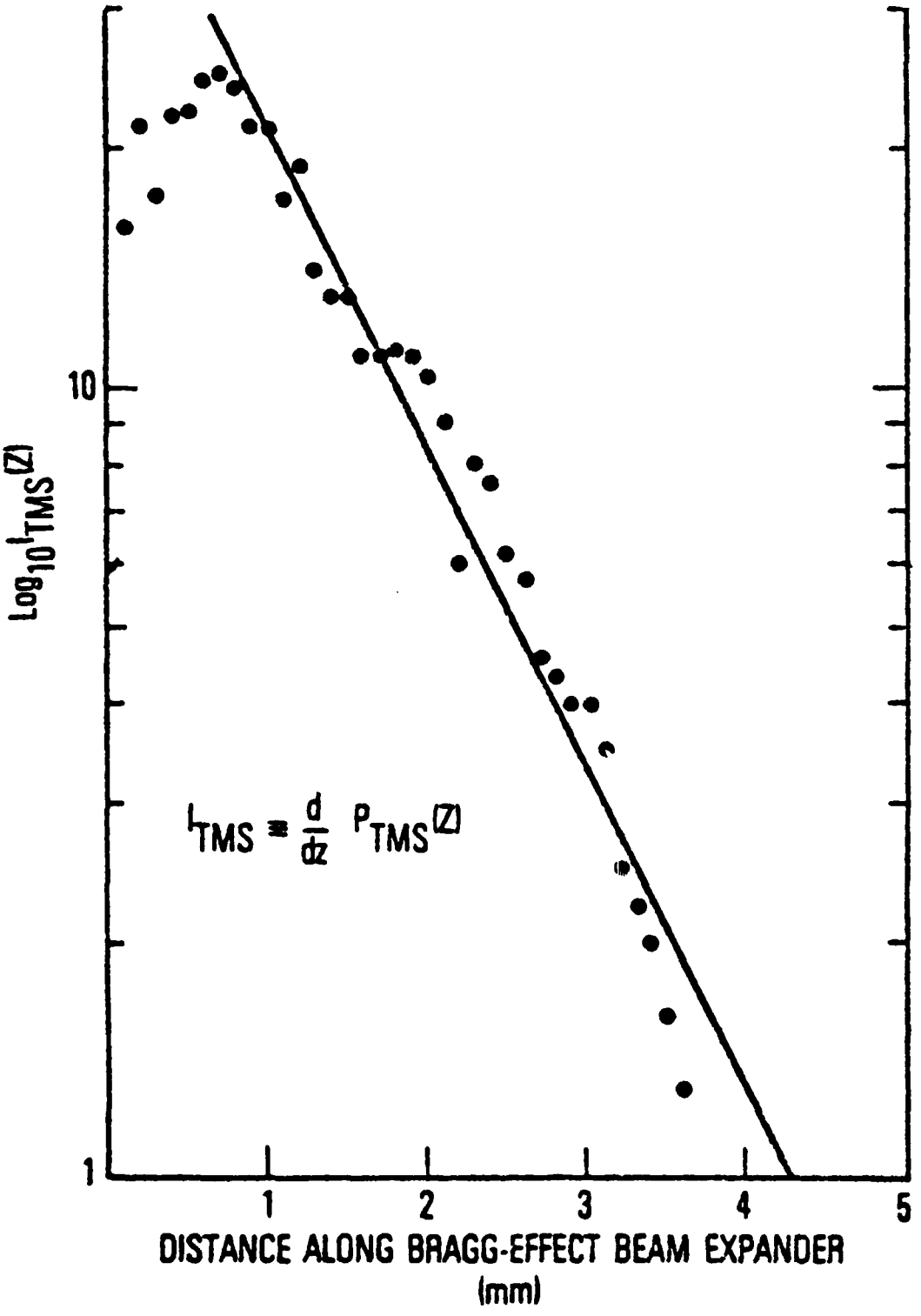

being equal to the ratio of T.M. - to T.E. -mode power deflected by the device, or

$$\rho = \frac{\gamma_{TM}}{\gamma_{TE}} \cdot \frac{\delta_{TE}}{\delta_{TM}} \frac{1 - \exp(-2\,\delta_{TM} L)}{1 - \exp(-2\,\delta_{TE} L)}, \tag{1-10}$$

and the T.M. deflection efficiency, η, which we define as being equal to the ratio of deflected to incident T.M. -mode power, or

$$\eta = \frac{\gamma_{TM}}{\delta_{TM}} \left[1 - \exp(-2\,\delta_{TM} L)\right]. \tag{1-11}$$

In Eqs.(1-10) and (1-11), δ_{TE} and δ_{TM} are the total (including background) T.E. - and T.M. -mode attenuation coefficients, respectively, and L is the device length.

Experiments were performed on the polarization dependence of beam deflection using the VPE GaAs waveguide beam expander shown in Fig. 1-2. By measuring the near field intensity profile of the beam which was Bragg deflected by the polarizer/analyzer, δ_{TM} was determined to be 4.19 cm^{-1}. Knowledge of δ_{TM} together with measurements of the undeflected throughput power,

$$P_{out}(\theta) = P_{in}\left[\cos^2\theta \exp(-2\,\delta_{TM} L) + \sin^2\theta \exp(-2\,\delta_{TE} L)\right] \tag{1-12}$$

for $\theta = 0$ and $\pi/2$, were then used to yield $\delta_{TE} = 3.11\ cm^{-1}$, $\gamma_{TM} = 0.154\ cm^{-1}$, and $\eta = 0.034$. Finally, direct measurement yielded an extinction ratio of 343 from which it was inferred that $\delta_{TE} = 3.6 \times 10^{-4}\ cm^{-1}$. Figure 1-5, which plots $P_{out}(\theta)$, $P_{TMS}(\theta)$ (the total T.M. power deflected), and the experimental data, summarizes the results.

The passive beam expander in VPE GaAs demonstrated that beam expansion was indeed possible using the Distributed Bragg Deflector. However, it was also demonstrated that the efficiency of deflection goes to zero for the TE mode at a deflection angle of 90°. Before we knew whether or not the 90° angle of deflection was suitable for use in a monolithic circuit together with the laser source, we needed to know what the polarization would be of the DBR lasers, whose characteristics will be described in the next chapter. It was

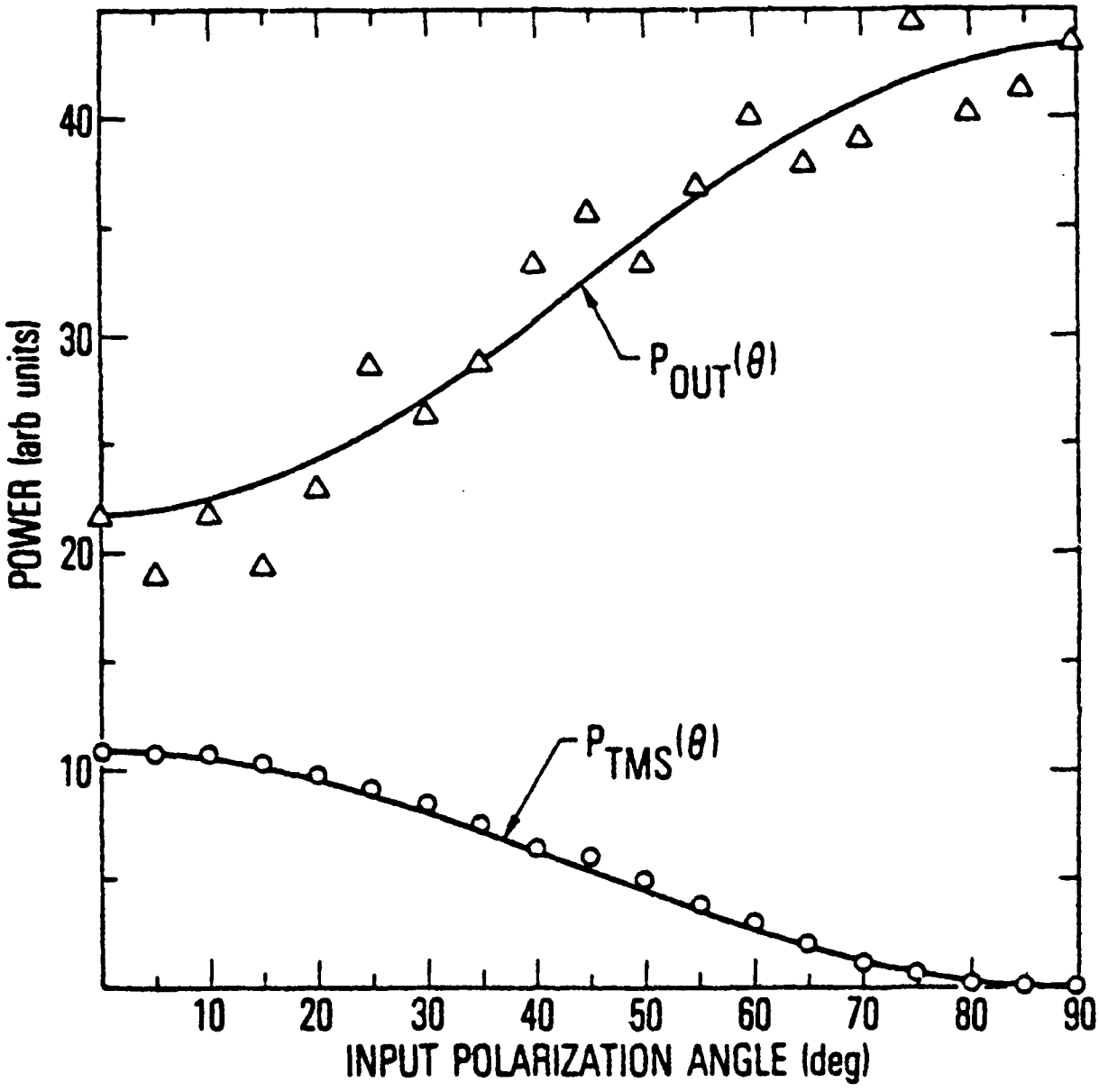

Figure 1-5 Plots of the throughput power, $P_{out}(\theta)$, and Bragg-scattered power, $P_{TMS}(\theta)$, as functions of the input beam polarization angle θ. Also shown are the experimental data (Λ and 0).

found that these lasers operated with a TE polarization. This means that the angle of deflection must be some angle other than 90°. The most convenient angle of deflection is 45°.

Figure 1-6 shows a 45° DBD which was fabricated in VPE GaAs. The beam expansion is shown in the lower photograph, as a streak to the left of the beam. The difficulty in observing this device is the necessity of polishing the end face to obtain the output at 45°. The advantage is that the grating can be used in fundamental order. The deflection of the DBD in the VPE waveguide was very weak because the waveguide was so thick. Experiments on 45° deflection in thinner LPE GaAs waveguides awaited the development of DBR lasers. Because the fabrication of the DBR lasers took more effort than anticipated, there was not time before the end of the contract to test the 45° beam expander in double heterostructure material.

It is possible to use the results of the DBR lasers and the coupling coefficients of their gratings to predict the behavior for the 45° beam expander, however.

The 45° beam expander used in conjunction with a GaAs DBR laser will be used with the grating in fundamental order and a spacing of 0.338 μm. To determine the expansion factor from the K value of the grating, we use Eq. (1-2) and obtain $\gamma_{TE} = (2K/\pi)^2 W \cos^2\theta_B = W \cos^2\theta_B/(\pi L_g)^2$. We wish to determine whether or not teeth of the shape used for the DBR laser can be satisfactory to produce beam expansion of the requisite factor of five. First we need to define an expansion factor, which includes the fact that the deflection is at an angle other than at 90°. The width of the expanded beam is $\sin\theta_B/(2\gamma_{TE})$. This gives an expansion factor of

$$F_\theta = \frac{1}{2}\left(\frac{\pi L_g}{W}\right)^2 \frac{\sin\theta_B}{\cos^2\theta_B} \quad . \tag{1-13}$$

The expansion factor increases rapidly as $\theta \to 90°$, but at this angle the TE reflectivity $\to 0$, so there is no inconsistency. From Eq. 1-6, it can be seen that the effective length of a grating used in first order differs from the effective length of a grating used in third order by a factor of 3.

The DBR lasers discussed in Chapter 2 had an average K = 0.0035 and effective grating length L_g = 140 μm. In first order these gratings would have L_g = 47μm. From Eq. 1-13 it can be seen that for W~15 μm, F_θ is too

45° Beam Expander

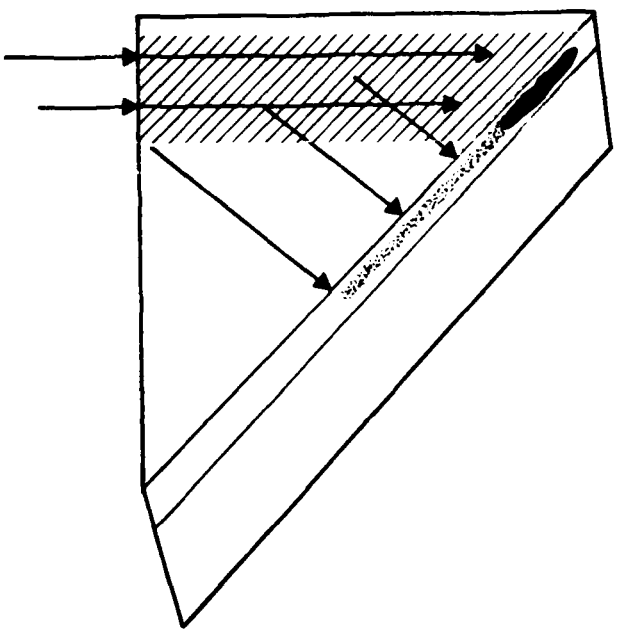

NEAR FIELD IMAGE
BEFORE AND AFTER ALIGNMENT

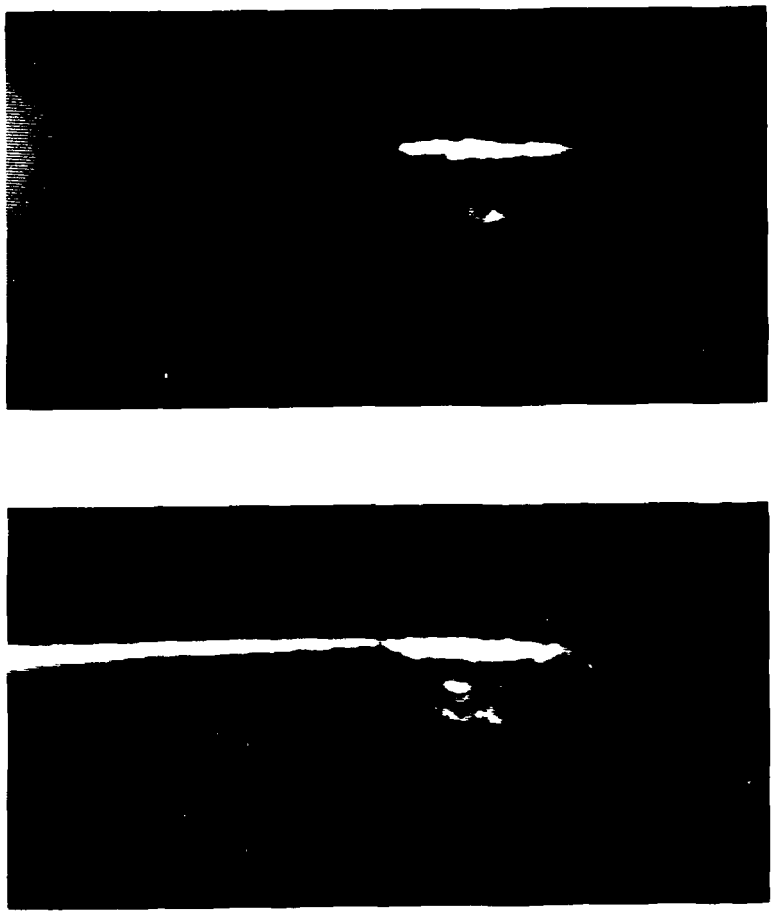

Figure 1.6. Geometry for 45° beam expander along with photographs of an IR television monitor of near field image of guided beam. The top photograph represents the unexpanded beam 50 μm wide before proper angular alignment. The bottom photograph demonstrates beam expansion with the streak to the left.

large to produce a beam which will match into fibers. Appropriate beam expansion will require larger coupling coefficients K and smaller L_g.

Progress was made during the second year in developing heterostructure material with thinner waveguides, so that K could be made smaller. Waveguides of half the thickness were fabricated, but the contract expired before DBR lasers could be fabricated or beam expansion measured.

CHAPTER 2 DBR LASERS FOR FIBER OPTICS AND OPTICAL SIGNAL PROCESSING SOURCES

It was proposed to fabricate DBR lasers as part of this program and to use these as sources together with the grating beam expander. This integrated laser and beam expander has applications both as a source which can be butt-coupled to multimode fiber optics and also for optical signal processing. The geometry of the integrated DBR laser and 45° DBD beam expander is shown in Fig. 2-1. The beam, which is expanded to approximately 100 μm, can be deflected acousto-optically to make a spectrum analyzer, or to make a beam whose output is one-dimensionally steerable, for use in optical signal processing. The application for multimode fibers suggested expansion to 60 μm and including a grating output coupler so that a fiber could be butt-coupled to the device. This geometry is shown in Fig. 2-2.

The program succeeded in fabricating DBR lasers, but did not produce the integration of the beam expander and the DBR laser. This is because it was discovered that it took longer to develop techniques for fabrication of DBR lasers than originally anticipated, and the first year was spent in developing a processing schedule for DBR lasers. This processing schedule is included as an appendix to this chapter. With the development of the processing schedule, it was possible to fabricate DBR lasers during the second year. This chapter will summarize the measurements made on those lasers, and describe how these properties affect expected performance of the integrated sources for fiber optic and optical signal processing.

The geometry of the DBR lasers which were fabricated is shown in Fig. 2-3. The gratings were third order, and the laser region was a large optical cavity. The design studies for this configuration were given in the interim report. This design was not optimum because the waveguide region was thicker than desired, but was the best material available at the time.

Measurements were made of the front-to-rear power ratio of DBR lasers of differing lengths to determine the coupling coefficient of the grating and to check for its reproducibility. Two devices were compared in detail; the data is shown in Table 2-I.

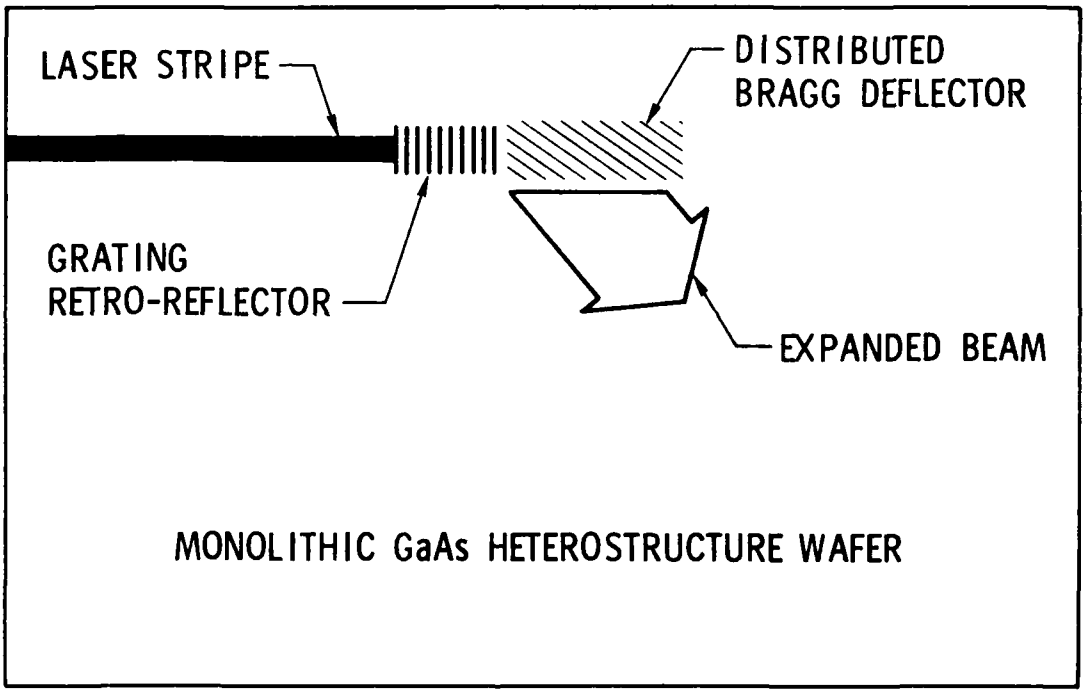

Figure 2-1 Distributed Bragg Deflector, acting to expand the beam from a DBR laser into a wide beam within the plane of the waveguide for use in optical signal processing.

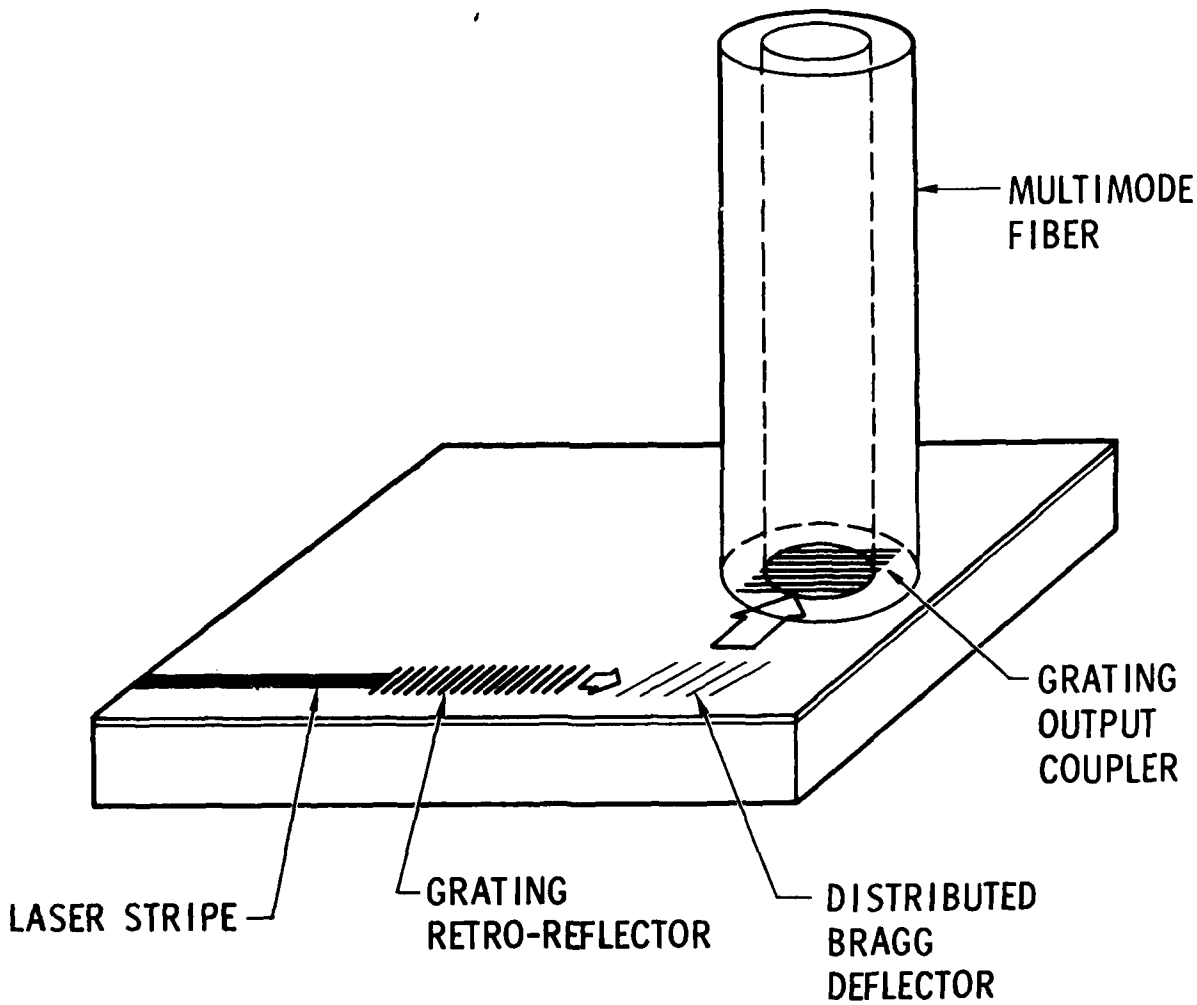

Figure 2-2 Distributed Bragg Deflector plus grating output coupler used to shape the beam from a stripe geometry laser to the mode pattern of a multimode fiber. The fiber attaches to the surface of the GaAs double heterostructure wafer, in a fashion analogous to the Burrus diode.

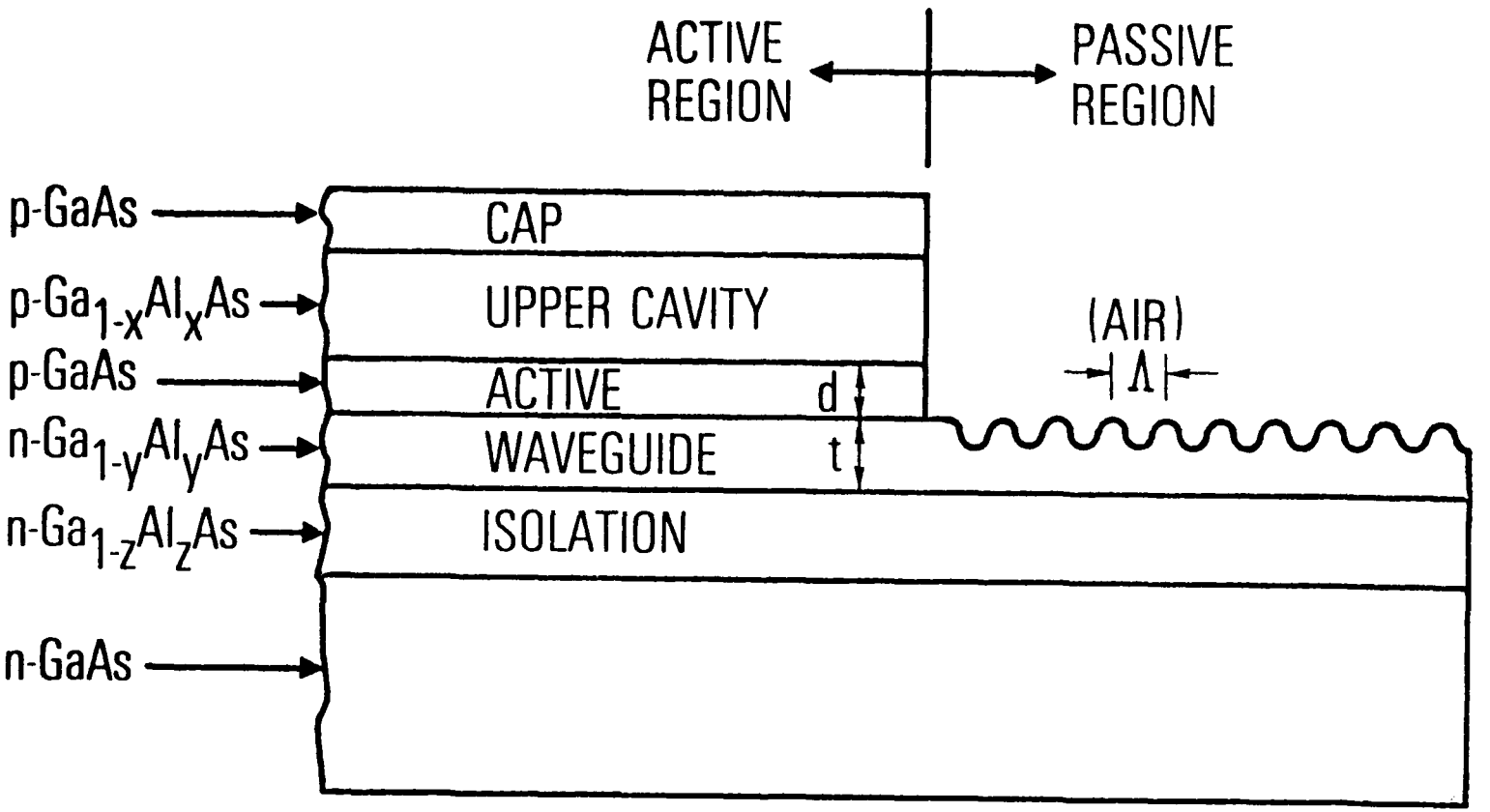

Figure 2-3. Geometry of the DBR laser fabricated and studied under this contract. The important parameters are d = 0.25 μm, t = 1.54 μm, x = 0.26, y = 0.1, z = 0.34, Λ = 0.36 μm

Table 2-I

Data to determine coupling coefficient of gratings in DBR lasers

Sample Number	g9	g5
Power out grating (mW)	1	0.5
Power out cleave (mW)	30	10
Power ratio (grating to cleave), T	0.03	0.05
Ln T/4	-5.3	-4.4
Grating Length	1000 μm	464 μm
K (μm^{-1})	0.0026	0.0047
$L_g = (2K)^{-1}$	192 μm	106 μm

According to the theory, a retro-reflector of length L on resonance, has the following behavior for transmission and refection:

Transmission:

$$T = \frac{1}{\cosh^2 KL} \tag{2-1}$$

Reflection:

$$R = \frac{\sinh^2 KL}{\cosh^2 KL} \tag{2-2}$$

When KL >> 1:

$$T = 4e^{-2KL}, \quad R = 1 - T \, . \tag{2-3}$$

The coupling coefficient was determined from Eq. (2-3) using the fact that the front-to-back power ratio will be the same as the ratio of the transmission of the grating to the transmission of the GaAs cleave on the front output face (85%).

The results give an average coupling coefficient of $K = 0.0036\ \mu m^{-1}$. We now compare these measurements with theoretical expectations.

The theoretical expression for the coupling coefficient of a grating was given for square teeth in Chapter 1. The experimental grating looked more like triangular teeth than square teeth, however. The comparison between square and triangular shapes may be made by comparing the fourier transforms for the third order coefficients for square and triangular shapes. Using the calculations shown in Fig. 2-4, we see that the polarization induced by a triangular grating will be 2/3 that induced by the step index. Thus we expect the grating coupling coefficient to be

$$K = \frac{4\pi^2(n^2-1)}{9m\lambda n}\left[\frac{a}{t_{eff}}\right]^3\left[1 + \frac{3\lambda/a}{2\pi\sqrt{n^2-1}} + \frac{3\,(\lambda/a)^2}{n^2-1}\right] \tag{2-4}$$

(n = index of guide)

where we have taken the result of Yariv, multiplied by 2/3 and used t_{eff} instead of t for guides which are not infinitely well confining.

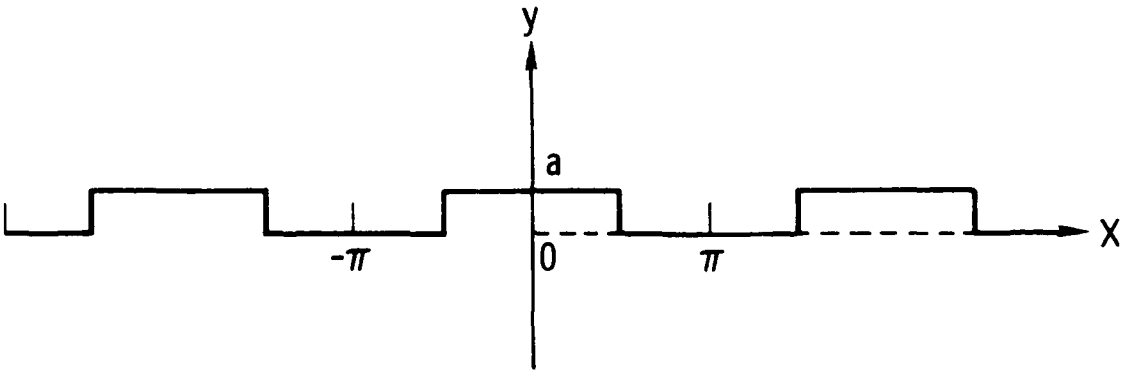

$$F = \int_{-\pi}^{\pi} y\,(x)\,\cos 3x\,dx = a\int_{-\pi/2}^{\pi/2} \cos 3x\,dx = \frac{-2a}{3}$$

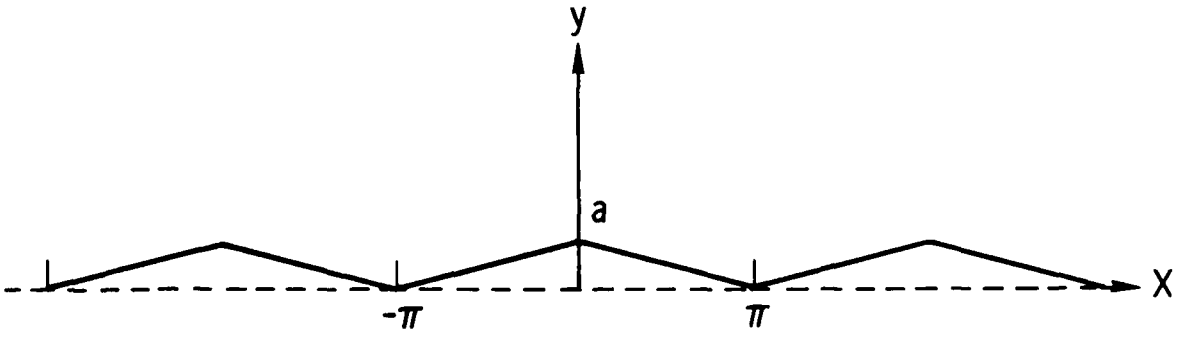

$$F = \int y\,(x)\,\cos 3x\,dx = -2a\int_{0}^{\pi} x\,\cos 3x\,dx = \frac{-4a}{9}$$

Figure 2-4 Calculation of third harmonic for square and triangular shape grating teeth.

From SEM photographs of the grating, we estimate $a = \Lambda/3$, $t = 1.54\ \mu m$, $\Lambda = 0.36\mu m$. The grating was used in third order, and the refractive index of GaAs at $0.88\ \mu m$ is 3.59. These numbers give the theoretically expected coupling coefficient of $K = 0.0044\mu m^{-1}$. In order to calculate this number, it was required to know the effective guide width. This was determined by solving the eigenvalue equation for the waveguide, to determine the exponential profile outside of the guide, and calculate $t_e = t + 1/\gamma$. For the DBR lasers, the V parameter for the waveguide was $\Delta\varepsilon k_o^2 d^2 = 146$, resulting in two modes, given by the following eigenvalue equation :

$$\tan u = \sqrt{\frac{146}{u^2} - 1} \quad .$$

The solutions are $kd = 1.7,\ 3.4$, and give $\gamma d = 12$. This makes the effective thickness $= 1.62\ \mu m$. This is the value used in Eq. (2-4) to determine the theoretical coupling coefficient.

The excellent agreement between theory and experiment allows us to predict behavior for other waveguides. Although the contract ran out before any more lasers were studied, we have fabricated a new set of material with waveguide thickness of $0.6\ \mu m$. These samples should yield devices with coupling coefficients as much as eight times larger.

Other properties relevant to DBR lasers as sources for fiber optics and signal processing were investigated. These include the spectrum, total power, the P-I characteristics, and the beam divergences in both planes, including whether or not the light was diffraction limited. The results are summarized here. A typical spectrum of a DBR laser is shown in Fig. 2-5. First, in order to prove that the laser action occurred from the grating and not from spurious reflections the following tests were applied. First, it was observed that the spectrum was a single mode. Comparable spectra for Fabry-Perot lasers from the same material were multimode, as shown in Fig. 2-6. Secondly, a DBR laser which operated at room temperature was cooled to liquid nitrogen temperature, and laser action ceased, since the reflectivity of the grating was no longer at the frequency of the fluorescence. This is in contrast to Fabry-Perot lasers whose frequency shifts with temperature.

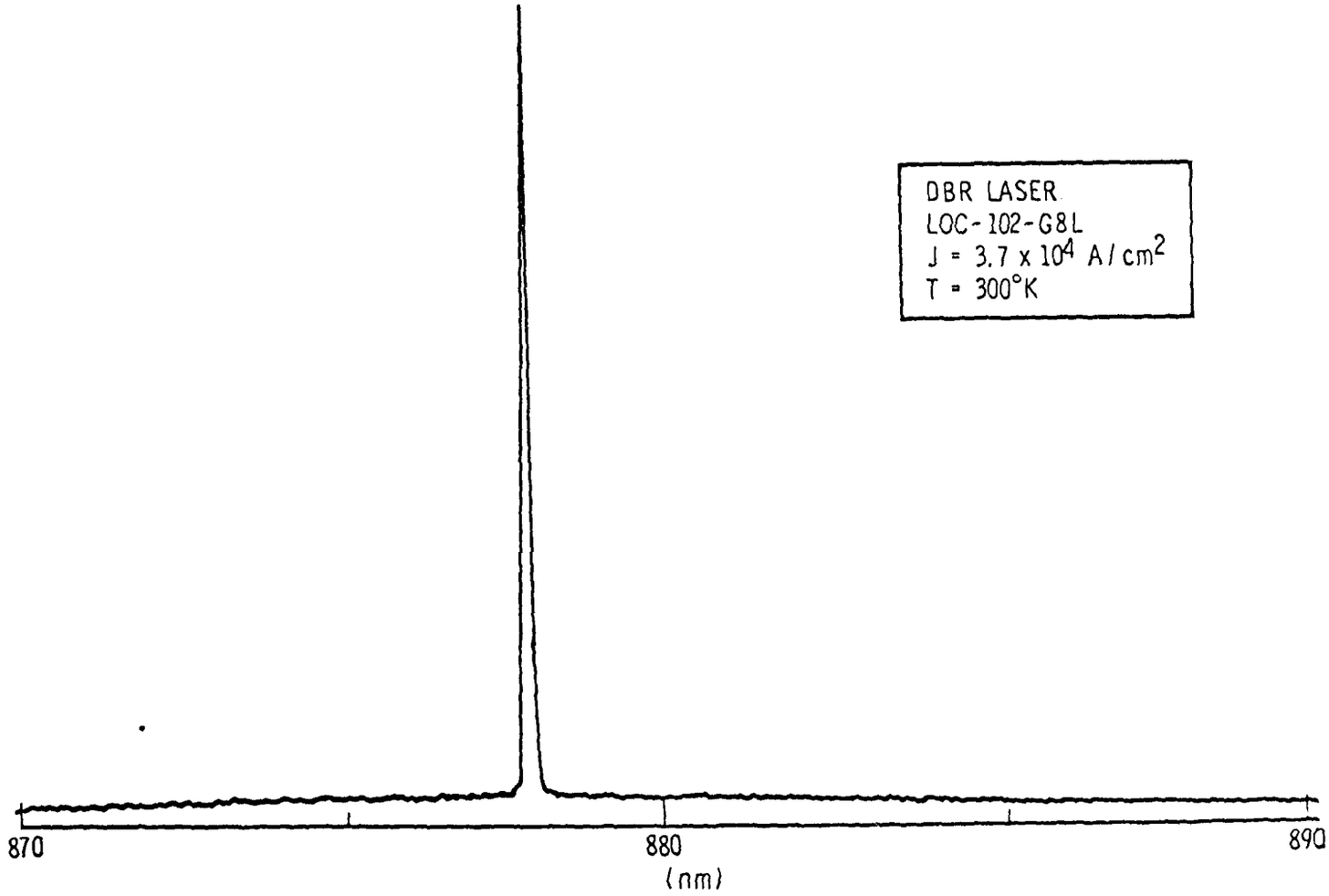

Figure 2-5. Spectrum of typical DBR laser.

Figure 2-6. Spectrum of Fabry-Perot laser, fabricated from the same material as in Figure 2-5.

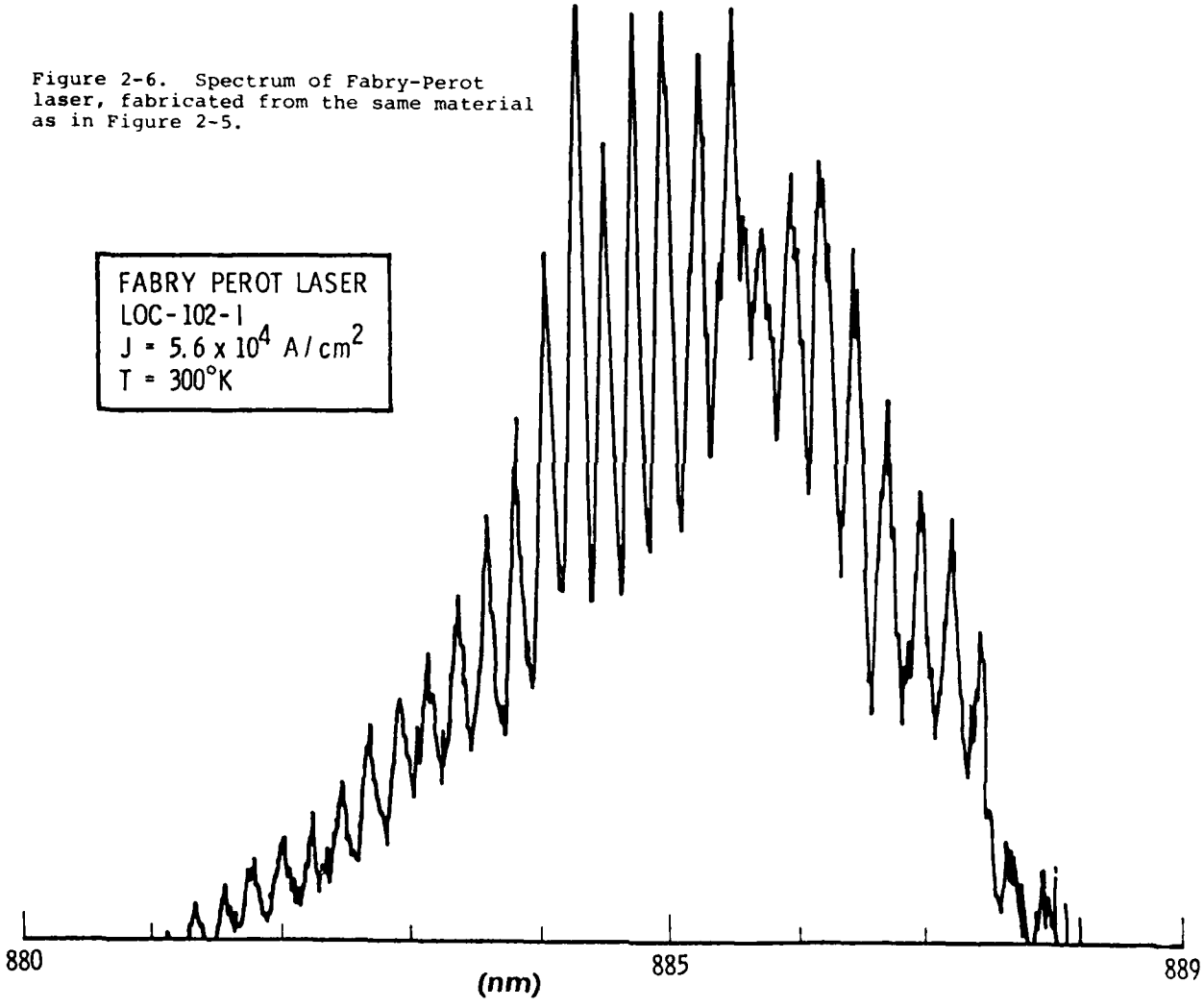

In some of the diodes two lines occurred, as shown in Fig. 2-7. This occurred because the waveguide was sufficiently thick that not only the lowest even mode, but also the lowest odd mode could be confined in the passive region. These modes are shown in Fig. 2-8. These two modes occur in the following way.

The laser wavelength is determined by the condition that the corrugation spacing is in resonance with the longitudinal propagation vector: i.e. $k_z = 3\pi/\Lambda$. However, the different modes have different propagation constants since the transverse propagation constant is different for each mode. The dispersion relation thus becomes

$$k_z^2 = n_g^2 k_o^2 - \left(\frac{(m+1)\pi}{t_{eff}} \right)^2 . \qquad (2\text{-}5)$$

To get a simple expression for the difference in frequencies for DBR laser lines operating on different waveguide modes, assume that the effective waveguide thickness is independent of mode, that the refractive index does not depend on frequency, and that the difference in wavelength between the two laser modes is much less than the wavelength. Then the equation for laser wavelength, given by

$$\left(\frac{3}{\Lambda}\right)^2 = \frac{4n_g^2}{\lambda^2} - \left(\frac{m+1}{t_{eff}}\right)^2 \qquad (2\text{-}6)$$

can be differentiated, yielding,

$$\Delta\gamma = \frac{3\lambda^3}{8t_{eff}^2 n_g^2} . \qquad (2\text{-}7)$$

For an effective wave guide thickness of 1.6 μm, the difference in wavelength between modes should be 75Å. In devices tested, the actual difference between modes was 40Å, indicating that the assumption that the waveguide refractive index was a constant value was only rough approximation. More exact results can be obtained by solving numerically for the eigenmodes of the waveguide and numerically solving the above equation. This has been done graphically in Fig 2-9. It can be seen that the laser is expected to operate at wavelengths in good agreement with the experimental results. Finally, it is observed that the longer wavelength is the lower order mode, and therefore the one with the lowest threshold, in agreement with experiment.

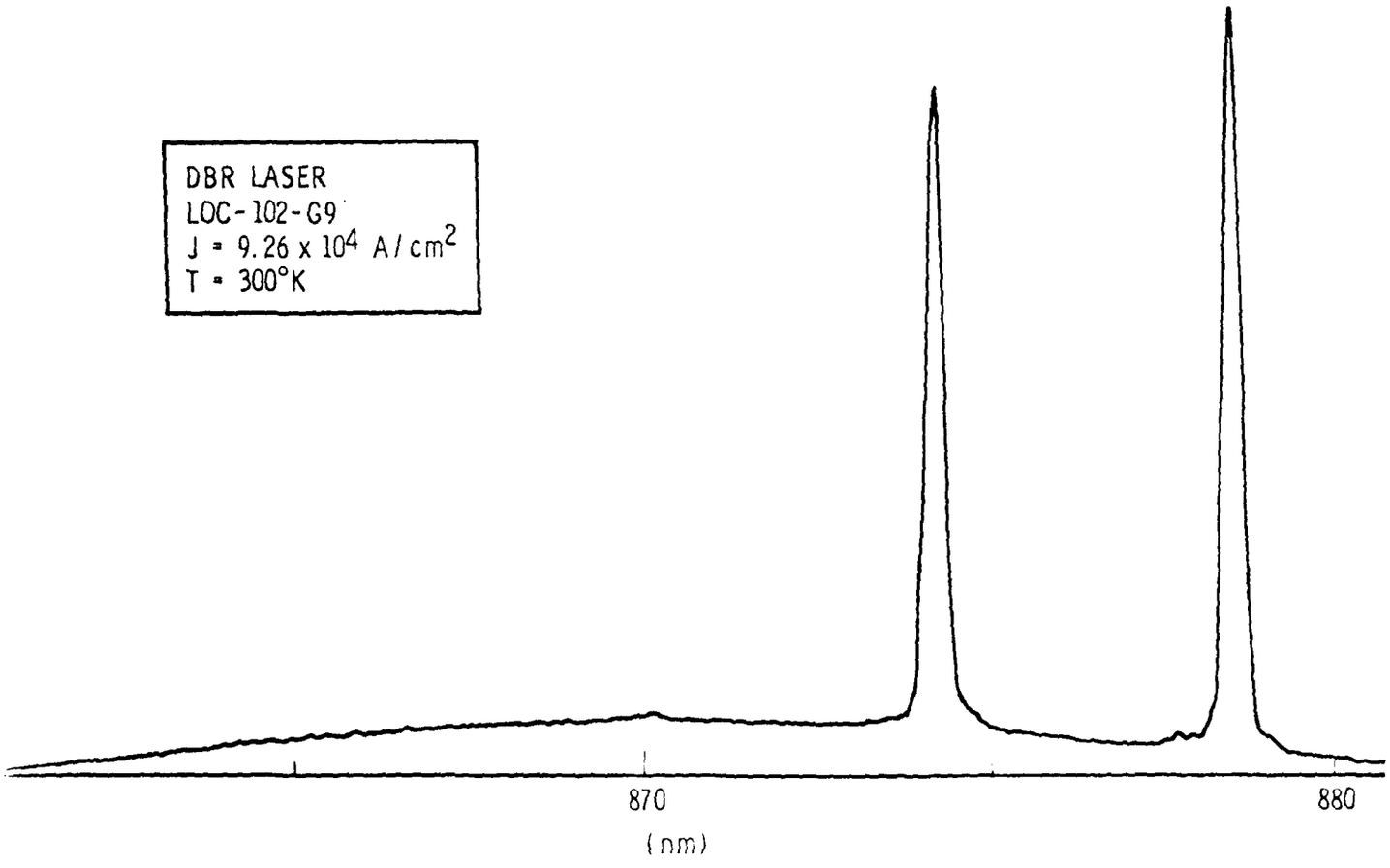

Figure 2-7. Spectrum of DBR laser which supports two waveguide modes and therefore has two oscillation frequencies.

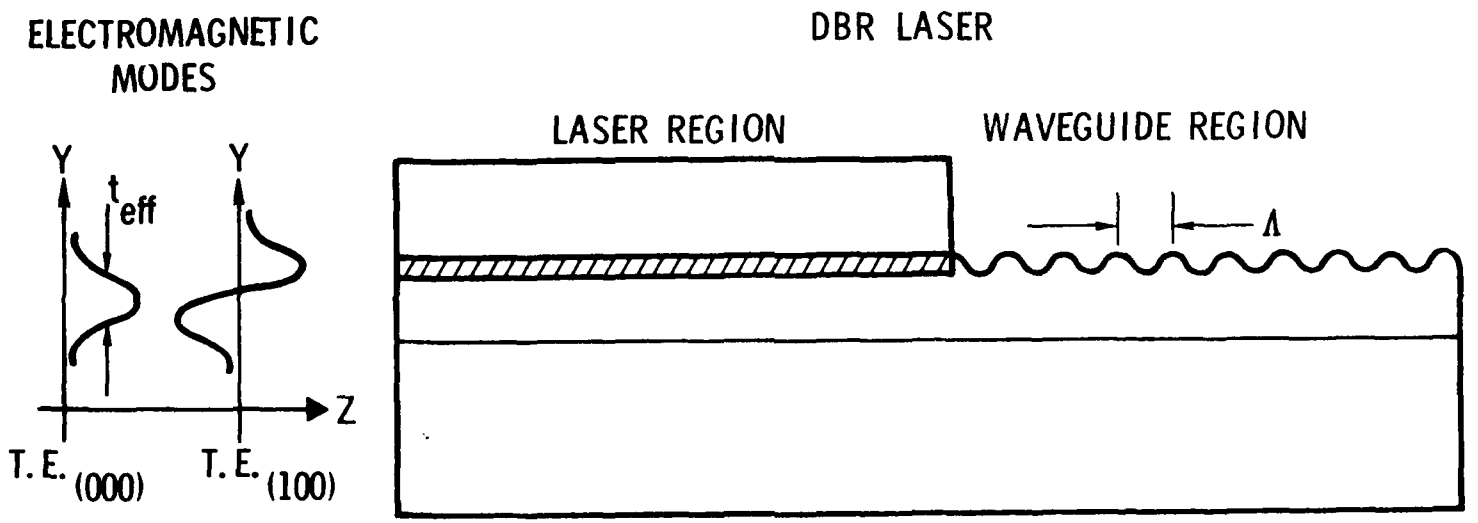

Figure 2-8 The two TE modes which exist in the DBR laser when the waveguide layer is fairly thick. Each of these modes has a different longitudinal propagation constant and therefore oscillates at a different frequency.

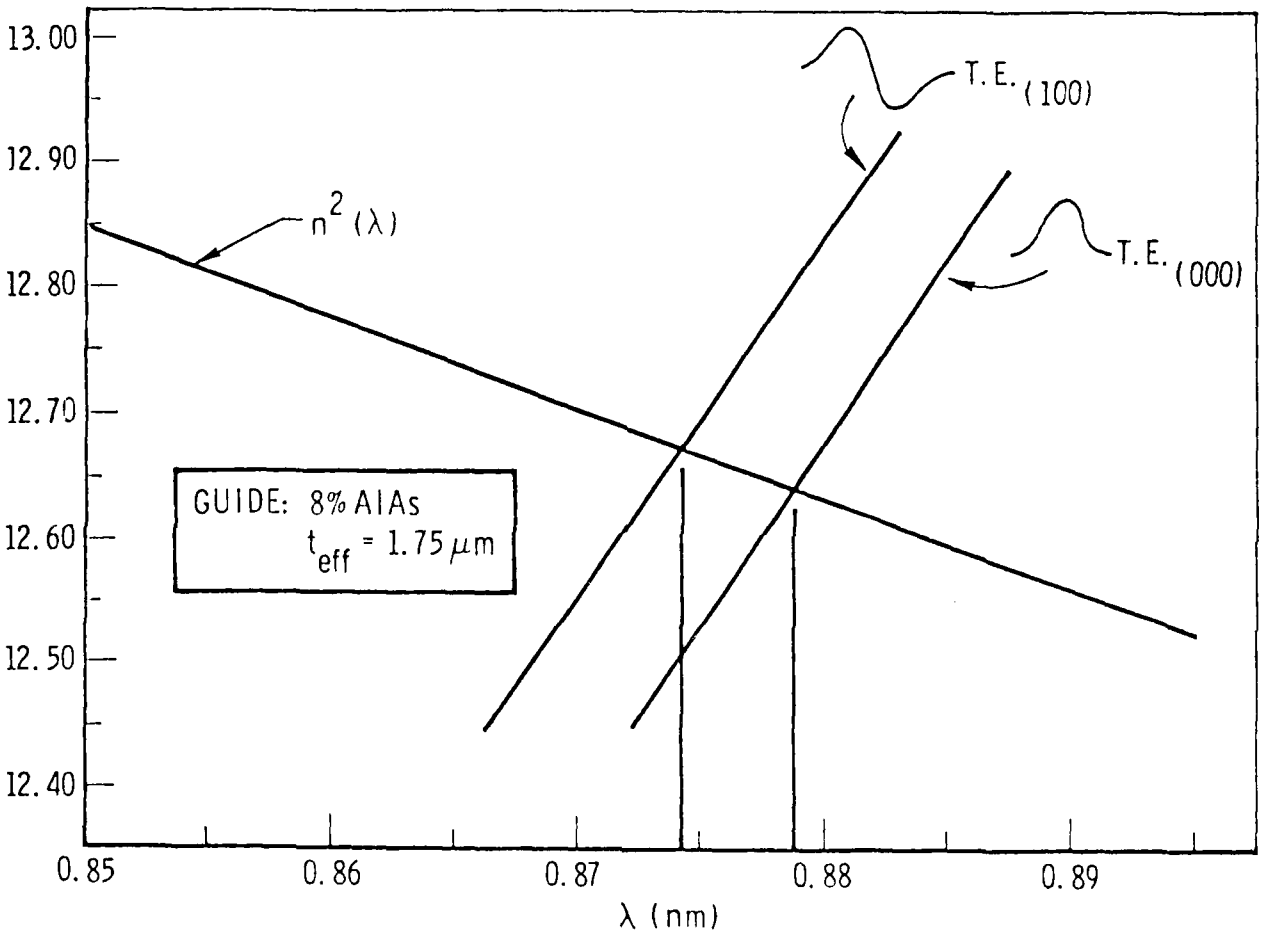

Figure 2-9. Graphical construction to solve for oscillation wavelengths of a DBR laser which can contain two waveguide modes in the structure.

The linewidths just above laser threshold were typically about 1Å. Diode G8, shown in Fig. 2-5, had a width of about 1.1 Å, and diode G9, shown in Fig. 2-10, had a width of 1.6 Å. The apparent linewidth broadened slightly with pumping, as shown in Fig. 2-10, in which diode g5 is pumped three times threshold. The line had broadened to about 3 Å, but is was observed on the oscilloscope that the frequency changed during the 100 nsec of the input pulse. The broadening was a chirp effect due to heating in the junction. Such effects have been seen before in Fabry-Perot diodes, but here are much smaller because of the smaller temperature sensitivity of DBR lasers.

Diode g9 had a complicated behavior, since the two frequencies corresponding to two guided modes occurred at high pumping rates. It was observed that at low excitation levels the shorter wavelength was the strongest peak and the longer wavelength occurred only during the initial portion of the pulse. Evidently heating caused the resonance condition to change and near the end of the pulse the shorter wavelength had a lower threshold and was the only frequency above threshold. This data demonstrates that even when a grating is used, it is possible to get several wavelengths oscillating, not necessarily simultaneously in time within the laser. Clearly DBR diodes must be optimized to have well-behaved results.

The complexity of this device can be seen from the P-I curve (Fig. 2-11), which are filled with kinks. The DBR laser causes only one or two frequencies to oscillate, but does not necessarily improve P-I characteristics over Fabry-Perot lasers.

Since kinks seem to be related to the filamentary structure of lasers, and since we were interest in beam quality, in order to perform beam expansion, we made a careful study of the diffraction qualities of the light emitted from the DBR lasers. Depending on the device, we were able to observe diffraction limited operation, just above threshold. This is demonstrated by studying the divergence of sample g9, right above threshold. Near field patterns were observed both out the cleave and the grating face (Fig. 2-12). In addition, the in-plane beam divergence was measured coming out of the cleave. This was done by monitoring the spot size as a function of distance from the cleave. The data are shown in Fig. 2-13.

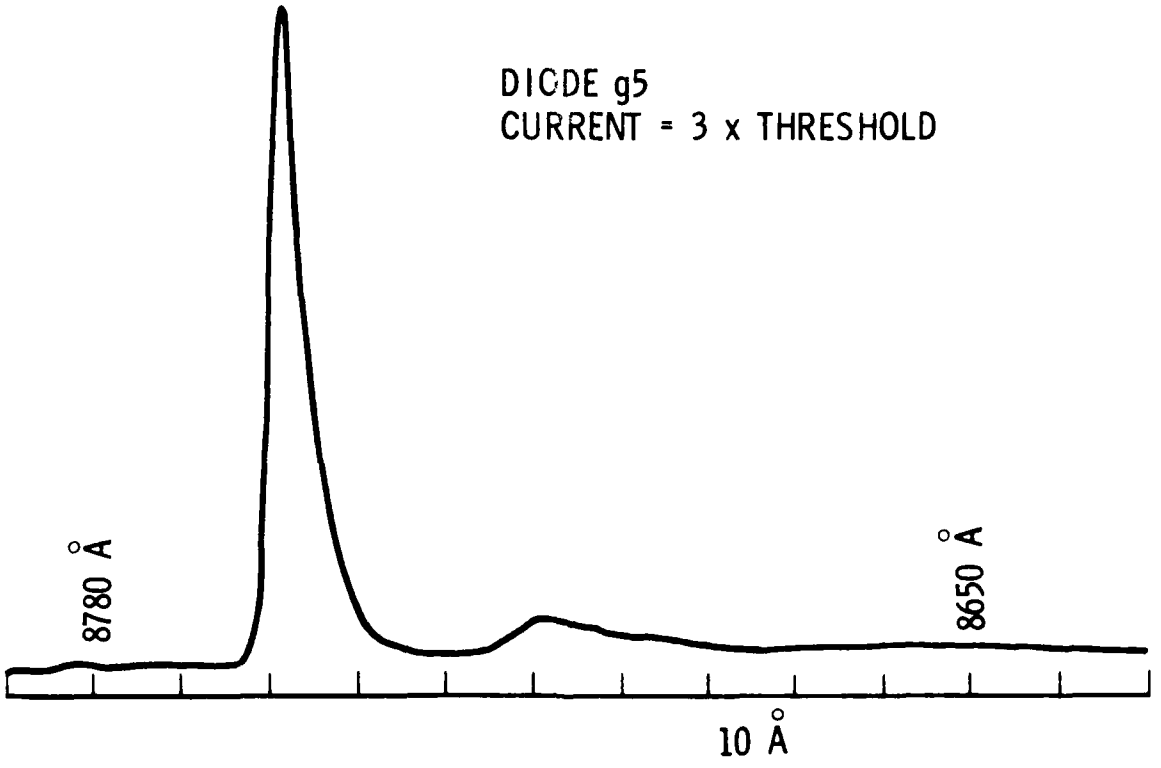

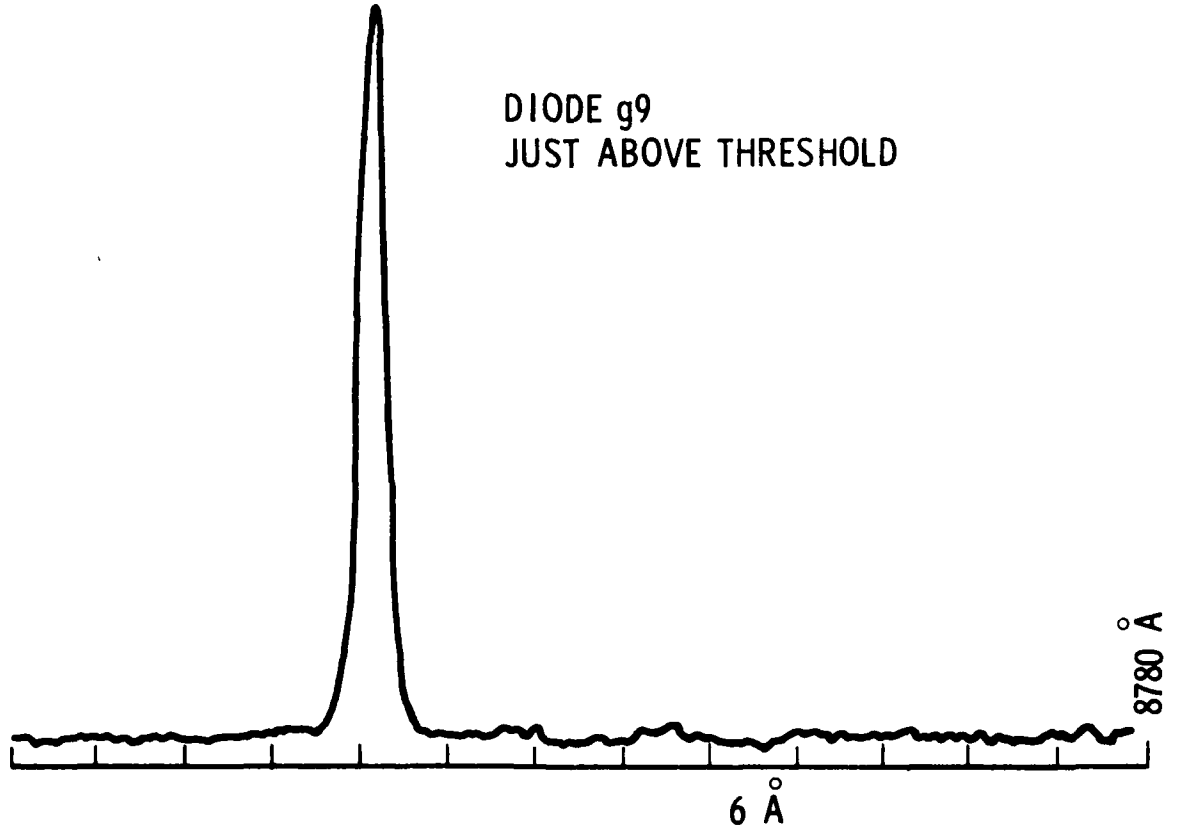

Figure 2-10 Spectra of diodes.

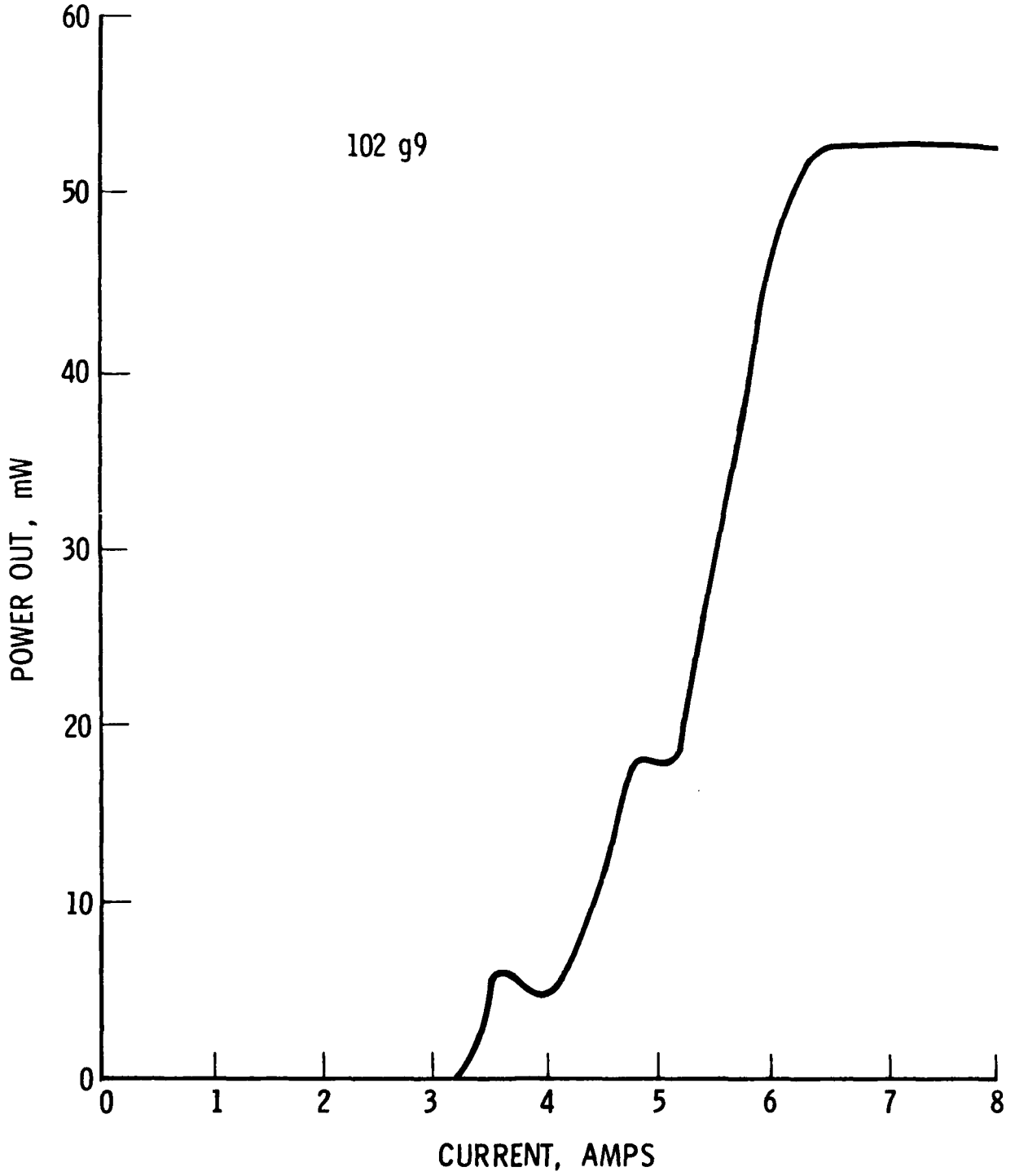

Figure 2-11 Emitted Light Power vs Current to Diode

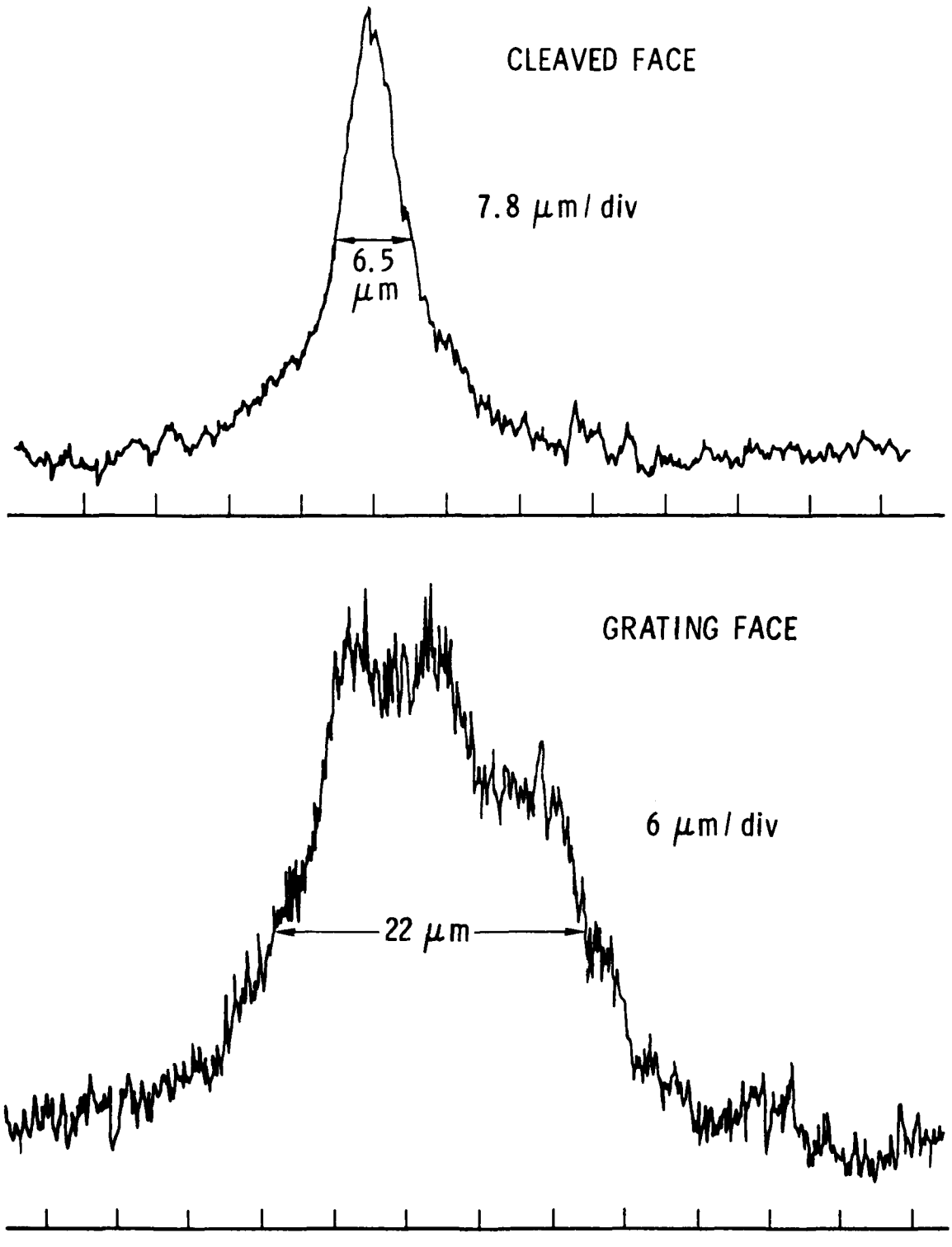

Figure 2-12 Near-field profiles of DBR laser. Diode g9, at threshold.

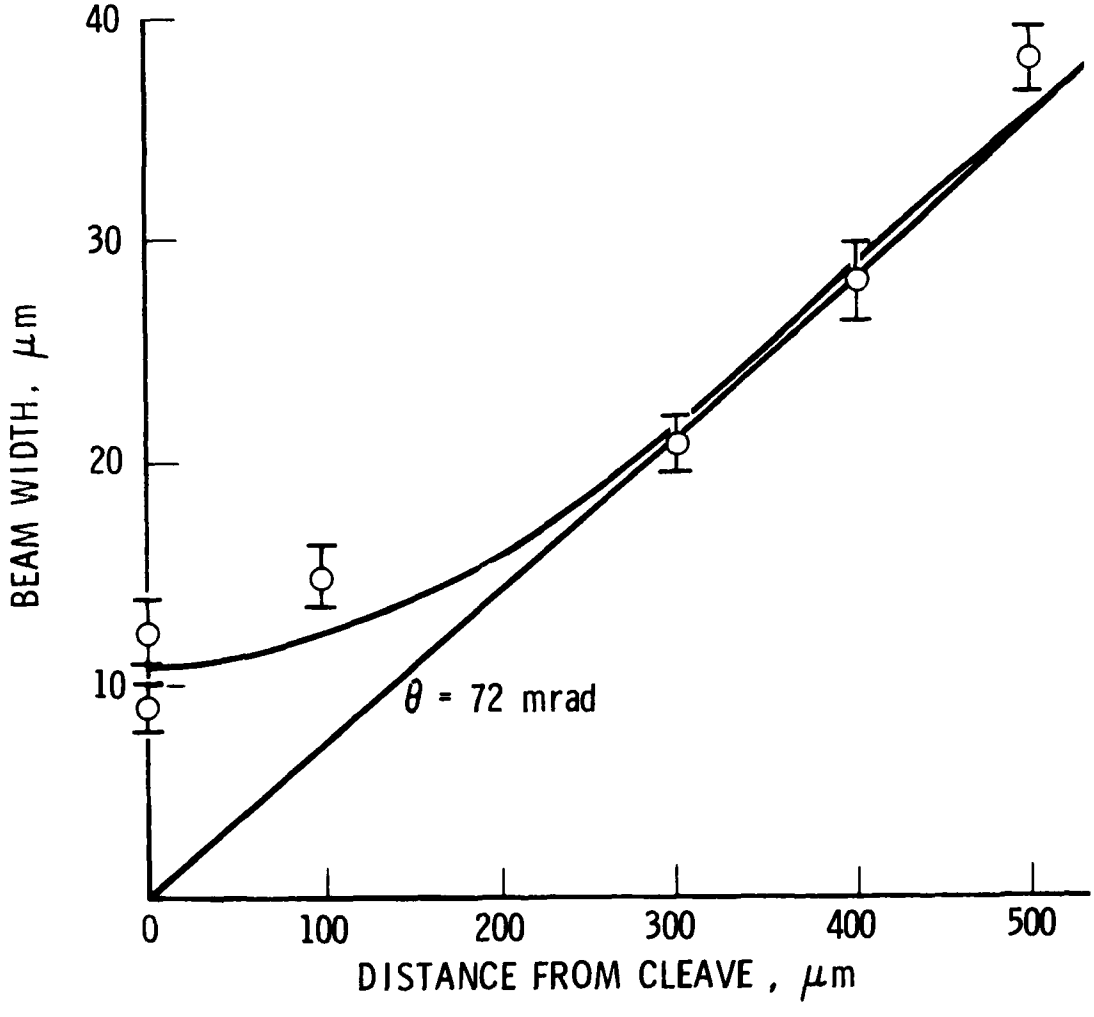

Figure 2-13 In-plane beam width as a function of distance from the exit face (as measured on a television monitor). Far field divergence angle is 72 m rad.

The data are analyzed by comparing the measured divergence with that expected for a Gaussian beam of the width determined from the near field intensity profiles (Fig. 2-12).

The angular divergence of a Gaussian beam is given by

$$\theta_o = \lambda/\pi\ \omega_o \tag{2-8}$$

where θ_o is the half-angle and ω_o is the half width of the beam at $1/e^2$ in intensity.

Redefining the quantities in terms of full width half maximum,

$$\theta = \frac{\lambda}{0.72\pi\omega} . \tag{2-9}$$

The filament measured in the near field had an apparent width of 6.4 μm (correction has not been made for resolution of the microscope objective used in this measurement). The far field beam divergence out the cleave was 0.072 rad, which corresponds to the diffraction expected from a filament of width 5.4 μm. This is in good agreement with the measured filament width, and supports the assumption that this laser operated in a single spatial mode.

The laser output from the grating face was observed to have a near field profile which was a single filament 22 μm wide. This profile is the beam which has diffracted from the 5.4 μm filament in the laser region due to the use of a 1 mm long grating as shown in Fig. 2-14. If the filament is assumed to extend the length of the active region of the laser diode, and begins to expand when it enters the grating, then the diffraction should occur for a distance of 1 mm, at an angle given by the far field divergence angle divided by the index of refraction of the medium (0.02 rad). This divergence would cause the output of the grating to have a width of 20 μm. This compares favorably with the measured filament width of 22 μm.

For completeness, out-of-plane beam divergence was measured also. It was observed that the frequency corresponding to the higher order waveguide mode caused a double-humped far field pattern from the cleave. The divergence was greater than 0.48 rad and could not be measured since it was limited by the

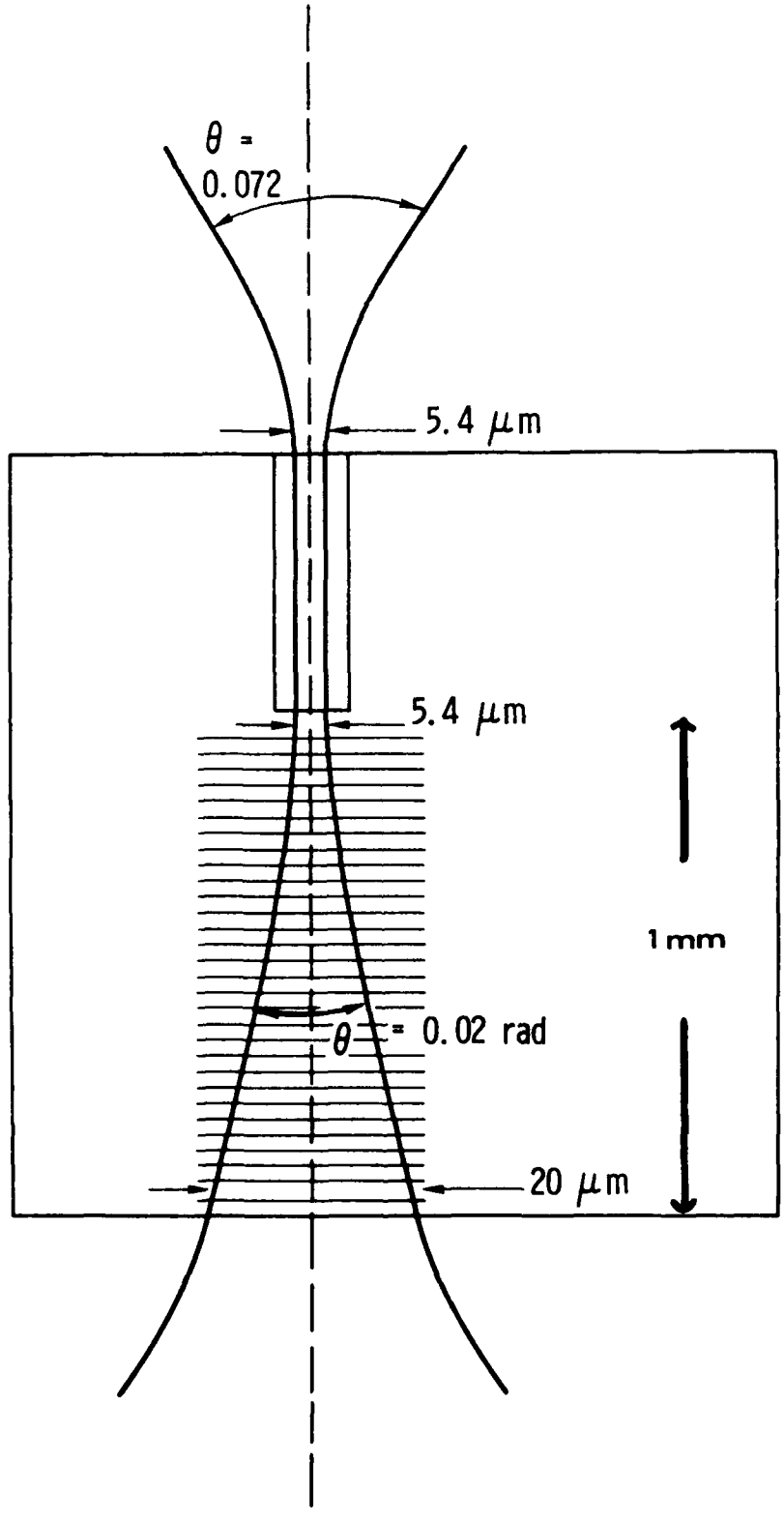

Figure 2-14 Geometry for the in-plane divergence of DBR lasers.

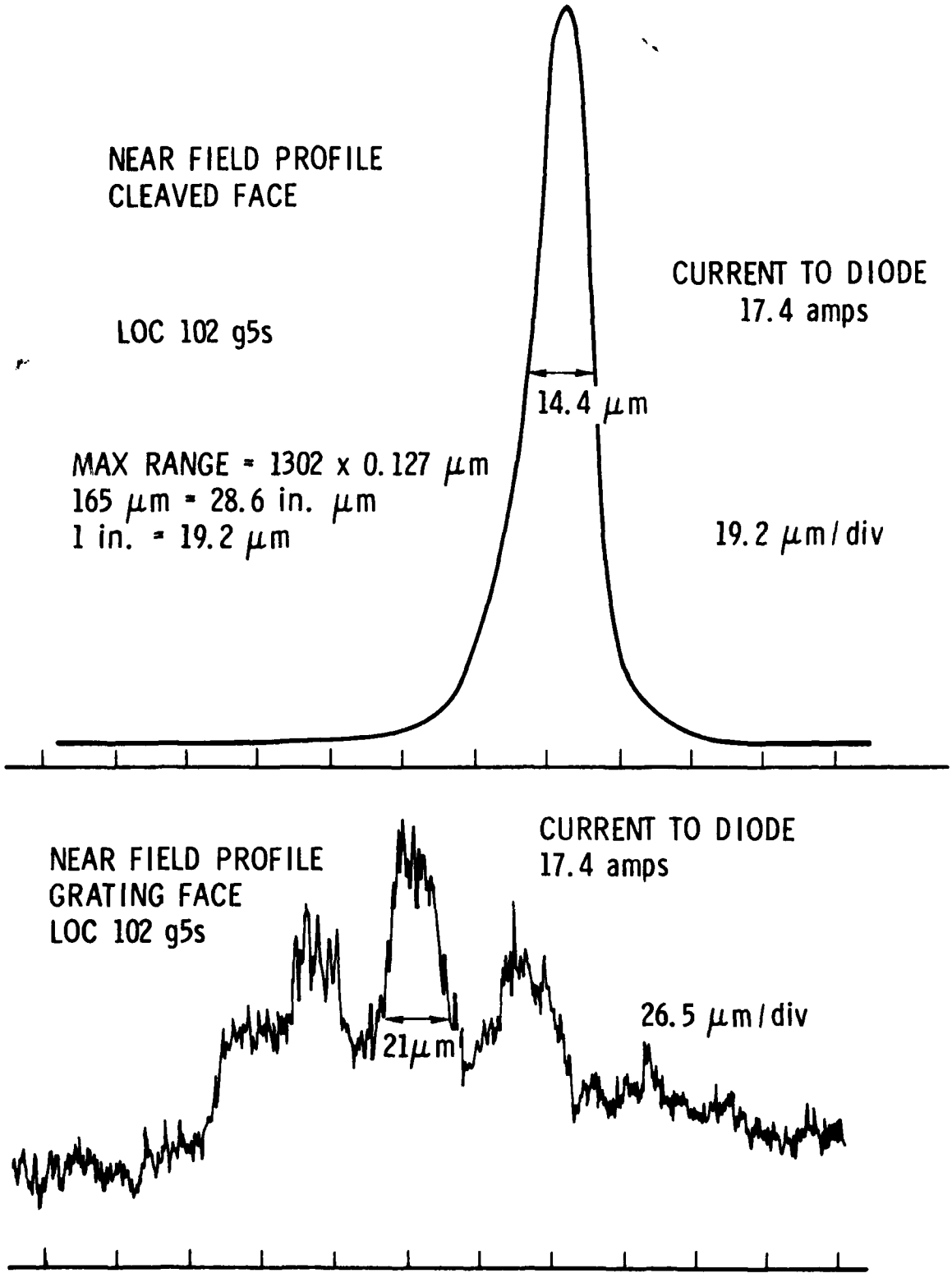

Figure 2-15 Near field profiles of DBR laser. Diode g5.

aperture of the lens which was used. The other frequency was a lowest order waveguide mode and had a beam divergence of 0.3 rad. This proves the assumption discussed earlier that the two frequencies are due to different modes occurring in the laser region.

Other diodes did not necessarily show in-plane diffraction limited behavior. The near field profiles of diode g5 are shown in Fig. 2-15. Although the apparent near field profile was 15 μm wide, the beam divergence was 0.16 rad, corresponding to a filament size of 2.4 μm. In other words, the diode had a highly filamentary character which caused a great deal of beam divergence. This fact was made clear by looking at the profile out of the grating. The output had several filaments and an overall width of almost 100 μm. Diodes such as this would not be very useful for signal processing applications because of large beam divergence.

The result of this study is the fact that although DBR lasers control the longitudinal modes, they do not improve the spatial modes or ensure diffraction limited operation. It is necessary to control the spatial modes in order to obtain *diffraction limited guided beams* which can be expanded and used for coupling to fiber optics and for signal processing. The spatial control must be obtained by the same techniques used in producing single mode Fabry-Perot lasers: narrow stripes, tapered junctions, and other modes control devices. Experiments to add these devices to the DBR lasers were beyond the scope of this project.

APPENDIX

Process Schedule - DBR Laser Fabrication

I. Cap layer Examination

1. Cleave sample from main specimen
2. Etch sample for 5 sec. in 1:1:8 (A:B:DI H_2O) A-B etch.
3. Photograph all four corners of sample to determine cap thickness variations.

II. Cap Layer Removal

4. Pre-photoresist application sample cleaning: Swab with methanol; flow trichloroethylene over surface; blow dry with dry nitrogen.
5. Spin coat sample with (unthinned) AZ1350J photoresist @ 5000 RPM for 30 sec. Allows removal of up to 54 microns of gallium arsenide.
6. Pre-exposure age coated sample at room temperature for 30 min.
7. Expose coated sample for 45 sec. using mask consisting of 0.5 mm wide bars separated by 1.0 mm clear spaces.
8. Develop photoresist for 1 min. using 1:1 developer (Shipley MF312:DI H_2O).
9. Post exposure bake at 100°C for 1 hr.
10. Ion mill to remove cap layer: 0.931 mA beam current; 1 KV accelerating potential; 4.6×10^{-4} atmos. argon.

III. P-isolation Layer Removal

11. Observe photoluminescence of valleys in order to be assured of proper cap layer removal. Check mesas for inadvertent photoresist removal.
12. Chemically etch p-isolation layer and active layer aluminum concentrations.
13. Observe photoluminescence of valleys in order to be assured of proper p-isolation layer removal. Check mesas for photoresist integrity.

IV. Active Layer Removal

14. Ion mill to remove active layer: 0.931 mA beam current; 1 kV accelerating potential; 4.6×10^{-4} atmos. argon.
15. Observe photoluminescence of valleys in order to be assured of proper active layer removal.
16. Remove photoresist with plasmaline etcher (using O_2 for 10 min).

V. Stripe Geometry Mask Application

17. Clean sample in boiling xylene: isopropyl alcohol (1:1) for 2-3 minutes. Blow dry with dry nitrogen.
18. Deposit 3000 Å thick SiO_2 layer over entire sample surface.
19. Pre-photoresist application sample cleaning: Swab with methanol; flow trichloroethylene over surface; blow dry with dry nitrogen.
20. Spray deposit 5000 Å layer of thinned AZ1350B (Az1350B; thinner - 1:1). Spray for 0.77 sec. @ 5 inches from sample.
21. Pre-exposure age coated sample at room temperature for 30 min.
22. Expose coated sample for 45 sec. using dark room exposure machine. Mask consists of a four-row matrix of 25 μm by 400 μm windows.
23. Develop photoresist for 1 min. using 1:1 developer (Shipley MF312:DI H_2O).
24. Post develop bake at 100°C for 1 hr.
25. Etch SiO_2 strip windows with plasmaline etcher (using CF_4 for 20 min.).
26. Remove photoresist with plasmaline etcher (using O_2 for 20 min.).

VI. Laser Metallization and Fabrication

27. Clean sample in boiling xylene: acetone (1:1) for 3 min. Rinse in three changes of hot xylene. Blow dry with dry nitrogen.
28. Mount sample on plating fixture with "Dotite" paint. Coat all areas except those to be plated, or those areas already protected by photoresist, with apiezon solution (apiezon wax in xylene). Let dry.
29. Immerse sample in $HCl:H_2O$ (1:1) for 3 min. Do not rinse. Transfer directly to plating solution.

30. Platinum plate back contact: 20v open circuit voltage, 100 mA. Current for 3 min. (for ~0.25 cm^2 sample).
31. Repeat step 28 for front contact.
32. Repeat step 29.
33. Platinum plate front contact: 20v open circuit voltage, 50 mA current for 2 min. (insufficient trials have been made to determine optimum current-time parameters for pattern area plating, but these values have been used. For Fabry-Perot samples of approximately 0.25 cm^2 area time should be increased to 3 min.).
34. De-mount sample. Clean with hot xylene and blow dry with dry nitrogen.
35. Dice samples
36. Mount on headers and bond.

VII. Test Active/Passive Fabry-Perot

37. Measure area of p-side contact and begin pulse testing at 1000 Amps/cm^2. (Total current passing through diode, I, is related to monitor voltage, V, by I = V/0.27.).

VIII. DBR Grating Application

38. Pre-Photoresist application sample cleaning: Swab with methanol; flow trichloroethylene over surface; blow dry with dry nitrogen.
39. Spray deposit ~0.15 μm thick layer of thinned AZ1350B photoresist (AZ1350B: thinner 1:1). Spray for 0.125 sec. @ 5" from sample.
40. Pre-exposure bake @ 65°C for 25 min.
41. Expose with interfering 0.4579 μm Argon laser beams for 35 sec @ combined beam intensity of 10mW/CM^2 (0.370 VDC on volt meter as detected by solar cell). Sample is aligned using He-Ne laser prior to exposure. Null standing wave pattern observed at beam splitting prism. Both laser beams must be of equal intensity.
42. Develop photoresist in diluted, Shipley MF312 developer (MF312:DI H_2O - 1:1).
43. Measure grating periodicity using ellipsometer, littrow angles of left and right, first-order diffracted beams are measured to within 20 sec. of arc and averaged. Grating orientation with

respect to crystal cleave is simultaneously measured using rotatable stage mounted on ellipsometer. The latter measurement is accurate to within one minute of arc.

44. If either the grating period or grating orientation is wrong, beam angle-of incidence must be adjusted and steps 38 through 43 repeated.

IX. Test DBR Laser

45. Same as step 37.

CHAPTER 3. STUDIES OF $LiNbO_3$ WAVEGUIDE LOSS

The research at USC during the first year centered on the development of the multimode bistable optical switch. This work was described fully in the interim report, and in several publications listed in the introduction. Continuations of this research were funded by AFOSR allowing research on this contract during year two, to focus on the sources of loss in $LiNbO_3$ waveguides, and on efforts to fabricate $LiNbO_3$ multimode polarization-independent waveguides. This work was motivated by the fact that good quality waveguides and also multimode polarization-independent modulators do not exist, and because there are no low-loss multimode and polarization-insensitive waveguides in $LiNbO_3$. The first part of this study involved investigations of losses in $LiNbO_3$ waveguides. The second part of the study involved searching for techniques to fabricate $LiNbO_3$ multimode waveguides which guide both TE and TM modes and be mode-matched to multimode fibers. This is described in Chapter 4.

a. Sources of Loss in Waveguides

In waveguides fabricated by a diffusion process such as $LiNbO_3$, mechanisms for loss are absorption, scattering within the waveguide and scattering from the surface of the waveguide. Absorption losses may come from either the bulk substrate material or from the diffusant. If the substrate is transparent and the diffusant is properly chosen, absorption loss

should be negligible. We used calorimetry to measure the absorption losses in $LiNbO_3$ waveguides, experiments which will be discussed in Section c below. We found, indeed, that with proper preparation, this loss mechanism was much lower than scattering loss in $LiNbO_3$ for both in-diffused and out-diffused waveguides.

There are several sources of scattering loss. The first is from the surface of the waveguide. Any imperfections in the flatness of the waveguides causes scattering from guided modes into radiation modes. Because of this it is reasonable to assume that the loss would be lower for waveguides which are buried below the surface of the waveguide. In order to test the validity of this idea, we calculated the power loss due to surface imperfections for waveguides which were diffused at the surface and compared them to those which were buried below the surface. We compared these results with the losses from step-index guides. We found, as expected, that the losses were lowest for guides which were buried below the surface. This theoretical study is described in Section b.

Scattering may also occur from nonuniformities in the refractive index caused by the diffusant or present in the substrate material. These nonuniformities in refractive index may be due to aggregates of the diffusant, occlusions, crystallites, or variations in stoichiometry or composition. These refractive index fluctuations will be small, as long

as the bulk substrate material is of optical quality and as long as the diffusant enters the material in a sufficiently dispersed fashion. In order to investigate the amount of scattering from the nonuniformities in the refractive index and compare that to the amount of scattering from the surface of the waveguide, we made comparative studies of losses and identified the mechanism of loss in $LiNbO_3$ waveguides. These experiments are described in section d.

As part of our experimental studies of waveguide losses, we tried several experiments to reduce the insertion loss for $LiNbO_3$ multimode waveguides. We found that the quality of the polish on the end faces was an important factor in reducing waveguide losses. Other techniques we tried to reduce the losses were not so satisfactory. The details of these experiments are described in Section e.

b. A Comparison of Losses in Imperfect Surface-Diffused and Buried Optical Waveguides

The recent advances in integrated optics technology have put a great deal of emphasis on $LiNbO_3$ and $LiTaO_3$ devices whose waveguides are fabricated by diffusion.[1] In most cases, these waveguides are formed near the surface and have graded refractive index profiles usually represented by exponential functions. Early experimental work on diffused glass waveguides indicated that buried guides had considerably lower loss than surface guides[2,3]. In this section we present the results of a theoretical analysis which show that in principle, the loss in a buried guiding layer formed by diffusion is at least one order of magnitude lower than that of a diffused waveguide in which the guiding layer adjoins the surface. These results suggest, therefore, that for low loss applications, $LiNbO_3$ and $LiTaO_3$ waveguides should be buried[4] to minimize scatter losses.

We assume single mode waveguides and consider the loss due to radiation from waveguide surface imperfections. It is the intent of this paper to consider a number of comparable waveguide geometries to determine which, in principle, has the lowest loss. For this purpose it is sufficient to use sinusoidal wall perturbation.

We shall compare graded index guides, formed by diffusion, with step index guides, such as formed by thin film deposition or crystal growth. In both cases we compare both surface (asymmetric) and buried (symmetric) guides. It will be shown that the buried guides have considerably lower

loss. In addition, it will be shown that graded index waveguides are inherently less sensitive to short wavelength surface roughness than are abrupt uniform guides.

The approximate formula for the power loss is obtained by assuming that the fields of the perfect guide are only slightly perturbed by wall imperfections, which can be shown to yield a coupled system of differential equations for the coefficients of the perturbed fields[5-7]. Discrete solutions are then obtained with the help of orthogonality relations, together with initial and final conditions. The general solution for scattering loss in a single mode guide is given by:

$$\frac{\Delta P}{P} = \left| \frac{k_o}{4\omega \mu_o P} \{ \int_o^\infty d\rho \int_o^L dz \int_{-\infty}^{\infty} E^*(\rho)\ \eta(x,z)\ E\ dx \} \right|^2 \qquad (1)$$

where $E(\rho)$ is the radiation field, E is the guided mode field, and $\eta(x,z)$ is the refractive index discontinuity function defined as:

$$\eta(x,z) = n^2(x,z)\Big|_{\text{perfect}} - n^2(x,z)\Big|_{\text{imperfect}} \qquad (2)$$

It can be shown that the resulting calculation performs the fourier transform of wall imperfections. Thus the physical processes and comparisons of different geometries of waveguide profile can be determined by looking at sinusoidal perturbations

First we discuss symmetric buried layers whose index profile is represented by the following distribution:

$$n(x) = n_s + \Delta n \cosh^{-2}((x - x_o)/d) \quad (3)$$

where n_s is the substrate index and Δn is the peak index discontinuity. Solutions of the guided TE modes for this profile have been obtained previously in the form of a hypergeometric series[8]. When waveguide fabrication is done by diffusion, surface irregularities can be thought of as causing an uneven diffusion depth. This will yield an index profile which, under sinusoidal imperfections, takes the following form:

$$n(x,z) = n_s + \Delta n \cosh^{-2} [(x - x_o - a \sin\Theta z)/d] \quad (4)$$

where Θ is the wave-vector of the perturbation and is given by $\Theta = 2\pi/\Lambda$ where Λ is the assumed periodicity of the perturbation. It is assumed that the ripple amplitude a is much smaller than the effective thickness of the guiding layer. Actual radiation modes of this profile are complex oscillatory hypergeometric series. However, when $\Delta n << n_s$, the exact solutions approach pure oscillatory solutions. Approximating with sinusoidal fields greatly simplifies calculations without introducing substantial error. This assumption has been shown valid for step-index fibers and for waveguides with small index discontinuities[9,10]. We have solved (1) under single

mode operation just below the cutoff of the next order mode and obtained the following normalized power loss in the range $0 < |\beta| < k_o n_s$:

$$\frac{\Delta P}{P}\left(\frac{\lambda^3}{a^2 L}\right) = \frac{2\pi^5}{9} n_s (\Delta n)^2 \frac{\rho d (1 + (\rho d)^2)^2}{\cosh^2(\rho d \pi/2)} \tag{5}$$

where λ is the free space wavelength, L is the length of the guide. The quantity $\rho^2 = (k_o n_s)^2 - (\beta_o - \Theta)^2$ where β_o is the propagation constant of the guided mode and k_o is the propagation constant in free-space.

Next, we consider diffused surface waveguides with an index profile given by:

$$n(x) = \begin{cases} n_s + \Delta n\, e^{-(x/d)} & x \geq 0 \\ n_2 = n_{air} & x < 0 \end{cases} \tag{6}$$

In this case, imperfections are represented by sinusoidal perturbations of the air-substrate surface such that n(x,z) of the imperfect guide is:

$$n(x,z) = n_s + \Delta n\, e^{-(x + a \sin \Theta z)/d)} \tag{7}$$

The evaluation of the losses as defined in (1) was carried out by using the exact radiation fields rather than the oscillatory approximation. However, it was assumed that the radiation

fields become sinusoidal as $x \to \infty$. Furthermore, because of the large air-dielectric discontinuity, we consider scattering only into the substrate as the predominant type of radiation loss. The normal radiation loss in the range $k_o n_2 < |\beta| < k_o n_s$ becomes:

$$\frac{\Delta P}{P}\left(\frac{\lambda^3}{a^2 L}\right) = \frac{2\nu\pi^3 (n_s^2 - n_2^2)^2 J_\nu^2(V) \left| J_{i\mu}(V) \right|^2}{\mu n_s}$$

$$\lim_{T \to o} \left\{ \left| J_{i\mu}(T) \right|^2 + \frac{T^2}{2\mu^2} \left| J_{i\mu+1}(T) \right|^2 - \frac{T}{\mu} \operatorname{Re}\left(i J_{i\mu}(T) J^*_{i\mu+1}(T) \right) \right\}^{-1}$$

where $V = 2d\, k_o \sqrt{2 n_s \Delta n}$

$$\nu = V\sqrt{b}$$

$$b = \frac{n_{eff}^2 - n_s^2}{2 n_s \Delta n}$$

$$\mu = 2d\left((k_o n_s)^2 - (\beta_o - \Theta)^2 \right)^{1/2}$$

Equations (5) and (8) were plotted in Fig. 1 illustrating the radiation losses in buried and diffused surface waveguides. In order to numerically evaluate comparable waveguides, the same propagation vector was chosen for both cases, consistent with single mode operation just below the cutoff of the next order mode. The parameters were $n_s = 1.5$, $\Delta n = 0.0035$ and $k_o d = 13.8$ for the buried waveguide, and $n_s = 1.5$, $\Delta n = 0.01$

and $k_o d = 15.9$ for the diffused surface waveguide.

It can be seen that over the entire range of periodicities for the surface roughness, the buried guide is at least one order of magnitude less lossy than the diffused guide. Furthermore, the losses of the buried guide are negligibly small for short range roughness. This indicates that burying the guiding layer results in a significant reduction in scattering losses and is therefore advantageous when scattering loss is of major concern. This is in agreement with the experimental results in glass[2,3] .

For completeness, we compare these losses to those of abrupt uniform waveguides, symmetric and asymmetric, again requiring the same propagation vector in each waveguide. These losses were calculated from equations of Marcuse[5-7] . In order to make correct analogy with diffused and buried guides, we assumed both boundaries of the abrupt guide were perturbed in parallel with the same periodicity. This corresponds to $\alpha = 0$ in Marcuse's notation,[5] and has been termed microbending[5]. These results are shown as the solid lines in Fig. 2. In order to make numerical comparison with the results in Fig. 1, the same substrate refractive index propagation constant were assumed. By comparison with Fig. 1, it can be seen that the peak loss of the symmetric abrupt guide is similar to that of the buried guide, and the peak loss of the asymmetric abrupt guide is also similar to that of the surface

Fig. 3b-1 Normalized radiation power loss of equivalent surface diffused and buried waveguides with sinusoidal surface irregularity. Included on the figure are sketches of the refractive index profiles.

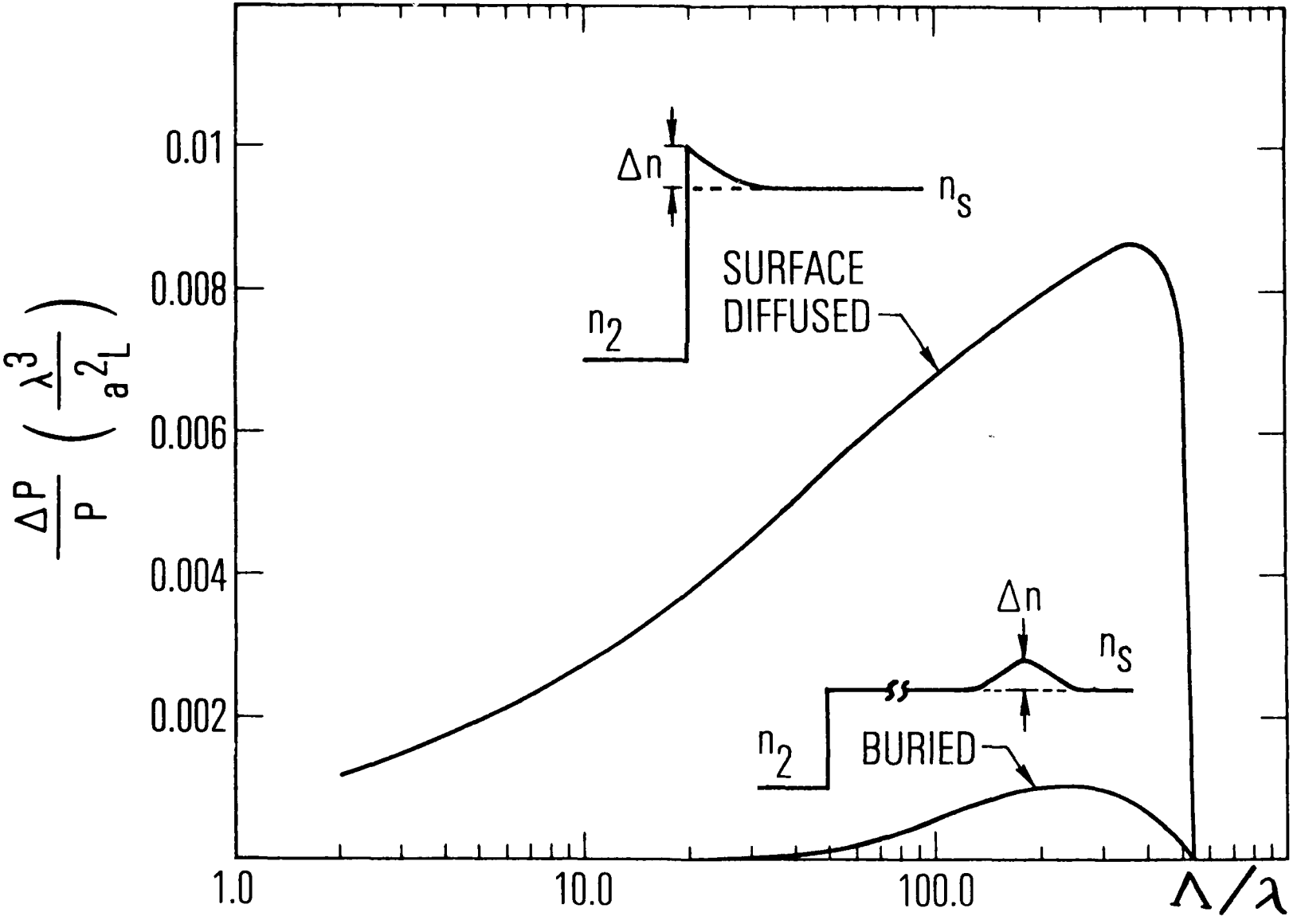

Fig. 3b-2 Normalized radiation power loss of symmetric and asymmetric step index waveguides with sinusoidal surface irregularity. Solid lines are for waveguides whose walls are perturbed in parallel. The dotted line is for symmetric waveguide whose walls are perturnbed symmetrically about the center of the waveguide. Included on the figure are sketches of the refractive index profiles.

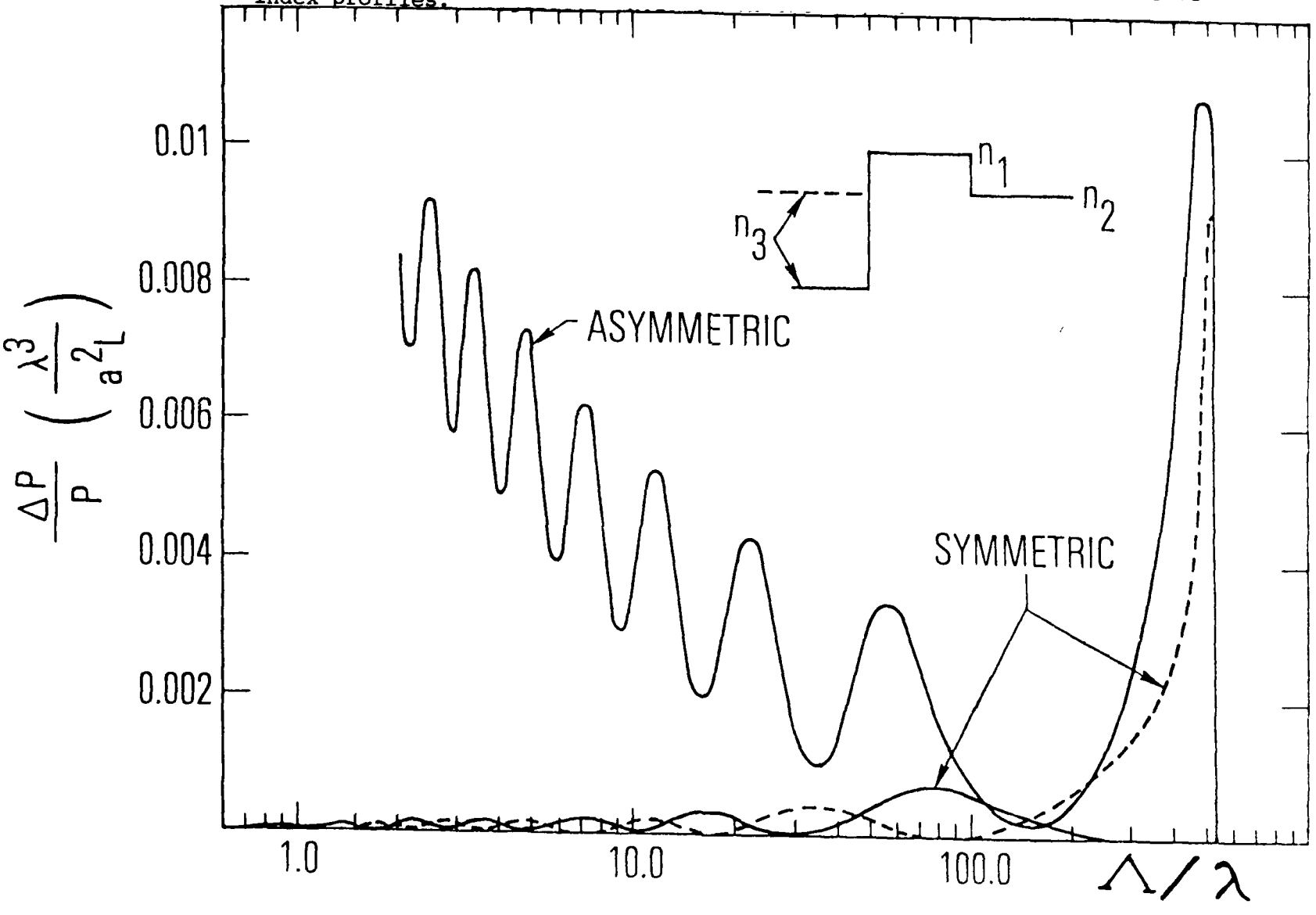

diffused guide. In general, it can be said that abrupt guides have comparable losses to their equivalent graded index guides.

The abrupt guides, however, can be seen to have higher losses at particular values of Λ corresponding to resonances of the leaky modes of the radiation fields. Such leaky modes do not exist in graded index waveguides, which are therefore less sensitive to short wavelength perturbations. This result was also observed by Marcuse in microbend loss calculations of slab guides with a parabolic index profile[11]. This reduction of radiation loss at small periodicities of surface roughness in graded index guides is significant since short range random roughness is the predominant type on most polished surfaces[12].

It should be mentioned that for abrupt waveguides fabricated by various deposition techniques, there is a good possibility that the perturbation of the two walls is uncorrelated. To show the effect of a phase difference between the perturbation in both walls, the radiation loss for the symmetric case in which the waveguide walls are perturbed symmetrically about the center of the waveguide is plotted as the dotted line in Fig. 2. It can be seen that in this case the guide is more sensitive to long period wall roughness than when the perturbations occur in parallel. Uncorrelated surfaces will, in general, have losses somewhere between the

two extremes. The situation when the two boundaries are uncorrelated and the loss is correspondingly higher is more likely to be found in abrupt films than in graded guides, making graded layers more attractive in this respect.

In conclusion, we have shown quantitatively that buried graded index guides have, in principle, lower losses due to surface roughness than do surface diffused. It is therefore clear that techniques must be developed to bury the guiding layer for low loss integrated optic circuitry.

SECTION 3b

REFERENCES

1. See, for example, the Technical Digest of the Topical Meeting on Integrated and Guided Wave Optics (Opt.Soc. Am. Wash., DC, 1978).
2. T. Izawa and H. Nakagome, Appl. Phys. Lett. 21, 584, (1972).
3. T.G. Giallorenzi, E.J. West, R. Ginther, R.A. Andrews Appl. Opt., 12, 1240 (1973).
4. J. Noda, T. Saku, N Uchida, Appl. Phys. Lett., 25, 308, (1974).
5. D. Marcuse, Theory of Dielectric Optical Waveguides Academic. Press, N.Y., (1974).
6. D. Marcuse, BSTJ, 48, 3187, (1969)
7. D. Marcuse, Light Transmission Optics, VNR, N.Y.,(1972).
8. H. Kogelnik, in Integrated Optics, Springer-Verlag, N.Y. (1975).
9. D. Marcuse, Appl. Optics, 14, 3021, (1975).
10. I. White and A. Snyder, Appl. Optics, 16, 1470, (1977)
11. D. Marcuse, Appl. Opt., 17, 755, (1978)
12. J.M. Bennett, J.M. Elson, Laser Induced Damage in Optical Materials: 1977, ed. Glass and Guenther (NBS Spec. Publ. 509, Washington D.C., 1977) p. 142.

c. Absorption Loss in $LiNbO_3$ Waveguides

Absorption loss was measured in $LiNbO_3$ waveguides by using calorimetry. This technique was demonstrated to be excellent and very sensitive method for determining this loss mechanism. The results of our first work was published in Applied Physics Letters. A reprint of this work is included in this section, describing the technique and tabulating the losses measured in $LiNbO_3$ outdiffused waveguides. Later measurements were made in $LiNbO_3$ Ti in-diffused waveguides as well as with another series in Table I. More complete details on comparison of mechanisms for loss is contained in Section d.

TABLE 3-I

Absorption Loss in $LiNbO_3$ Waveguides

	Polarization	λ μm	α_{ABS} db/cm	α_{TOT} db/cm
Bulk	Ext-Ord	.633	.045 ± .01	.18 ± .05
Bulk	Ord	.633	.09 ± .01	.23 ± .05
Ti-Diff	TE-Mode	.633	.06 ± .01	1.7 ± .5
Ti-Diff	TM-Mode	.633	.18 ± .02	2.8 ± .5
Out-Diff	TE-Mode	.633	.06 ± .01	1.6 ± .5
Out-Diff	TE-Mode	1.06	.02 ± .005	1.5 ± .5
Bulk	Ext-Ord	1.06	.01 ± .003	<.13

The results of these measurements can be summarized by the following facts:

1. The absorption loss in waveguides is much smaller than the scattering loss, for both in-diffused and out-diffused waveguides.
2. The TM mode has more absorption than the TE mode (in-diffused waveguides). The reason for this is not understood at this time. Nevertheless, these losses are much smaller than the total loss, and at the present time are negligible.
3. The TE mode has the same loss whether the waveguide is fabricated by out-diffusion or by in-diffusion of Titanium. This means that the Ti ions do not introduce significant absorption.
4. The absorption loss in TE modes is very close to that in bulk $LiNbO_3$. Because of the errors in the measurements and the small value of the absorption loss, it is not known whether the loss in waveguides is the same as in bulk, or bigger by a factor of two. Nonetheless, the absorption losses are an order of magnitude smaller than the total loss.
5. The loss at 1.06 μm is three times smaller than at 0.63 μm.
6. There is a dichroism in bulk $LiNbO_3$, which exhibits twice the absorption for the extraordinary polarization than for the ordinary polarization. This effect has not been reported before. Experiments are underway to study the dichroism at other wavelengths.
7. The total loss in $LiNbO_3$ bulk is about twice the absorption loss. The difference being presumably due to scattering.

8. The total loss in $LiNbO_3$ waveguides is about an order of magnitude bigger than the total loss in bulk $LiNbO_3$.

This is the first time that several of these facts have been reported, and not all these properties can be explained at the present time. However, clearly absorption loss is not a dominant mechanism in $LiNbO_3$ waveguides.

Calorimetric measurement of $LiNbO_3$ waveguide absorption losses

S. D. Allen, E. Garmire, M. Bass, and B. Packer

Center for Laser Studies, University of Southern California, University Park, Los Angeles, California 90007

(Received 6 November 1978; accepted for publication 23 January 1979)

This paper reports the first measurement of optical-absorption loss in $LiNbO_3$ waveguides and bulk material. This is also the first demonstration of calorimetry as a feasible technique for measuring waveguide absorption in integrated optics. Results indicate that in $LiNbO_3$ out-diffused waveguides the absorption is two orders of magnitude lower than the total loss, implying that the predominant loss mechanism is scattering. The ultimate sensitivity limit for calorimetric determination of absorption losses appears to be $\sim 10^{-4}$ dB/cm for optimized geometries.

PACS numbers: 42.80.Lt, 42.80.Sa, 42.82. + n, 42.70.Fh

Measurement of absorption losses by laser calorimetric techniques is common in the fields of high-power laser optics[1] and fiber optics.[2] The application of this technique to determine the absorption loss in $LiNbO_3$ waveguides and bulk material at 1.06 μm is reported. The results are compared to total loss measurements at this wavelength in order to elucidate the loss mechanisms.

In a calorimetric measurement the temperature rise of a sample during laser irradiation is detected. Such data permits a sensitive and absolute determination of the absorption loss in a sample. Bulk absorption coefficients of less than 2×10^{-3} cm^{-1} (10^{-3} dB/cm) have been measured at infrared wavelengths.[3] In contrast to transmission measurements, calorimetrically determined waveguide losses depend only to second order on insertion losses. Since the absorption is independent of the laser-beam diameter and since a waveguide will confine the beam along the entire length of the sample, the sensitivity of a waveguide-loss measurement can be comparable to that of a bulk-loss measurement in samples of equal thermal mass. Measurements in samples of different geometries are reported, and we estimate that for proper choice of sample geometry, the minimum measurable waveguide absorptivity is only 10 times larger than the minimum measurable bulk absorptivity. We therefore conclude that laser calorimetry is capable of measuring much lower absorption losses than any of the integrated-optics techniques in current use.

$LiNbO_3$ is an important material for active devices in integrated optics and is known to form low-loss waveguides by out-diffusion and Ti in-diffusion.[4,5] Much of the work to date on losses in $LiNbO_3$ waveguides has been directed toward understanding optical damage effects in the visible.[6] At 1.06 μm there is negligible optical damage, and this wavelength region is of particular interest because of the minimum optical-fiber loss. Total losses (absorption plus scattering) in $LiNbO_3$ bulk material have been shown to be less than 0.1 dB/cm at 1.15 μm.[7] Total losses in a Ti in-diffused waveguide have been measured at 0.63 μm (at power levels below the optical damage threshold) and yielded a value of 1.0 dB/cm.[7] In this paper, we report the losses at 1.06 μm in waveguides prepared on y-cut $LiNbO_3$ substrates by out-diffusion in flowing oxygen for 1 h at 950 °C.

The laser used in this experiment was Nd : YAG operated cw at 1.06 μm and producing 200 mW of TEM_{00} incident power. No optical damage effects were observed at this power level. The initial laser-beam diameter was 0.76 mm FWHM and the polarization was aligned to excite the TE mode of the waveguide. The focusing optics consisted of a cylindrical lens (f.l. = 80 mm) and a microscope objective (10×, N.A. = 0.25). A simple lens (f.l. = 40 mm) and a cylindrical lens (f.l. = 40 mm) collected the output of the waveguide and focused it onto a power meter with a slit positioned to block scattered light. For measurements of bulk absorption and transmission, the slit was removed. The samples were mounted on glass capillary tubing with cyanoacrylic cement to minimize conduction losses. Small-diameter copper/Constantan thermocouples (0.003 in., Omega Engineering) were similarly glued to the samples. The reference thermocouple was embedded in an aluminum block. A Plexiglas enclosure provided isolation of the sample and thermocouples from air currents. Relative sample temperature changes before, during, and after laser irradiation were monitored with a nanovoltmeter (Keithley 147).

In order to explore the usefulness of calorimetry as a measurement technique for integrated optics, we measured the losses in two very different geometries, representing the worst and best cases. The results are summarized in Table I. Sample A (dimensions $0.3 \times 2.4 \times 2.5$ cm, $m = 8.6$ g) had a relatively large cross-sectional area and a long thermal time constant, which produced a heating curve linear with time, as shown in Fig. 1(a). The absorption coefficient was determined as follows[8]:

$$\alpha\ (\mathrm{cm}^{-1}) = \frac{mC}{lP_0}\left[T_2' - T_1' - (T_3' - T_1')\left(\frac{T_2 - T_1}{T_3 - T_1}\right)\right], \quad (1)$$

where m is the mass of the sample, C is the specific heat, l is the length of the sample, and P_0 is the incident laser power. The quantities T_i' and T_i are, respectively, the slopes of the temperature-vs-time curves and the temperatures of the samples for the three regions shown in Fig. 1(a).

 0003-6951/79/070435-03$00.50

FIG. 1. Temperature-vs-time behavior for the two sample geometries.

Sample B (dimensions $0.1 \times 0.1 \times 2.5$ cm, $m = 0.14$ g), on the other hand, had a small cross-sectional area and a thermal behavior which was dominated by convection and radiation losses, as shown in Fig. 1(b). For this case, the absorption coefficient was given by

$$\alpha \ (\text{cm}^{-1}) = mC\Delta T / l\tau P_0, \tag{2}$$

where ΔT is the steady-state sample temperature rise and τ is the measured thermal time constant of the sample.[9] The values of the absorption coefficients obtained for the two different geometries agree within experimental error, and the waveguide loss is only about twice that observed in the bulk. This indicates that out-diffusion does not introduce significant absorption centers in $LiNbO_3$ at 1.06 μm. Both the bulk and waveguide absorption losses are considerably lower than the total losses, as will be discussed below.

The total loss in the optical system through either the bulk or the waveguide can be described by

$$\frac{P_T}{P_0} = L_0 L_c \left(\frac{(1-R)^2 \exp[-(\alpha+\beta)l]}{1-R^2 \exp[-2(\alpha+\beta)l]} \right) L_T, \tag{3}$$

where P_T and P_0 are the transmitted and incident powers, respectively, L_0 and L_T are the fractional transmissions of the focusing and collecting optics, respectively, L_c is the waveguide coupling efficiency, R is the reflectivity for a single interface, α and β are the length-dependent absorption and scattering losses, respectively, and l is the sample length. The term in large parentheses in Eq. (3) is the equation for loss in a sample including noncoherent multiple reflections.[10] The transmission coefficients of the input and output lenses were $L_0 = 0.73$ and $L_T = 0.81$. The coupling efficiency was determined by calculating the overlap between the 10-μm-deep waveguide and the incident spot size (9.8×23 μm). The coupling efficiency was >0.90 with the lower bound used in the data reduction.

The total loss in bulk $LiNbO_3$ (0.13 dB/cm, sample A) is comparable to that reported by Kaminow and Stulz[7] at 1.15 μm (0.1 dB/cm). In both cases, this is only an upper bound on the true total bulk loss. The total waveguide loss is approximately the same for both samples and almost two orders of magnitude greater than the absorption loss. This indicates that the dominant optical-loss mechanism in these waveguides is scattering. It is interesting to note that the total waveguide loss at 1.06 μm is comparable to the loss

TABLE I. Results of loss measurements on $LiNbO_3$.

	Waveguide		Bulk	
Sample	Absorption loss (10^{-3} dB/cm)	Total loss (dB/cm)	Absorption loss (10^{-3} dB/cm)	Total loss (dB/cm)
A	2.2(±0.6)	1.5(±0.5)	0.7(±0.3)	<0.5
B	1.7(±0.4)	1.7(±0.5)	1.1(±0.3)	a

[a] Laser-beam divergence prevented accurate bulk transmission measurements for this long thin sample.

reported for a Ti in-diffused waveguide at 0.63 μm using an interferometric technique (1.0 dB/cm).[7]

For the optimized geometry of small rodlike samples whose length is much greater than both the width and the height, the minimum measurable absorptivity is proportional to the perimeter of the entrance face. Therefore, only small gains in sensitivity are made by decreasing the size of the sample. The minimum measurable absorption coefficient of samples similar in size to sample B is estimated to be 5×10^{-4} dB/cm. The sensitivity in this case will be limited by scattering directly onto the thermocouple and may be further improved by optimizing the coupling efficiency of the laser into the waveguide. For large samples whose thermal behavior is best analyzed by Eq. (1), the minimum measurable absorptivity is proportional to the cross-sectional area of the entrance face of the substrate. As a rule of thumb, for experimental condition similar to those in this work, the minimum measurable absorptivity is

$$\alpha_{\min} \ (\text{cm}^{-1}) = 3 \times 10^{-3} A,$$

where A is the area in cm^2. In general, the sensitivity of the calorimetric measurements could be improved for both the large and small samples by (a) increasing the thermal isolation by placing the samples in a vacuum; (b) improving the laser stability; (c) eliminating unguided light.

In conclusion, we have demonstrated the usefulness of the calorimetric technique for measuring absorption loss in planar waveguides. It is estimated that the minimum waveguide absorption coefficient measurable for samples with optimum geometry is on the order of 10^{-4} dB/cm. For the specific example of $LiNbO_3$ out-diffused waveguides, the absorption coefficient at 1.06 μm is 2×10^{-3} dB/cm. This result is to be compared with the first measurement of absorption coefficient in bulk $LiNbO_3$, 1×10^{-2} dB/cm reported here. The total losses measured in both the bulk and waveguide were found to be comparable with previously reported results.[7] These results show that in the waveguide the absorption loss is considerably less than the total loss, giving the first indication that the absorption losses in $LiNbO_3$ are negligible at 1.06 μm and demonstrating that scattering is the limiting mechanism in the waveguide transmission.

The authors would like to acknowledge the help with the Nd : YAG laser given by Alan Stewart and the loan of a sample from Carl Verber of Battelle Columbus Laboratories. This work supported in part by RADC/ESO Hanscom

Air Force Base, Mass., and in part by AFOSR, Air Force Systems Command, USAF. One of the authors (B. Packer) acknowledges the support of a Xerox Research Traineeship.

[1] M. Hass and B. Bendow, Appl. Opt. **16**, 2882 (1977), and references therein.
[2] R. L. Cohen, K. W. West, P. D. Lazay, and J. Simpson, Appl. Opt. **13**, 2522 (1974).
[3] S. D. Allen and J. E. Rudisill, Appl. Opt. **16**, 2914 (1977).
[4] I. P. Kaminow and J. R. Carruthers, Appl. Phys. Lett. **22**, 326 (1973).
[5] R. V. Schmidt and I. P. Kaminow, Appl. Phys. Lett. **25**, 458 (1974).
[6] R. L. Holman, P. J. Cressman, and J. F. Revelli, Appl. Phys. Lett. **32**, 280 (1978).
[7] I. P. Kaminow and L. W. Stulz, Appl. Phys. Lett. **33**, 62 (1978).
[8] M. Hass, J. W. Davidson, P. H. Klein, and L. L. Boyer, J. Appl. Phys. **45**, 3959 (1974).
[9] D. A. Pinnow and T. C. Rich, Appl. Opt. **12**, 984 (1973).
[10] ASTM Publication No. F-120-75 (unpublished).

d. Loss Mechanisms in $LiNbO_3$ Waveguides

Loss mechanisms in optical waveguides can be classified into three types; absorption, volume scattering due to refractive index irregularities within the interior of the guide, and surface scattering due to waveguide boundary imperfections. We have separated these mechanisms and proved that the latter is the main source of length-dependent loss in $LiNbO_3$ waveguides.

We showed in Section c that absorption is negligibly small compared to the overall guide loss. It remains, therefore, to differentiate between volume and surface scattering loss mechanisms for length dependent losses.

The basic technique used for differentiating between scattering due to surface roughness and scattering due to volume inhomogenienities is the comparison of in-plane and out-of-plane scatter. Scattering from volume inhomogenieties will be roughly isotropic, while scattering from surface roughness will cause primarily out-of-plane scatter. This latter face is because, for this case, one-dimensional phase matching occurs, in which surface roughness couples guided modes into small-angle radiation modes.

These modes radiate out-of-plane and are much stronger than the in-plane radiation caused by surface roughness.

Estimations of in-plane scatter are relatively simple to obtain, because the beam profile of light travelling in the waveguide can be compared to the beam profile of light travelling in the bulk of the sample. Any broadening, or wings on the profile of the guided light will be due to scatter within the waveguide. In order to obtain these profiles, $LiNbO_3$ samples were polished and end-fire coupled. The near field of the exit face was imaged onto a scanning detector. Intensity scans were taken of the light when it was guided and compared to those when the light was traveling through the bulk substrate.

The overlap integral between the two profiles determined the fraction of in-plane scattering of the guide relative to that of the bulk. Measurements of $LiNbO_3$ out-diffused guides showed that the in-plane scatter was less than 0.05 dB/cm, proving that volume scatter is not a predominant loss mechanism in these waveguides.

All $LiNbO_3$ waveguides were studied in with end-fire coupling, in the configuration with which they will be used for fiber optics switches. Typical near-field profiles of the exit light are shown in Fig. 3-1. It can be seen that there is a considerable amount of light in both the substrate and the air above the waveguide. The ratio of the energy inside the waveguide to that in the wings gives a measure of the insertion loss of the waveguide. This insertion loss will be due to the

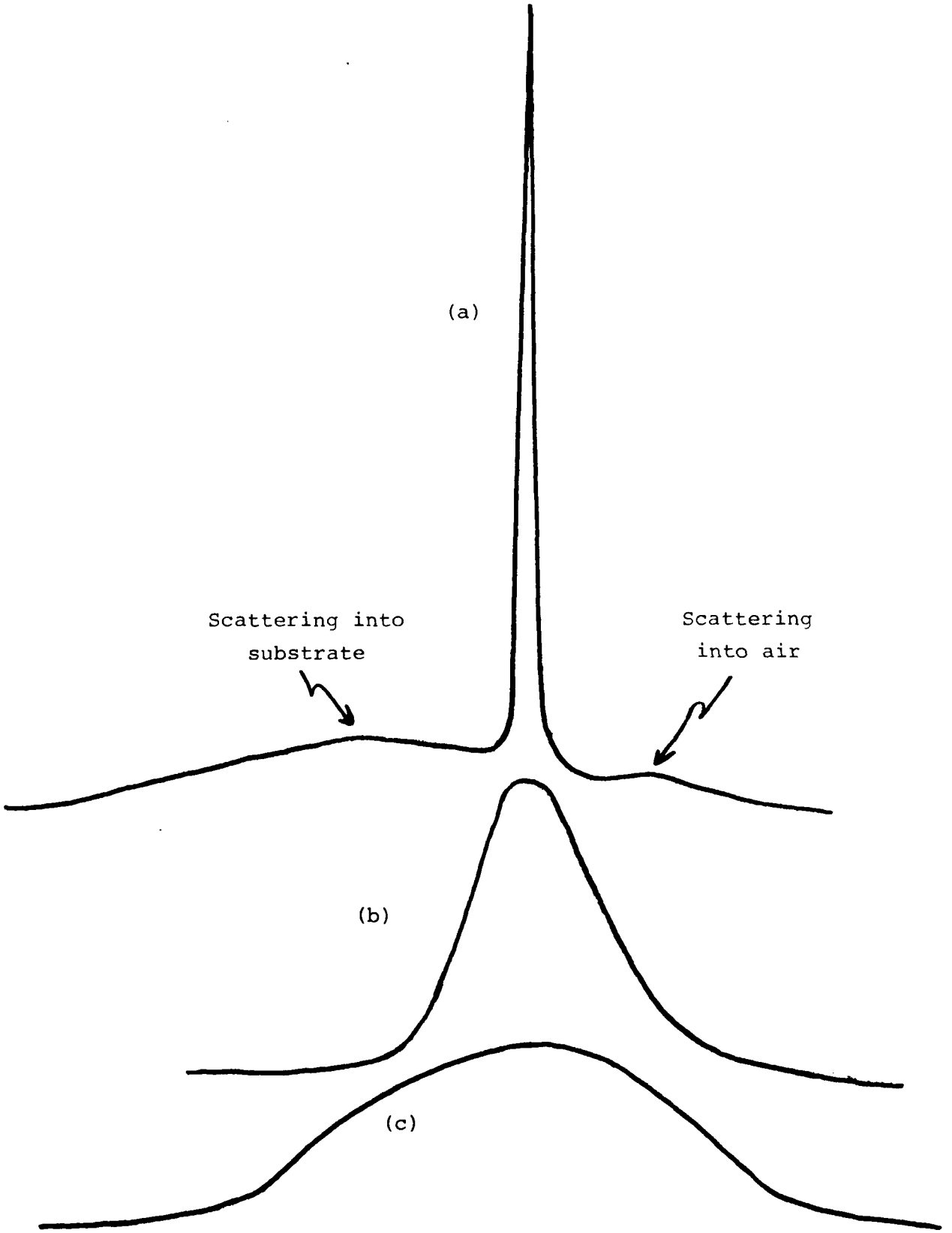

Figure 3-1. Out-of-plane intensity profiles of near-field image for incident light focused into the a) guide, b) substrate and c) air.

mode-mismatch between the incident light and the waveguide and also due to small angle scatter loss in the waveguide. Typical numbers for the fraction of light in each regime is shown in the first column of Table II, for both out-diffused and in-diffused waveguides. Included in the table is the amount of light which was undetected. All measurements were normalized to the transmission in the bulk. Since bulk losses were an order of magnitude smaller than waveguide losses (section c), and we wanted to eliminate the need to calculate reflection losses, the normalization to the bulk transmission gave a simple way to do this. It can be seen that the undetected light (lost due to absorption or large-angle scatter) is very much smaller than small angle scatter or input coupling losses.

It was possible to get a direct measure of the light which was scattered into the air by surface roughness. We placed a block above the guide at the entrance face to eliminate all light due to mode mismatch, and measured the output in the air due to surface scatter. The difference between this signal and the signal measured without the block represents a measure of the coupling mismatch or small angle scattering into the air due to roughness of the entrance edge. In order to estimate the difference between these two quantities, we assumed a Gaussian mode input and a Bessel function guided wave and calculated the overlap. The results are listed in the table

TABLE II

Contributions of Various Mechanisms at the Exit Face of $LiNbO_3$ Waveguides 1 inch Long at .633 μm. Measurements normalized to bulk transmission

OUT-DIFFUSED

	Total Measured	(t = 10 μm, TE mode; Guided mode width = 5 μm) Small Angle Scatter	Coupling Mismatch	Entrance Edge loss
In Guide	43.5%			
In Air	9%	3%	(3%)	(3%)
In Substrate	46%	43%	(4%)	(<3%)
Undetected Light	1.5%			

IN-DIFFUSED

		(t = 3 μm, TE mode; Guided mode width = 2.6 μm)		
In Guide	33%			
In Air	14%	6.5%	(3.5%)	(4%)
In Substrate	50%	43%	(7%)	(<3%)
Undetected Light	3%			

under "coupling mismatch" and are placed in brackets to show that they are the result of calculations. The light which is in the air and not represented by the coupled mode mismatch or by the small angle scatter, is due to an entrance edge scatter, and is listed in the last column.

It is not possible to make separate measurements in the substrate. However, we made a few gross assumptions to develop some estimates. We calculated the light in the substrate due to the expected mode mismatch, and then assumed that the rest of the light in the substrate was due to small angle scatter. These numbers are included in the table, in brackets. Also included is the fact that we assumed the entrance edge scatter into the substrate to be less than that in the air.

With the assumption that the coupling mismatch and entrance edge loss all occur at the beginning of the waveguide, before length/dependent scatter loss becomes appreciable, the length-dependent small angle scatter loss can be calculated. For out-diffused waveguides, the initial transmission at the front edge was 87%, corresponding to a 0.6 dB loss (excluding reflections). The remainder of the total 3.6 dB loss is due to small angle scattering, yielding a length-dependent loss of 1.1 dB/cm. For the in-diffused guide, the transmission loss of the front edge is 17.5% corresponding to a 0.83 dB loss. The remainder of the total 4.8 dB loss is distributed along the length and corresponds to a loss of 1.6 dB/cm. Finally, the

reflectivity has not been included in this analysis, since these measurements were all made relative to the bulk transmission. The reflection losses for two faces of $LiNbO_3$, with a reflectivity of 15% each is 1.3 dB. This means that the total insertion loss for the two samples was 5 and 6 dB respectively. The samples were carefully prepared to have the same waveguide thickness and good quality edges, so that rounding and chips were eliminated. The plot of these losses as a function of waveguide length yields the loss per unit length. The results are shown in Fig. 3-2, for samples up to 7.5 cm in length.

The results of the longest sample do not belong on the same graph since that guided mode was a different thickness. We have included the measurements for completeness, however. The best estimate we have for the length dependence of the loss is drawn in as a straight line and corresponds to α = 0.6 dB/cm. The results are also consistent with α = 0.3 dB/cm. These numbers are somewhat lower than obtained previously. The difference is real, because these waveguides were thicker than those studied previously and will therefore have less loss. The insertion loss at zero thickness includes the Fresnel reflection loss of 1.3 dB. The remainder of 3.5 dB is due to any mode-mismatch and edge-coupling loss.

The results of this study have indicated that the mechanisms for loss in end-coupled $LiNbO_3$ waveguides are both length-dependent losses due to scatter from the waveguide surface

Figure 3-2. Insertion loss of out-diffused $LiNbO_3$ waveguides of different lengths, in d
Samples marked ● were pure out-diffused. Samples marked X were measured i
the presence of in-diffused titanium. Guided modes were 10 μm thick.
Samples marked □ had guided mode profiles 5 μm thick.

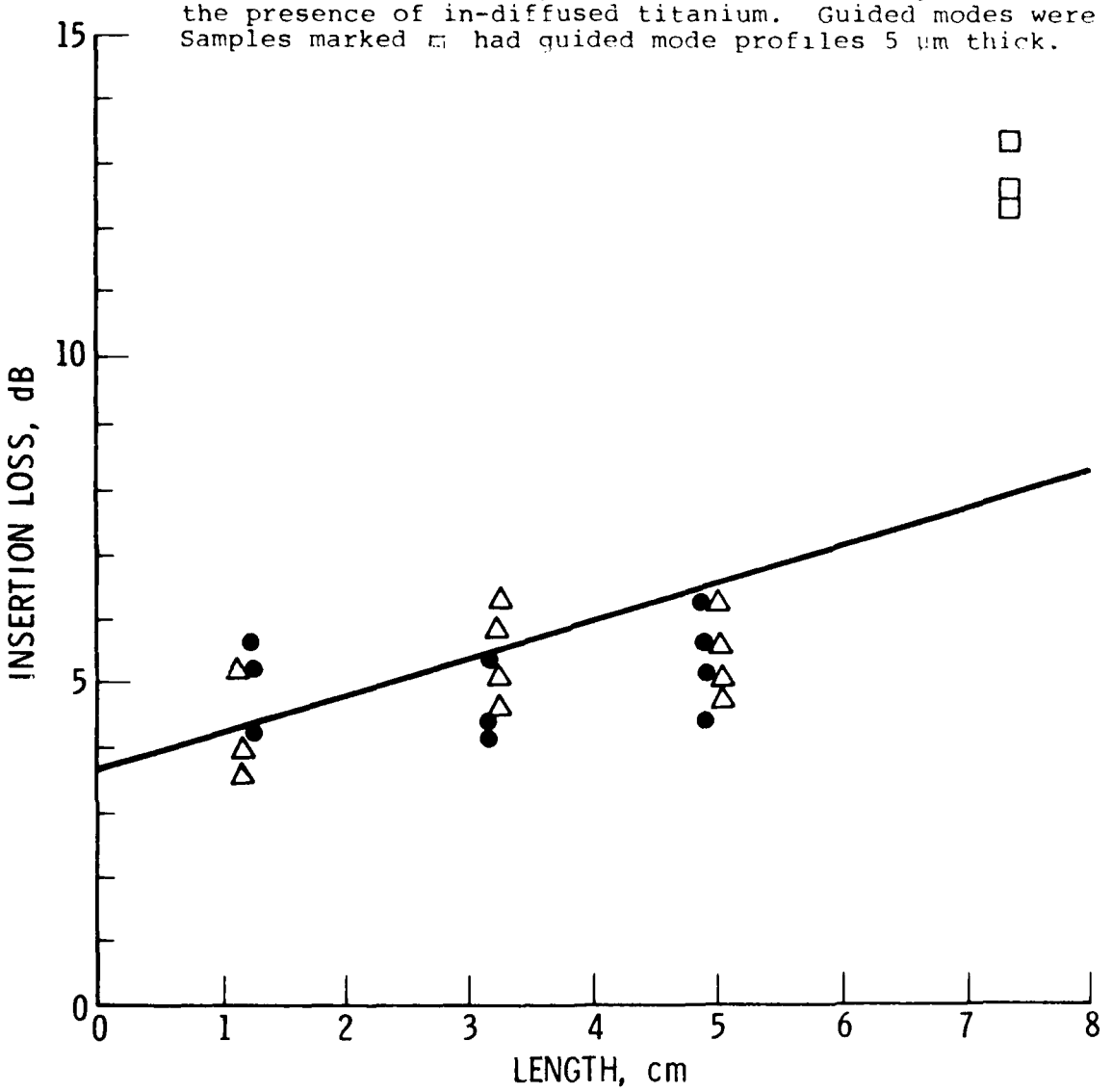

and also losses due to poor coupling, mode mismatch and reflection at the entrance edge. The first set of measurements indicated a relatively large value for the length-dependent loss, making this the predominant loss mechanism. The second set of measurements indicated that the edge losses were, in general, larger than the length dependent losses. More work is needed to sort out these effects in order to reduce the loss.

e. Techniques to Reduce $LiNbO_3$ Waveguide Insertion Loss

In order to determine whether the primary source of loss was due to surface scatter and to reduce this effect we tried several experiments. First we tried polishing the top of the samples. It is well known that in-diffusion of Titanium causes the surface of the sample to be raised slightly, and a surface roughness to appear. We therefore decided to measure the losses before and after the surface was polished. The results are shown in Table III. It can be seen that the waveguide became 10 μm thinner during the polishing and the waveguide losses typically increased. Unambiguous interpretation of these measurements is not possible since there were several mechanisms which may have contributed to higher losses in the thinner waveguides after polish. First, thinner waveguides typically have higher scatter losses. Second, thinner waveguides have higher input coupling losses. Both these effects were reported in Section d.

The losses of the samples reported in table III are higher than those reported in section d. These were some of the first measurements we made, and it was discovered after these measurements that the corners of the waveguides tended to be rounded. Commercially polished edges were found to be inadequate for good input coupling efficiencies. Careful polishing procedures were introduced on the front edge of the samples and the insertion losses were reduced to typically 3 dB.

In order to establish definitively the success of surface polish, new measurements should be made with samples whose edges have been properly prepared and also which have not been thinned to such an extent. It was not possible to make these measurements before the end of the contract.

In order to further investigate the cause of the loss in samples with good end faces another experiment was performed. Losses due to surface scatter depend on the index difference between the waveguide and the medium above the surface. If the medium above the surface is changed from air to a transparent medium with a higher index, the amount of surface scatter should be reduced. We performed this experiment by measuring the losses before and after coating the top of a $LiNbO_3$ waveguide with a polymer.

The results are shown in Table 3-IV. The polymer was in the form of a glue with refractive index 1.4, and it was applied carefully in order not to disturb the entrance and

TABLE 3-III

Insertion loss (reflection loss included) of TE modes at 0.63 μm in 2.54 cm $LiNbO_3$ waveguide before and after 10 minutes of hand polishing with Syton on a silk pad.

	Before		After	
Sample Number	Guided Mode Thickness Micrometers	Loss dB	Guided Mode Thickness Micrometers	Loss dB
A	20	9.0	10	15.0
B	25	9.0	10	8.8
C	30	7.9	30	9.4
D	30	5.0	20	6.2

TABLE 3-IV

Insertion Loss Change of TE Guided Mode for Y-cut Propagating $LiNbO_3$ Waveguides
The cladding refractive index was 1 without glue and the glue index was 1.4

Measurement error ± 10%

Sample ID	Waveguide Types	ℓ Length cm	Thickness of Guided Mode μm	Insertion Loss L in dB		Change in Loss	
				Without Glue	With Glue	$\Delta\alpha$ dB/cm	Percentage*
071879B	In-diffused	4.8	10	5.8	5.5	+ 0.06	+ 10%
071879B'	Out-diffused	4.8	10	5.6	5.4	- 0.04	- 6.7%
062979C	In-diffused	7.2	5	11.8	12.8	+ 0.03	+ 5.0%
062979C	In-diffused	1.25	10	3.9	3.7	- 0.16	- 10.4%
062979C'	Out-diffused	1.2	10	5.6	5.6	0.0	0%
062979C	In-diffused	3.1	10	6.4	6.4	0.0	0%
062979C'	Out-diffused	3.1	10	9.5	10.0	+ 0.16	+ 10.4%

$$\Delta\alpha = \frac{\Delta L}{\ell}$$

*assuming
α = 0.6 dB/cm

exit faces to the waveguide, lest it affect the input and output coupling efficiencies. All the measurements listed in Table 3-IV were consistent with no change in transmission due to the polymer in the waveguide surface. The error for these measurements is about 10%, expressed as a percentage of the length-dependent loss (assumed to be 0.6 dB/cm). This number can be compared to that expected from theory.

It was shown in Section b (Eq. 8) that the normalized radiation loss due to surface roughness is

$$\frac{\Delta P}{P}\left(\frac{\lambda^3}{a^2 L}\right) = \frac{2\pi^3 (n_s^2 - n_c^2)^2}{n_s} F$$

where F is a function which depends on the details of the mode profile and the amplitude and periodicity of the roughness. The quantity n_s is the index of the substrate and n_c is the index of the cladding. If the refractive difference between the guide and the substrate is much smaller than the difference between the guide and air (or polymer), the mode profile is determined primarily by the diffusion profile and does not depend on the index of the cladding layer. Under this approximation, the scatter loss should be reduced due to the reduction in quantity $(n_s^2 - n_c^2)^2$. This difference between $n_c = 1$ = air and n_c = polymer is 40%. We measured ~10% change.

Our inability to measure a 40% reduction in waveguide loss may be due to several causes. First, the large amount of insertion loss error due to mode mismatch, reflections, and edge defects may have swamped the length-dependent losses which we seek to

reduce. Second, the assumption that the mode profile does not change due to introduction of a larger index cladding layer may be inaccurate. In addition to making the theoretical estimate wrong, a mode-change due to the polymer cladding will cause a mode-mismatch between light initially guided in an air-cladded layer and the mode when it enters the polymer-clad region. The mode mismatch at this transition may introduce additonal loss masking the loss reduction we intended to measure. Thirdly, the polymer we used may have been lossy or not have formed a perfect interface between the waveguide and the polymer. Bubbles or inhomogeneities in the polymer would introduce additional sources of loss. Finally, our assumption that the length-dependent losses are due to scatter from the surface imperfections may be erroneous. More measurements are required to determine whether or not reducing the index discontinuity between the waveguide and cladding layer reduces the waveguide loss.

In conclusion, the only technique we have found which significantly reduces the insertion loss of end-coupled $LiNbO_3$ waveguides is to use great care in polishing the endfaces of the waveguides, to eliminate any rounding of the corners. Techniques attempted to reduce the loss due to surface scatter did not produce any noticeable improvement.

Clearly, if the waveguide could be buried below the surface, the requirements on the polish of the end faces would be reduced. In addition, any loss due to surface roughness would be reduced.

CHAPTER 4. STUDIES OF MULTIMODE WAVEGUIDE FABRICATION IN C-PROPAGATING $LiNbO_3$

In the first chapter it was described how the 90° distributed Bragg deflector can act as a polarization analyzer, deflecting one polarization and transmitting the other. This is the integrated optical analog of the Glan-Thompson prism. This suggests its use, along with the electro-optic effect, to make a multimode integrated optics fiber switch. This occurs when phase modulation is used to cause polarization modulation, converting TE to TM modes. The distributed Bragg deflector then transmits the TE polarization and deflects the TM polarization. If two exit fibers are placed as shown in Fig. 4-1, an integrated optics multimode fiber optics switch is the result.

Our studies of the beam expander, therefore, led to an interest in demonstrating the device in $LiNbO_3$, in conjunction with an integrated optical multimode switch. This, in turn, led to the requirement to develop good quality waveguides in $LiNbO_3$ which would confine both the TE and TM modes equally well.

Typical diffused waveguides in $LiNbO_3$ have a strong polarization dependence. The polarization dependence of in-diffused waveguides occurs because the titanium ions affect the extraordinary index more than the ordinary index. In addition, unless careful procedures are introduced, out-diffusion causes a refractive index profile for the extraordinary polarization separate from that caused by in-diffusion. For these reasons we decided to investigate waveguides fabricated in y-cut, z-propagating $LiNbO_3$, where both TE and TM modes see an ordinary index.

Figure 4.1. Multimode fiber optics switch using electro-optic polarization modulation with DBD polarizer and polarization-sensitive deflector.

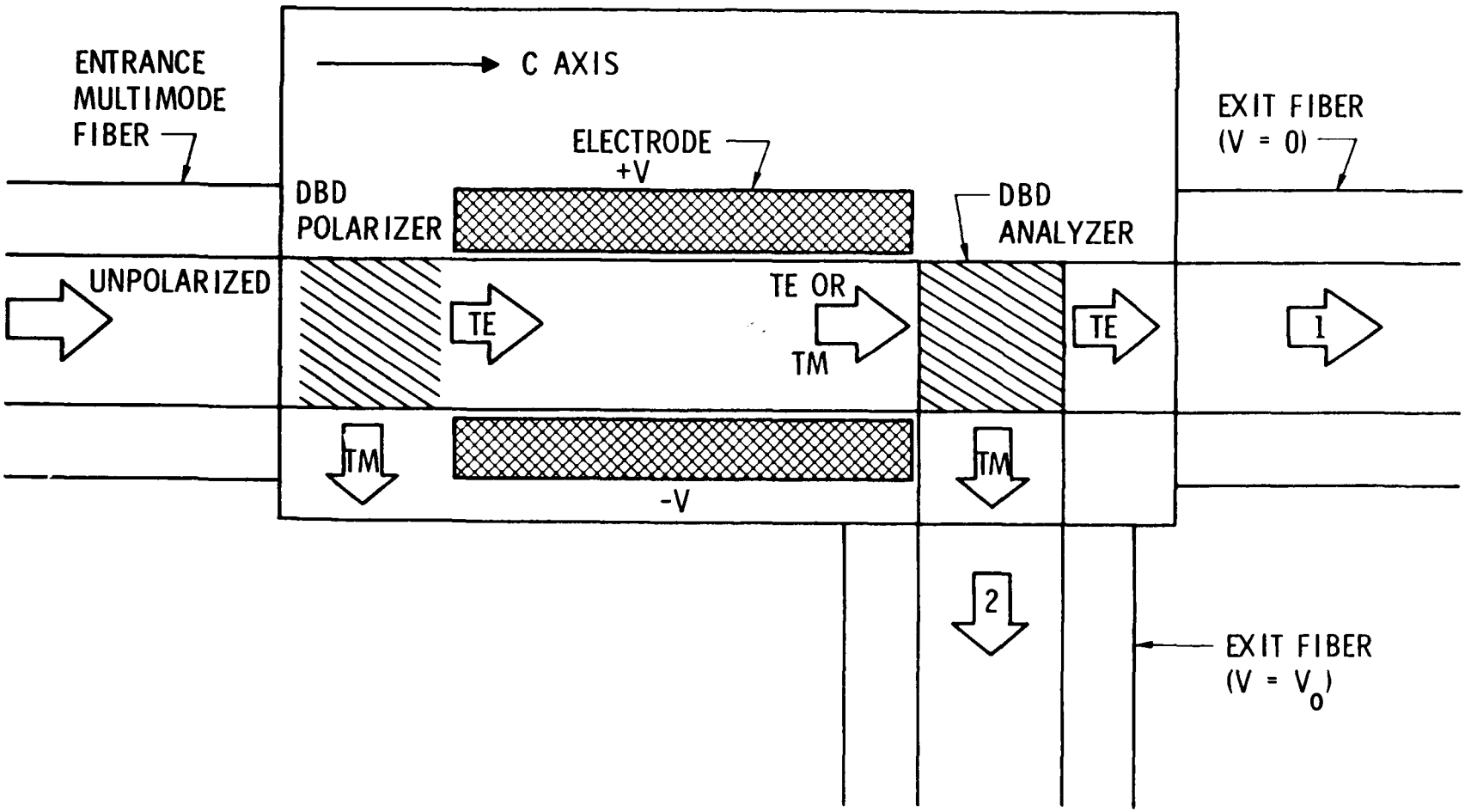

Another reason for being interested in this orientation is that it can be used with the electro-optic effect to convert TE to TM modes, and vice versa. Either an x or y-cut $LiNbO_3$ plate is used with the channel waveguide in-diffused along the z direction. The electric field is applied in the plane of the waveguide, perpendicular to the direction of propagation. The input polarization can be either TM or TE, and the applied field causes a rotation of the optic axes in the $LiNbO_3$.

When this rotation is 45^o, a mode which was originally pure TE can be converted into pure TM, and vice versa. The exact solution involves terms in r_{51}^2, but these terms are much less than those introduced by any alignment errors and can justifiably be ignored. The phase retardation for this case is

$$\Gamma = \frac{2\pi \ell}{\lambda_o} E\, n_o^3\, r_{22} \quad .$$

The half-wave voltage for this orientation is only 10-20% higher than for the usual geometries.

A bulk modulator of this orientation was demonstrated in the experiments on optical bistable switches which were described in the interim report.

We have, in principle, a design for a multimode switch, and the problem becomes one of making waveguides which guide both TE and TM modes and are thick enough to be butt-coupled to multimode fibers. Out-diffused waveguides are thick enough,

but act only on the extra-ordinary polarization. Out-diffusion increases the ordinary index but has thus far not produced thick enough waveguides in reasonable times. One technique for increasing the depth of the diffused waveguides is electro-diffusion, where, in addition to the concentration gradient driving force, an electric field is introduced. This method has been used to produce Cu in-diffused waveguides in $LiTaO_3$, (Appl. Phys. Lett. 25 308 (1974)) at much lower temperatures and shorter times than are usually required.

We have investigated titanium in-diffusion in c-propagating samples with and without an applied electric field. We have results which are inconclusive and require more experimentation before the full understanding is developed. The work described here represents a progress report and describes our status at the end of the contract.

Titanium diffusion in the presence of an electric field was studied both with electrodes separate from the samples and with the electrodes in contact with the samples.

The preliminary measurements indicated that electro-thermal diffusion might indeed be very satisfactory. In an initial run, waveguides were fabricated by depositing 500 Å of Ti on c-propagating $LiNbO_3$ and diffusing in flowing O_2 at 1000°C for eight hours. The electro-diffused sample was placed in a field of 10 V/mm during diffusion, oriented in the direction of the Ti motion. A control sample was placed outside the region of

Table 4-I. Results of Titanium In-diffusion in c-propagating Waveguides

Sample Number	Thickness Titanium Å	Time Hours	Gas	Guided Mode Thickness (μm) TE	TM	
0529 A	600	14	O_2	10	10	
0713 B	450	7	Ar	5	5	
0608 A	450	6½	Ar	4	4	
0608 B	450	9	O_2	5	5	
0622A	450	6½	Ar	10	10	(near cutoff)
		+1	O_2	--	--	
	+200	+4½	Ar	--	30	(near cutoff)
0622 B	450	8½	Ar	--	20	(near cutoff)
0807 C	450	6	Ar	--	20	(near cutoff)
0807 D	450	6	Ar	--	20	(near cutoff)
0530 A	300	7	O_2	--	30	(near cutoff)
0525	300	7	O_2	--	--	

The symbol -- means that no waveguide was observed.

the electric field. The electro-diffused sample demonstrated good confinement of light inside the waveguide with a high N.A. and a guide thickness of 70 μm. The control sample demonstrated weak guiding in a mode of 30 μm width (the diffused region was 10 μm thick), with low N.A.

With these encouraging preliminary results, experiments were undertaken to systematically study the process of electro-diffusion, and its impact on the fabrication of waveguides in c-propagating $LiNbO_3$. The results shown in Table IV-I were obtained.

The results are somewhat unreproducible because we had not yet developed a good method for monitoring the titanium film thickness, and the numbers used here are only approximate. The results show that reasonable waveguides can be fabricated with film thickness of at least 450 Å. However, a number of the waveguides were right near cutoff, and the results were somewhat unreproducible. We were surprised to find that in many samples there was weak guiding of TM modes, but TE modes were not confined. This is due to the fact that the waveguide is anisotropic. We developed a theory to explain this phenomenon, which is included in the appendix. The result of this study is the conclusion that even though the waveguide is c-propagating, the TE and TM modes do not have the same propagation vectors.

Further diffusion of waveguides near cutoff caused all guiding to disappear. This was also an unexpected result because,

theoretically, the longer the diffusion time, the farther the waveguide should be from cutoff. This is shown theoretically in Appendix II. Evidently the theoretical models for the diffused waveguide are not exact, when samples are operating right at cutoff.

Additional experiments were attempted with the samples diffused in an electric field and compared to those diffused without an electric field. The same conditions were used as in the previous experiments: 450 Å titanium, 6 hour diffusion at 1000°C in Argon. None of the samples showed guiding of the TE mode. The sample whose diffusion occurred in the direction of the electric field showed no guiding in the TM polarization either. A sample whose diffusion direction was counter to the applied field, and the samples which did not have an applied field showed weak guiding for the TM polarization, without much difference between them. For comparison, an X-propagating sample was studied, with a 1000 Å titanium film and 2½ hour diffusion in Argon. Both guides showed 20 μm TE modes and 10 μm TM modes, with very little difference between the sample with the applied field and that without the applied field. The results of these measurements were inconclusive and did not confirm the dramatic behavior measured in the first preliminary experiments.

It was decided to try electro-diffusion with the electrode contracts directly applied to the $LiNbO_3$. It was expected that

the effects would be bigger with this geometry. A sample was prepared with titanium on the top surface, and then both the bottom and top were overcoated with gold. Gold wires were attached in one corner of the samples with a thermocompression bonder. The observations can be summarized as follows:

1. The sample was heated to 350°C for a total of 38 hours under an electric field of between 10 and 40 V/mm. It was observed that at temperatures greater than 200°C, the $LiNbO_3$ sample began to pass current. With the voltage constant at 20 V/mm, the furnace warmed up to full temeprature in 20 minutes, and the current rose from 5 μ amp at 200°C to a maximum of 32 μ amps, ten minutes after the furnace reached its maximum temperature. The current then began to decrease to about 5 μ amps about 80 minutes after the oven reached its maximum value. After a long period of steady state, the electric field was suddenly switched to 40 V/mm. The current rose slowly again to about 30 μ amps, reaching a peak 40 minutes after the change of electric field. After saturating at its maximum value, the current slowly decreased to 17 μ amps, 170 minutes after the voltage change.

At the temperature of 350°C, when the electric field was suddenly switched from 0 to a final value of 20 V/mm, the current responded immediately without any delay, to a new peak value.

2. During the experiment, Ohm's law did not hold; i.e. the resistivity appeared to be voltage dependent. These results are shown in Table 4-II. The cause is not understood.

3. After electro-diffusion at 350°C, there was a crack across the substrate. In addition, there was no evidence of a waveguide.

Table 4-II. Resistivity Measured at 300°C and 600°C

Temp. °C	Voltage Across the Sample V	Current mA	Resistivity Calculated from Ohm's Law cm	Measured Resistivity cm
300	12	2.5×10^{-3}	6.0×10^{7}	
	18	4.3×10^{-3}	5.2×10^{7}	
	40	18.1×10^{-3}	2.8×10^{7}	
600	6	14	$5,4 \times 10^{3}$	2.5×10^{4}

AD-A086 115 UNIVERSITY OF SOUTHERN CALIFORNIA LOS ANGELES F/G 20/6
WAVEGUIDE STUDIES FOR FIBER OPTICS AND OPTICAL SIGNAL PROCESSIN--ETC(U)
APR 80 E GARMIRE F19628-77-C-0221
UNCLASSIFIED RADC-TR-80-82 NL

The sample came out black in the vicinity of the wire bond. Studies of this darkened area on the Xray dispersive SEM indicated Si and Mg contamination. It is not clear how these metals got in from the bond, but it was decided to redesign the electrode arrangement. No waveguiding was observed with this sample; it was too dark.

A new electrode arrangement was developed, whereby the sample was mounted between two platinum plates. With this arrangement no darkening occurred. However, cracks still appeared. Only one sample cut of four was not cracked. That sample also was the only sample that did not pass current during the diffusion process. This leaves the experiments at a very interesting stage. Perhaps the current is caused by the crack and when there is no cracking, there is no current. Perhaps, instead, there was not good electrical contact for that one sample. That sample was the only one that could be tested for waveguiding. None was observed. However, until we demonstrate clearly that there was electrical contact with the sample during diffusion, we cannot conclude that electro-thermal diffusion was not successful.

We suggest that it would be useful to continue experiments on electro-thermal diffusion to develop the conditions under which it works. Since the effect has been reported in $LiTaO_3$, we expect that we should be able to develop it for $LiNbO_3$.

One advantage of electro-thermal diffusion is the potential for driving the waveguide below the $LiNbO_3$ surface. This has

two distinct advantages: first, it reduces losses due to surface scatter; second, it causes a symmetric refractive index profile and results in a mode profile that more closely matches that of the optical fiber. The theoretical analysis of the effect of the applied field on the mode profile is shown in Appendix III.

In conclusion, the experiments on electro-thermal diffusion in $LiNbO_3$ do not yet show any dramatic evidence for multimode guides which confine both TE and TM modes. More experiments should be done to determine whether or not this technique will work.

APPENDIX 4-I TM-Selective Guiding in c-propagating $LiNbO_3$

TM-selective guiding is observed near cut-off. This Appendix contains a theoretical explanation using the model of a step-index planar waveguide in an anisotropic medium, with the same symmetry as $LiNbO_3$.

For simplicity we choose a weakly guiding model, assuming that the refractive index components of the guiding layer are only slightly larger than those of the bulk.

Abbreviations to be used are as follows:

n_o = ordinary refractive index of bulk

n_e = extraordinary refractive index of bulk

N_o = ordinary refractive index of waveguide

N_e = extraordinary refractive index of waveguide

$\vec{k}$ = wave vector

$\vec{D}$ = displacement vector

θ = angle between the optic axis (propagation direction) and the direction of the ray propagating in the waveguide.

θ' = angle between the optic axis (propagation direction) and the direction of the ray propagating in the bulk.

β = propagation constant of a guide mode

N = refractive index of an extraordinary ray in the guide

n = refractive index of an extraordinary ray in the bulk.

b = waveguide thickness

k_o = wave number in free space

Because of the anisotropy, it is required to talk about index ellipsoids rather than refractive indices. In this theory we employ two refractive index ellipsoids, in the bulk and waveguide respectively. The waveguide ellipsoid is slightly enlarged compared with that of the bulk due to the Ti-indiffusion and Li out-diffusion. In Fig. 4I-1 the two ellipsoids are shown. The index increase is shown to be much larger along the c axis than perpendicular to it. This note will describe why this is so.

In the ray optics picture of propagation in a waveguide, the guided modes can be considered to be bouncing back and forth between the waveguide walls at an angle θ. Those rays which are polarized TE, are pure ordinary rays and do not experience the anisotropy of the waveguide. The TM modes, however, have a polarization which lies in the plane of incidence of the rays, and have a component of polarization which lies along the c-axis. This is shown in Fig. 4I-2.

We know from birefringence theory that the TM-polarized ray shown in Fig. 2, traveling at an angle θ, will experience a refractive index given by

$$N(\theta) = \frac{N_e N_o}{(N_e^2 \cos^2\theta + N_o^2 \sin^2\theta)^{\frac{1}{2}}} \qquad \text{(I-1)}$$

The light traveling in the substrate, which has an exponential profile, can be considered to be composed of rays traveling at an imaginary angle, θ'. This makes it possible to write

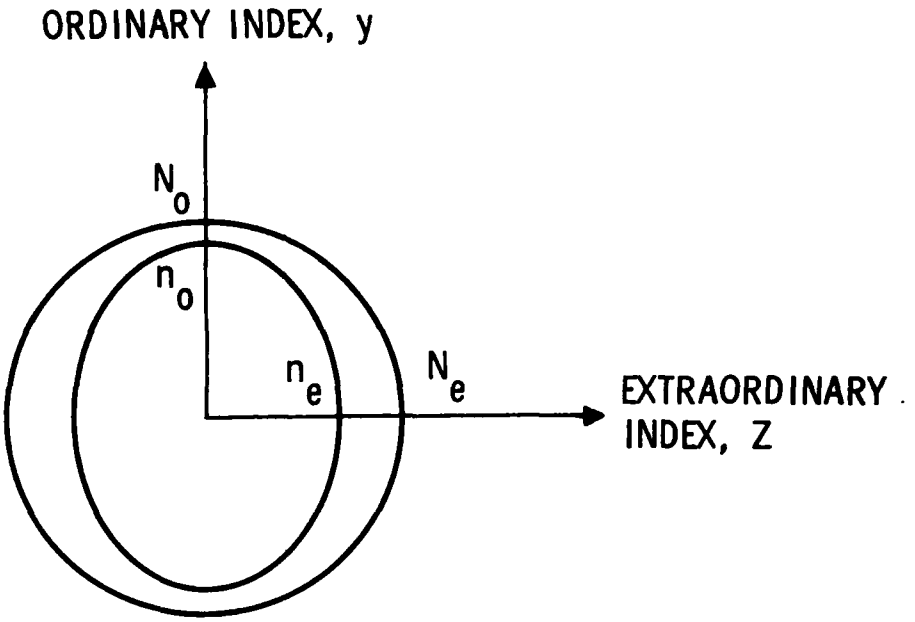

Fig. 4I-1. Index ellipsoid for anisotropic substrate (inner ellipse) and for waveguide (outer ellipsoid).

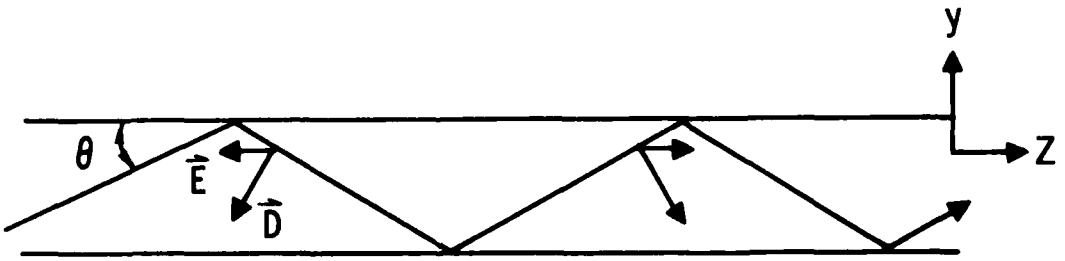

Fig. 4I-2. Polarization components for TM mode, using ray optics picture of guided wave.

$$N \cos \Theta = n \cos \Theta' = \beta / k_o \tag{I-2}$$

with

$$n(\Theta') = \frac{n_e \, n_o}{(n_e^2 \cos^2 \Theta' + n_o^2 \sin^{-2} \Theta')^{\frac{1}{2}}} \tag{I-3}$$

N and n are written in terms of β

$$N^2 = \frac{1}{N_o^2} \left\{ N_e^2 N_o^2 - (N_e^2 - N_o^2 \frac{\beta^2}{k_o^2} \right\} \tag{I-4}$$

and

$$n^2 = \frac{1}{n_o^2} \left\{ n_e^2 n_o^2 - (n_e^2 - n_o^2) \frac{\beta}{k_o^2} \right\} \quad . \tag{I-5}$$

We can write the waveguide equation in the bulk

$$\left\{ \frac{\partial^2}{\partial y^2} + (n^2 k_o^2 - \beta^2) \right\} \begin{bmatrix} E \\ H \end{bmatrix} = 0 \tag{I-6}$$

and in the waveguide

$$\left\{ \frac{\partial^2}{\partial y^2} + (N^2 k_o^2 - \beta^2) \right\} \begin{bmatrix} E \\ H \end{bmatrix} = 0 \tag{I-7}$$

The condition for guided waves is

$$(n^2 K_o^2 - \beta^2) < 0 \text{ and } (N^2 k_o^2 - \beta^2) > 0$$

If we use abbreviations

$$v = (\beta^2 - n^2 k_o^2)^{\frac{1}{2}} b \text{ and } u = (N^2 k_o^2 - \beta^2)^{\frac{1}{2}} b$$

we write

$$u^2 > \quad \text{and} \quad u^2 > 0.$$

For TE modes the relationship between u and v is the same as for isotropic guides:

$$u^2 + v^2 = V^2$$

where

$$V = (N_o^2 - n_o^2)^{\frac{1}{2}} k_o b \tag{I-8}$$

For TM modes, however, u and v satisfy the equation for an ellipse, which does not appear in the isotropic guide:

$$\frac{u^2}{A^2} + \frac{v^2}{B^2} = 1 \tag{I-9}$$

where

$$A = \frac{N_e}{N_o} (N_o^2 - n_o^2)^{\frac{1}{2}} k_o b$$

and

$$B = \frac{n_e}{n_o} (N_o^2 - n_o^2)^{\frac{1}{2}} k_o b \quad .$$

To obtain the eigenvalue equation, we apply the same analysis as applied for isotropic waveguides, since all the procedure in the boundary condition matching between the waveguide and the bulk must be followed exactly in the same fashion. Thus we can use the result of a weakly guiding isotropic step guide to get for both TE and TM modes

$$v = -u \cot u \qquad \text{(I-10)}$$

We have confirmed that the quasi-ray analysis employed coincides with the results of the field treatment done by Yamamoto et.al.[1]

The eigenvalues for β will be determined by the crossing points of Eqs. (9) and (10) for TM mode and Eqs. (8) and (10) for TE mode. In Fig. 3 the characteristic Eq. (10) and Eqs. (8) and (9) are plotted. From this we can readily determine the three different cases of guiding:

TE if $V > \frac{\pi}{2}$

TM if $A > \frac{\pi}{2}$

TM only if $A > \frac{\pi}{2}$ and $V < \frac{\pi}{2}$.

Since $\frac{A}{V} = \frac{Ne}{N_o}$ it is possible to guide TM mode only when

$$\frac{Ne}{N_o} > 1 \quad . \qquad \text{(I-11)}$$

With the extraordinary index increase Δn_e and the ordinary index increase Δn_o in the guiding layer we can relate the refractive

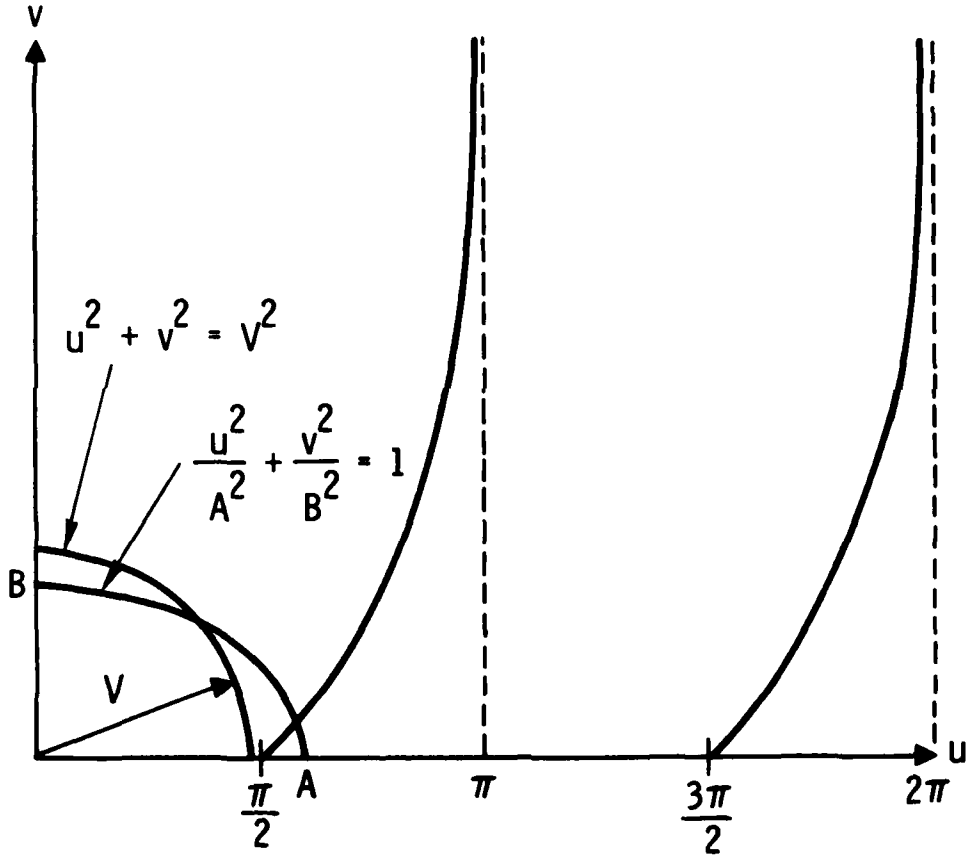

Fig. 4I-3. Graphical determination of the conditions for TM-selective guiding.

indices of the bulk and the waveguide by

$$Ne = n_e + \Delta n_e \quad \text{and} \quad N_o = n_o + \Delta n_o \quad .$$

For $LiNbO_3$ ($n_o = 2.29$ and $n_e = 2.20$ at 0.63 μm) the condition of TM mode - selective guiding is determined to be

$(\Delta n_e - \Delta n_o) > 0.09$.

We should point out that the step guide analysis is not good for the quantitative analysis of a real graded index guide and therefore we cannot judge this theory from the value calculated with this model. However, an estimate of $\Delta n_e - \Delta n_o = 0.03$ [2] is typical for Ti-indiffused guides. Thus we consider that the above theory is undoubtedly the explanation for the TM-only guides which we observed.

REFERENCES IV-I

1. S. Yamamoto, Y. Koyamoda, and T. Makimoto, "Normal-mode Analysis of Anisotropic and Gyrotropic Thin-film Waveguides for Integrated Optics", J. App. Phys. 43, 5090 (1972).
2. J.R. Carruthers, I.P. Kaminow, and L.W. Stultz, "Diffusion Kinetics and Optical Waveguiding Properties of Out-diffused Layers in Lithium Niobate and Lithium Tantalate", Appl. Opt. 13, 2333 (1974).

APPENDIX 4-II. Waveguide Cutoff Condition Dependence on Diffusion Time

Let us consider diffusion from a finite source of diffusant, such as a thin film of $LiNbO_3$. The refractive index will have its peak value at the surface, where it will be n larger than its value in the bulk, N_b. As the diffusion time gets longer, the surface value of Δn decreases by $t^{\frac{1}{2}}$, while the diffusion profile spreads, increasing the diffusion depth by $t^{\frac{1}{2}}$. Thus, while the index step decreases, the effective waveguide thickness increases. This contradictory behavior of the two waveguide parameters does not allow us to make a quick judgment as to whether increasing the diffusion time will increase or decrease the waveguide cutoff. In this appendix we examine the cut-off condition for a diffused guide index profile.

It is well known that for a sufficiently long time diffusion of a limited amount of diffusion source, the diffused concentration profile follows the Gaussian distribution. We can reasonably assume the refractive index change will follow the same profile. In order to judge whether a sample forms a guiding layer, it is necessary only to determine the cut-off condition for a single mode. The lowest order mode cut-off condition is [1]

$$k_o \; 2 \, n_b \, \Delta n \int_o^{\infty} e^{-x^2/2b^2} \, dx - 3 \, \pi/4 \qquad (1)$$

where k is the free space wave number, x is the position variable measured from the surface and b is the $\frac{1}{e}$ width of the Gaussian index profile. Equation (1) can be calculated to give

$$k_o \, b \quad 2 \, n_b \, \Delta n \quad = \quad 3 \, \pi/4 \quad . \tag{2}$$

For finite source diffusion, the quantities n and b are related by

$$\frac{\Delta n}{t/b} = \frac{2}{\pi} \quad \frac{dn}{dc} \quad \alpha \tag{3}$$

where t is the deposited metal film thickness, α is the metal atom concentration of the film and dn/dc is the rate of change of the refractive index with diffusant concentration. The quantitity dn/dc has been shown to be constant by Schmidt and Kaminow[2] as well as Naitoh et.al. [1] Two sets of measurements give almost the same value, $dne/dc = 1.6 \times 10^{-23}$ cm^3, for the extraordinary index change due to Ti- diffusion. Now, if we assume dn/dc to be constant, substitution of Eq. (3) into Eq. (2) gives

$$k_o \quad 2 \, n_b \, t(dn/dc)\alpha b \quad = \quad \frac{3}{4} \pi^{3/4} \quad . \tag{4}$$

In other words, the film thickness required to ensure confinement of at least one mode is

$$t = \frac{\left(\frac{3}{4k_o}\right)^2 \pi^{3/2}}{n_b \alpha \left(\frac{dn}{dc}\right) b} \qquad (5)$$

Since b is proportional to $t^{\frac{1}{2}}$, a longer diffusion time decreases the film thickness required to produce a waveguide.

For a given deposition thickness of diffusant, the longer the diffusion time, the better confined the mode should be. This theoretical result does not agree with our experiments. This is not totally unexpected, however, because the left hand side of Eq. (4) is a slowly varying function of time. A little discrepancy between the assumptions made in this theory and the real diffusion parameters could revert the increasing time dependence. After a long diffusion time, the refractive index profile may deviate substantially from the theoretical Gaussian profile. In addition to Ti in-diffusion, there are three other diffusion processes which may be participating in forming the refractive index profile. Those are suggested as Li_2O out-diffusion, NbO_2 diffusion and oxygen revolution with $Nb^{5+} \rightarrow Nb^{4+}$ reduction.[3] Near 1000°C, Li_2O and oxygen diffusions are significant but NbO_2 diffusion is not, because of its extremely low vapor pressure. Li_2O out-diffusion is well known to affect only the extraordinary index. It is not known to us how much the oxygen diffusion affects the refractive

index profile. However, we expect that it could have a large effect because an oxygen ion has bigger electronic polarizability 3.88 in c.g.s. unit than 0.19 of Ti^{4+}.[4] Thus the resultant refractive index profile after diffusion in $LiNbO_3$ will be determined as well as the superposition of diffused Ti contribution and the side effects due to other three contributions and may deviate from the Gaussian profile based on a single ideal diffusion theory.

REFERENCES I-II

1. H. Naitoh, M. Numoshita, and T. Nakayama, "Mode Control of Ti-diffused $LiNbO_3$ Slab Optical Waveguide", App. Opt. 16, 2546 (1977).
2. R.V. Schmidt and I.P. Kaminow, "Metal-diffused Optical Waveguides in $LiNbO_3$", App. Phys. Lett. 25, 458 (1974).
3. I.P. Kaminow and J.tR. Carruthers, "Optical Waveguiding Layers in $LiNbO_3$ and $LiTaO_3$", Appl. Phys. Lett. 22, 326 (1973).
4. C. Kitlel, "Introduction to Solid State Physics", 5th ed., John Wiley & Sons, Inc., New York/London/Sydney/Toronto, 411 (1976).

APPENDIX 4-III

Previous experiments on buried waveguides have used a double diffusion technique, following an in-diffusion of one species to raise the index, with another to lower the index closer to the surface. Theoretically a single diffusion with the help of an electric field can make a buried wave guide. The diffusion equation under an external field is

$$\frac{\partial c}{\partial t} = D \frac{\partial^2 c}{\partial x^2} - E \mu \frac{\partial c}{\partial x} \qquad \text{(III-1)}$$

where C is the diffusant concentration in the substrate, x is the coordinate measured from the surface of the sample, D is the diffusion constant, μ is the mobility of the diffusant, and E is the applied external field.

It is well known that the diffusion profile without an external field becomes Gaussian for a long diffusion time from a limited source. The solution of the diffusion equation without a field is:

$$c_1 = \frac{2C_o}{\sqrt{\pi} b} \exp\left(-x^2/b^2\right) \qquad \text{(III-2)}$$

where b is the diffusion depth and c_o is the number of metal ions per unit area which are available for the diffusion (C_o metal-thickness).

In order to solve equation III-1, take a coordinate transform such that $x \to x' + \mu t'$

$t \to t'$

The diffusion equation then has a very simple form:

$$\frac{\partial c}{\partial t}(x',t') = D \frac{\partial C}{\partial x^2}(x',t)$$

Immediately we get a solution of the form

$$C(x't) = A \frac{2C_o}{\sqrt{\pi}b} \exp(-x^{12}/b^2)$$

$$C(x,t) = A \frac{2C_o}{\sqrt{\pi}b} \exp\{-(x - E\mu t)^2/b^2\}$$

The new concentration represents a buried profile below the surface by a distance $X_o = E\mu t$. The constant, A, in the above equation is determined by requiring conservation of the amount of diffusant. Clearly the waveguide can be buried most effectively if the diffusant has a relatively high electrical mobility in the substrate.

This guided mode profile matches very well the symmetric profiles from optical fibers. Electrical burying of the waveguide below the surface would lower the insertion loss of $LiNbO_3$ switches used with fiber optics.

MISSION
of
Rome Air Development Center

RADC plans and executes research, development, test and selected acquisition programs in support of Command, Control Communications and Intelligence (C^3I) activities. Technical and engineering support within areas of technical competence is provided to ESD Program Offices (POs) and other ESD elements. The principal technical mission areas are communications, electromagnetic guidance and control, surveillance of ground and aerospace objects, intelligence data collection and handling, information system technology, ionospheric propagation, solid state sciences, microwave physics and electronic reliability, maintainability and compatibility.